FINAL REPORT

Practical UXO Classification: Enhanced Data Processing Strategies for Technology Transition

ESTCP Project MR-201421

JUNE 2020

Kevin Kingdon
Laurens Beran
Stephen Billings
Nicolas Lhomme
Leonard Pasion
David Sinex
Barry Zelt
Black Tusk Geophysics, Inc.

Distribution Statement A
This document has been cleared for public release

ESTCP

This report was prepared under contract to the Department of Defense Environmental Security Technology Certification Program (ESTCP). The publication of this report does not indicate endorsement by the Department of Defense, nor should the contents be construed as reflecting the official policy or position of the Department of Defense. Reference herein to any specific commercial product, process, or service by trade name, trademark, manufacturer, or otherwise, does not necessarily constitute or imply its endorsement, recommendation, or favoring by the Department of Defense.

REPORT DOCUMENTATION PAGE

Form Approved
OMB No. 0704-0188

Public reporting burden for this collection of information is estimated to average 1 hour per response, including the time for reviewing instructions, searching existing data sources, gathering and maintaining the data needed, and completing and reviewing this collection of information. Send comments regarding this burden estimate or any other aspect of this collection of information, including suggestions for reducing this burden to Department of Defense, Washington Headquarters Services, Directorate for Information Operations and Reports (0704-0188), 1215 Jefferson Davis Highway, Suite 1204, Arlington, VA 22202-4302. Respondents should be aware that notwithstanding any other provision of law, no person shall be subject to any penalty for failing to comply with a collection of information if it does not display a currently valid OMB control number. **PLEASE DO NOT RETURN YOUR FORM TO THE ABOVE ADDRESS.**

1. REPORT DATE	**2. REPORT TYPE**	**3. DATES COVERED** *(From - To)*
30-06-2020	**ESTCP Final Report**	9/15/2014 - 9/15/2019

4. TITLE AND SUBTITLE
Final Report: ESTCP MR-201421
Practical UXO Classification: Enhanced Data Processing Strategies for Technology Transition

5a. CONTRACT NUMBER
W912HQ-14-C-0054

5b. GRANT NUMBER
ESTCP MR-201421

5c. PROGRAM ELEMENT NUMBER

6. AUTHOR(S)
Kevin Kingdon, Laurens Beran, Barry Zelt, Nicolas Lhomme, Len Pasion, David Sinex

5d. PROJECT NUMBER MR-201421

5e. TASK NUMBER

5f. WORK UNIT NUMBER

7. PERFORMING ORGANIZATION NAME(S) AND ADDRESS(ES)
Black Tusk Geophysics
#401-1755 Broadway W
Vancouver, BC V6J 4S5
Canada

8. PERFORMING ORGANIZATION REPORT NUMBER
MR-201421

9. SPONSORING / MONITORING AGENCY NAME(S) AND ADDRESS(ES)
Environmental Security Technology Certification Program
4800 Mark Center Drive, Suite 16F16
Alexandria, VA 22350-3605

10. SPONSOR/MONITOR'S ACRONYM(S)
ESTCP

11. SPONSOR/MONITOR'S REPORT NUMBER(S)
MR-201421

12. DISTRIBUTION / AVAILABILITY STATEMENT
Distribution A: Approved for public release; distribution is unlimited

13. SUPPLEMENTARY NOTES

14. ABSTRACT

This project demonstrated advanced methods for the detection and classification of unexploded ordnance (UXO) in production settings. Advanced Geophysical Classification (AGC) software and hardware were developed and tested under the following project tasks:

1. **Software development**: software tools were developed to facilitate the application of AGC methods and transfer this technology to industry. An application for in-field verification of measurements quality objectives has been developed and transitioned to industry.
2. **AHRS testing**: the performance of commercial Attitude and Heading Reference Systems (AHRS) was tested to verify they can meet requirements for AGC.
3. **AGC in challenging scenarios**: we tested processing algorithms for classification of small targets of interest (TOI).
4. **UltraTEM testing**: data collected with the UltraTEM AGC sensor at test sites was processed to verify capabilities for informed source selection and classification.
5. **Technology transfer**: advancements in AGC processing workflows and lessons learned from this project were shared with the MMRP industry

Software tools and processing algorithms tested under this project have been transitioned to industry and have been successfully used on commercial MMRP projects. The UltraTEM Classifier system tested under this project has been validated under DAGCAP and is expected to reduce project costs via one-pass classification capabilities.

15. SUBJECT TERMS
Advanced Geophysical Classification, UltraTEM, UXOLab, MPV, AHRS

16. SECURITY CLASSIFICATION OF:			**17. LIMITATION OF ABSTRACT**	**18. NUMBER OF PAGES**	**19a. NAME OF RESPONSIBLE PERSON**
a. REPORT	**b. ABSTRACT**	**c. THIS PAGE**			Kevin Kingdon
UCLASS	UCLASS	UCLASS	UCLASS	106	**19b. TELEPHONE NUMBER** *(include area code)* 604-428-3382

FINAL REPORT
Project: MR-201421

TABLE OF CONTENTS

Page

ABSTRACT X
1.0 INTRODUCTION 1
1.1 BACKGROUND 1
1.2 OBJECTIVE OF THE DEMONSTRATION 1
1.3 REGULATORY DRIVERS 2
2.0 SOFTWARE DEVELOPMENT 3
2.1 DATA QUALITY TEST TOOLS 4
2.1.1 Function test 4
2.1.2 Lag test 7
2.1.3 Spin test 10
2.2 ADDITIONAL TOOLS FOR ANALYSIS OF AGC DATA 13
2.3 BTG IN-FIELD APP 29
2.3.1 Overview 30
2.3.2 QC tests 30
2.3.3 Sensor function test 34
2.3.4 Spin test 36
2.3.5 Background validation and verification 38
3.0 AHRS TESTING WITH THE LORD MICROSTRAIN 3DM GX4-25 AND GX5-25 42
3.1 APPLICATION OF THE GX4-25 AHRS WITH THE MPV 43
3.2 INTEGRATION OF THE GX5-25 45
3.3 AZIMUTH BIAS WITH THE GX5-25 47
3.4 TESTS WITH GX5-25 50
3.5 TESTS WITH GX4-25 53
3.6 RECOMMENDED PARAMETERS FOR THE GX4-25 55
3.7 CONCLUSION 56
4.0 AGC IN CHALLENGING SCENARIOS 57
4.1 LOWRY 20MM INVESTIGATIONS 57
4.1.1 Summary 57
4.1.2 Results 57
5.0 ULTRATEM SHAKEDOWN TESTING AND VALIDATION 63
5.1 PROCESSING OF INITIAL SENSOR DATA ACQUIRED AT STRATHALBYN TEST SITE 63
5.2 SHAKEDOWN TESTING AT BLOSSOM POINT 65

TABLE OF CONTENTS (Continued)

Page

5.3 ULTRATEM HARDWARE DEMONSTRATION OF CAPABILITIES AT ABERDEEN PROVING GROUNDS (APG) 69
5.4 SYNTHETIC SEEDING A HIGH TARGET DENSITY DATASET FOR TESTING ONE PASS CLASSIFICATION WORKFLOW 69
6.0 TECHNOLOGY TRANSFER 74
7.0 PERFORMANCE ASSESSMENT 75
8.0 COST ASSESSMENT 76
9.0 IMPLEMENTATION ISSUES 77
APPENDIX A POINTS OF CONTACT A-1
APPENDIX B WHITE PAPER: VALIDATION OF ULTRATEM SCREENER FOR INFORMED SOURCE SELECTION B-1

LIST OF FIGURES

Page

Figure 1. Detection Modeler Interface Showing Threshold Calculations for the MPV Sensor... 3
Figure 2. Results for Two Function Tests for MPV Dynamic Data..... 5
Figure 3. Time Decay of the EMI Response for Each of the Receivers. 6
Figure 4. Function Tests Through a Day of Field Data Collection for Static MPV. 6
Figure 5. Time Decays for Multiple Function Tests with MPV Static Data..... 7
Figure 6. Lag Lines on the IVS. 8
Figure 7. Synchronization of the EMI and Positional Data to Match the Peak Location. 9
Figure 8. Illustration of the MPV Spin Test. 10
Figure 9 Failed Spin Tests. 12
Figure 10. Illustration of Spin Tests with an Azimuth Bias. 12
Figure 11. GridZilla in Target Picking Mode Showing Gridded Dynamic Classic MetalMapper Data and the Target Picking Parameter Menu. 13
Figure 12. GridZilla Showing an Example Contour Map of Target Density (targets/acre)..... 14
Figure 13. Background: QCZilla Window. 15
Figure 14. General Cluster Cluster Analysis Tool. 16
Figure 15. DigZilla Tool for Classification. 17
Figure 16. Left: GUI for Specifying Modeling Parameters for Validation of a Background Using a Standard Set of Five Measurements. Right: Five-point Background Validation Report..... 18
Figure 17. Sample Two-point Background Validation Report. 19
Figure 18. Utility for Converting DoD H5 Library Files to QCZilla Ordnance File Format. 20
Figure 19. GUI for Setting Auto QC Parameters. 21
Figure 20. Left: Reporting Tool GUI. On This Screen, Various Relevant Files Are Specified. Various Categories of Targets Can Be Overlain on a GridZilla Display of Gridded Data Using Dedicated Buttons. Middle: GUI for Specifying Cover Page Information. Right: GUI for Specifying Classification Summary Information..... 22
Figure 21. Example GridZilla Display Modified by the Reporting Utility to Show Target Locations Coded Based on Dig List Category. 22
Figure 22. Example MPV Dynamic Data Viewed in GridZilla. 23
Figure 23. Same Dynamic MPV Data as in Previous Figure, Overlain on Google Map Imagery. 24
Figure 24. Classic MetalMapper Dynamic Data (Channel 14; 0.818 ms). 25
Figure 25. Corresponding Map of Estimated Noise. 25
Figure 26. Example of The Earl of Slice in Action. 26
Figure 27. Spatial Background Tool Showing Background Ground Locations (Large Labeled Symbols) and Cued Measurement Locations (Small Symbols). 27
Figure 28. GUI for Specifying Contour Tiling Parameters. 28
Figure 29. Example of Tiling of a Large EM61 Anomaly. 28
Figure 30. Example Map of MPV Sensor Speed in m/s. 29
Figure 31. Main Window (Top) and UI Options for the Sensor Function Test (Bottom). 31
Figure 32. Main Window (Top) and UI Options for the Spin Test (Bottom). 32

LIST OF FIGURES

Page

Figure 33. Main Window (Top) and UI Options for the Background Validation and Verification Test (Bottom). 33
Figure 34. Function Test Results Window. 34
Figure 35. Function Test Decay Plot Comparing Time Decays for the Test Measurement Against the Reference Values. 35
Figure 36. Function Test Variation Comparison Plot Showing the Response Variation Values for Each Receiver. 35
Figure 37. Function Test Results Window. 36
Figure 38. Spin Test Location Plot Showing the Locations of the GPS or RTS Sensor Head (Green Line) and All Receiver Positions Pre-optimization (Blue) and Post-optimization (Red). 37
Figure 39. Spin Test History Plot Showing the History of Successful Spin Test Results for the Change in IMU Bias Metric. 37
Figure 40. 5-point Background Validation Results Window. 38
Figure 41. Example of a Successful 5-point Background Validation Report. 39
Figure 42. Example of a 5-point Background Validation Report with a Failure Due to Insufficient Offset of One of the Four Offset Measurements. 39
Figure 43. Example of a (Successful) 5-point Background Validation Report When No GPS or RTS Information Is Available. 40
Figure 44. Example of a Successful 2-point Background Verification Report. 41
Figure 45. Example of a 2-point Background Verification Report with a Failure Due to Excessive Offset from the Original Validation Measurement Location. 41
Figure 46. MicroStrain 3DM GX4-25 and GX5-25. 42
Figure 47. Picture of the MPV, Where the Upper Part of the Handling Boom Has Fixtures for a White Box Containing the AHRS and a Mast Holding the GPS Rover (or a Prism for RTS). 43
Figure 48. Illustration of the MPV Spin Test. 46
Figure 49. Illustration of Spin Tests with an Azimuth Bias. 46
Figure 50. Lag Lines on the IVS. 47
Figure 51. Sensor Path During a Detection Survey. 48
Figure 52. View of a Line Subset with Irregular Line Pattern. 49
Figure 53. Schematic Illustrating AHRS-related Positional Error. 50
Figure 54. AHRS Test Along a Lag Lines for a Given Set of Filter Parameters. 51
Figure 55. AHRS Testing with Filter Parameters Matching as Close as Possible BTG's GX4 Parameters. 52
Figure 56. Lag Line Tests with GX4 Out of the Box, Before Calibration. 53
Figure 57. GX4 Lag-Line Test After Soft and Hard Iron Calibration. 54
Figure 58. Lag Lines Tests with GX4 using BTG Filter Parameters. 54
Figure 59. EKF Parameters for the GX4-25 in MIP 2016 Software. 55
Figure 60. Left: Dynamic Test Line Data Over Eight Holes. Holes 1-5 Each Contain a Single 20mm Projectile. Holes 6, 7 and 8 Contain 2, 3 and 4 20mm Projectiles, Respectively. Right: Dynamic Polarizabilities. (a) Single Source Inversion Polarizbilities from Holes 1-5. (b-d) Two-, Three- and Four- Source Inversion Polarizabilities from Holes 6, 7 and 8, Respectively. 58

LIST OF FIGURES

Page

Figure 61. Cued Polarizabilities. 59
Figure 62. Gridded Dynamic Data (Leveled Channel 10; 0.338 ms) from Row 31 (High Density Area) of the 20mm Range. 60
Figure 63. Cued Polarizabilities Sorted by Polarizability Match Metric (Cyan Label at Lower Left in Each Panel). 61
Figure 64. Example of Comparison of Cued (Grey Lines) and Dynamic (Blue Lines) Polarizabilities for One Target. 62
Figure 65. Geometry of the 5Tx UltraTEM Classifier Sensor. 63
Figure 66. Geometry of the 1Tx UltraTEM Screener Sensor. 64
Figure 67. UltraTEM Classifier Acquiring Data at the Strathalbyn Test Site. 64
Figure 68. Strathalbyn Test Site Layout. 65
Figure 69. Comparison of UltraTEM and TEMATDS 2x2 Detection Data Over 60mm Mortars at the Blossom Point Test Site. 66
Figure 70. Left: Comparison of the SNR for Small ISO in Worst Case Orientation at 30 cm Depth. Right: Depth of Detection for a Small ISO When the Threshold Is Determined by 3 Times the Noise. 66
Figure 71. Recovered Polarizabilities for the UltraTEM Classifier Over 60mm Mortar Targets at the Blossom Point Test Site. 67
Figure 72. Multi Object Scenario Comprised of Two TOI and One Piece of Clutter Within the Footprint of the UltraTEM Classifier 68
Figure 73. Multi Object Scenario Comprised of Two TOI and Three Pieces of Clutter Within the Footprint of the UltraTEM Classifier 68
Figure 74. Multi Object Scenario Comprised of Two TOI and Four Pieces of Clutter Within the Footprint of the UltraTEM Classifier 69
Figure 75. Targets Synthetically Seeded Into the 4 Acre High Target Density Site Constructed for Testing a One Pass Classification Workflow. 70
Figure 76. Distribution of TOI and Scrap Synthetically Seeds to Create a High Density 4-acre UltraTEM Classifier Dataset. 71
Figure 77. Synthetically Seed Dataset for the Target Distribution Shown in Figure 76. 72
Figure 78. Target Density Map of Detected Anomalies. 72
Figure 79. ROC Curve for the Automated Classification Approach Applied to the Synthetically Seed High Target Density Four-acre Site. 73
Figure 80. UltraTEM Screener Form Factors (Top to Bottom): Man-portable, Pushcart, and Towed Array. B-2
Figure 81. Left: UltraTEM-III Receiver Bank. Right: UltraTEM-III Sensor (Receiver Cube). B-3
Figure 82. BTField Data Acquisition View for UltraTEM Screener. B-4
Figure 83. UltraTEM Classifier Collecting Data at Strathalbyn Test Site. B-5
Figure 84. Strathalbyn Test Site Data. B-5
Figure 85. Comparison of Polarizabilities Estimated from UltraTEM Screener (Left) and Classifier (Right) for Medium ISOs Seeded at the Strathalbyn Test Site. B-6
Figure 86. Comparison of Polarizabilities Estimated from UltraTEM Screener and Classifier for Small and Medium ISOs Seeded at the Strathalbyn Test Site. B-7

LIST OF FIGURES

Page

Figure 87. Deviation of Estimated Locations from Ground Truth Locations for ISOs Seeded at Strathalbyn Test Site. B-7
Figure 88. Informed Source Selection Parameters B-9
Figure 89. A Threshold of 7.6 Was Used to Select Data Anomalies. B-10
Figure 90. Dipole Source Locations from Inverting Each Data Anomaly with a 1, 2, and 3, Source Inversion. B-11
Figure 91. Selected Sources. All ISOs Within the Clearance Depth (i.e., Black Squares) Have Selected Sources. B-12
Figure 92. Nearest Selected Source Offset from Ground Truth for Seeded ISOs B-14
Figure 93. Left: Source Polarizability for Isolated 20 mm Not Screened by ISS. The Source Has a 3 cm Offset from the Groundtruth. However, the Depth for this Source Was Over Estimated, Resulting in a Size Metric of -0.96, Which was slightly higher than the -1 Size Threshold Used by the ISS. Right: The Data Fit for This Target, Showing Observed, Predicted, and Residual Data B-15

LIST OF TABLES

Page

Table 1. Number and Depth Range of Scrap and TOI Synthetically Seeded to Create the 4-acre High Target Density UltraTEM Classifier Dataset. 71
Table 2. Mean and Maximum Offsets of Estimated Locations from Ground Truth Locations for ISOs Seeded at Strathalbyn Test Site. B-6
Table 3. TOI Locations and Nearest Selected Source B-13
Table 4. 20mm Simulant Locations and Nearest Selected Source B-14

ACRONYMS AND ABBREVIATIONS

AHRS	Attitude and Heading Reference Sensor
AGC	Advanced Geophysical Classification
APG	Aberdeen Proving Ground
BTG	Black Tusk Geophysics
DAGCAP	DoD AGC Accreditation Program
DoD	Department of Defense
DGM	Digital Geophysical Mapping
DM	Detection Modeler
EKF	Extended Kalman Filter
EMI	Electromagnetic Induction
ESTCP	Environmental Security Technology Certification Program
FLBGR	Former Lowry Bombing and Gunnery Range
FUDS	Formerly Used Defense Site
GPS	Global Positioning System
IMU	Inertial Motion Unit
IVS	Instrument Verification Strip
ISO	Industry Standard Object
ISS	Informed Source Selection
MM	MetalMapper
MMRP	Military Munitions Response Program
MPV	Man Portable Vector
MQO	Measurement Quality Objective
MRS	Munitions Response Site
NRL	Naval Research Laboratory
QA	Quality Assurance
QAPP	Quality Assurance Project Plan
QC	Quality Control
ROC	Receiver Operating Characteristic
RTS	Robotic Total Station
SERDP	Strategic Environmental Research and Development Program
SVFUDS	Spring Valley Formerly Used Defense Site
TEMTADS	Time-domain Electromagnetic Multi-sensor Towed Array Detection System

TOI	Target of Interest
Tx	Transmitter
UI	User Interface
UXO	Unexploded Ordnance

ABSTRACT

INTRODUCTION AND OBJECTIVES

This project demonstrated advanced methods for the detection and classification of unexploded ordnance (UXO) in production settings.

TECHNOLOGY DESCRIPTION

AGC software and hardware were developed and tested under the following project tasks:

1. **Software development**: software tools were developed to facilitate the application of AGC methods and transfer this technology to industry. An application for in-field verification of measurements quality objectives has been developed and transitioned to industry.
2. **AHRS testing**: the performance of commercial Attitude and Heading Reference Systems (AHRS) was tested to verify they can meet requirements for AGC.
3. **AGC in challenging scenarios**: we tested processing algorithms for classification of small targets of interest (TOI).
4. **UltraTEM testing**: data collected with the UltraTEM AGC sensor at test sites was processed to verify capabilities for informed source selection and classification.
5. **Technology transfer**: advancements in AGC processing workflows and lessons learned from this project were shared with the MMRP industry

PERFORMANCE AND COST ASSESSMENT

Software tools and processing algorithms tested under this project have been transitioned to industry and have been successfully used on commercial MMRP projects. The UltraTEM Classifier system tested under this project has been validated under DAGCAP and is expected to reduce project costs via one-pass classification capabilities.

IMPLEMENTATION ISSUES

All technology developed under this project must comply with the requirements of DAGCAP when used by industry for commercial MMRP work.

PUBLICATIONS

All publications for this project are available on the ESTCP website.

1.0 INTRODUCTION

1.1 BACKGROUND

Advanced Geophysical Classification (AGC) is a method for detection and identification of buried munitions and explosives of concern, including unexploded ordnance, discarded military munitions, and munitions constituents. Developed and tested under the SERDP and ESTCP programs, AGC is now mandated by the DoD for Remedial Investigations and Actions (RIs and RAs) at Formerly Used Defense Sites (FUDS).

The AGC method involves detection of metallic targets with an electromagnetic sensor, followed by processing of measured data to classify detected targets. Electromagnetic sensors designed for AGC applications are optimized to illuminate targets from multiple directions and measure induced secondary fields using multiple vector receivers. These multi-static, multi-component data are input into inversion algorithms that estimate extrinsic (location, depth and orientation) and intrinsic (dipole polarizabilities) values for each target. The estimated dipole polarizabilities are then matched against a pre-defined library of ordnance polarizabilities to identify likely Targets of Interest (TOI).

Through the ESTCP Munitions Response Live-Site Demonstration program, AGC technology has been demonstrated to significantly reduce the number of non-TOI items that are intrusively investigated, while ensuring with high probability that all TOI are found.

1.2 OBJECTIVE OF THE DEMONSTRATION

The objective of this project was to develop and transition both hardware and software for use on AGC projects. The project encompassed a diverse set of tasks that arose during our participation in the ESTCP program:

1. **Software development**: software tools were developed to facilitate the application of AGC methods and transfer this technology to industry. An application for in-field verification of measurements quality objectives has been developed and transitioned to industry.
2. **AHRS testing**: the performance of commercial Attitude and Heading Reference Systems (AHRS) was tested to verify they can meet requirements for AGC.
3. **AGC in challenging scenarios**: we tested processing algorithms for classification of small targets of interest (TOI).
4. **UltraTEM testing**: data collected with the UltraTEM AGC sensor at test sites was processed to verify capabilities for informed source selection and classification.
5. **Technology transfer**: advancements in AGC processing workflows and lessons learned from this project were shared with the MMRP industry

This project was not carried out as a single live-site demonstration and so does not easily conform with the template for ESTCP demonstration reports. The remainder of this report therefore covers each of the above tasks in a separate section.

1.3 REGULATORY DRIVERS

Much of our work under this project has been driven by DAGCAP requirements. For example, in-field software for the MPV sensor was motivated by the need to verify measurement quality objectives during data acquisition.

2.0 SOFTWARE DEVELOPMENT

We developed tools to facilitate acquisition and processing of electromagnetic data for AGC. These include:

1. Enhancements to Detection Modeler software initially developed under SERDP-2226. This application allows a user to calculate the worst-case detection threshold for a specified target of interest at a maximum clearance depth.

   We extended the Detection Modeler (DM) software for the Man Portable Vector (MPV) sensor. Figure 1 shows the DM interface with calculations for the MPV, all existing functionality (detection thresholds, clearance depths) has been extended to this sensor for both dynamic and cued modes.

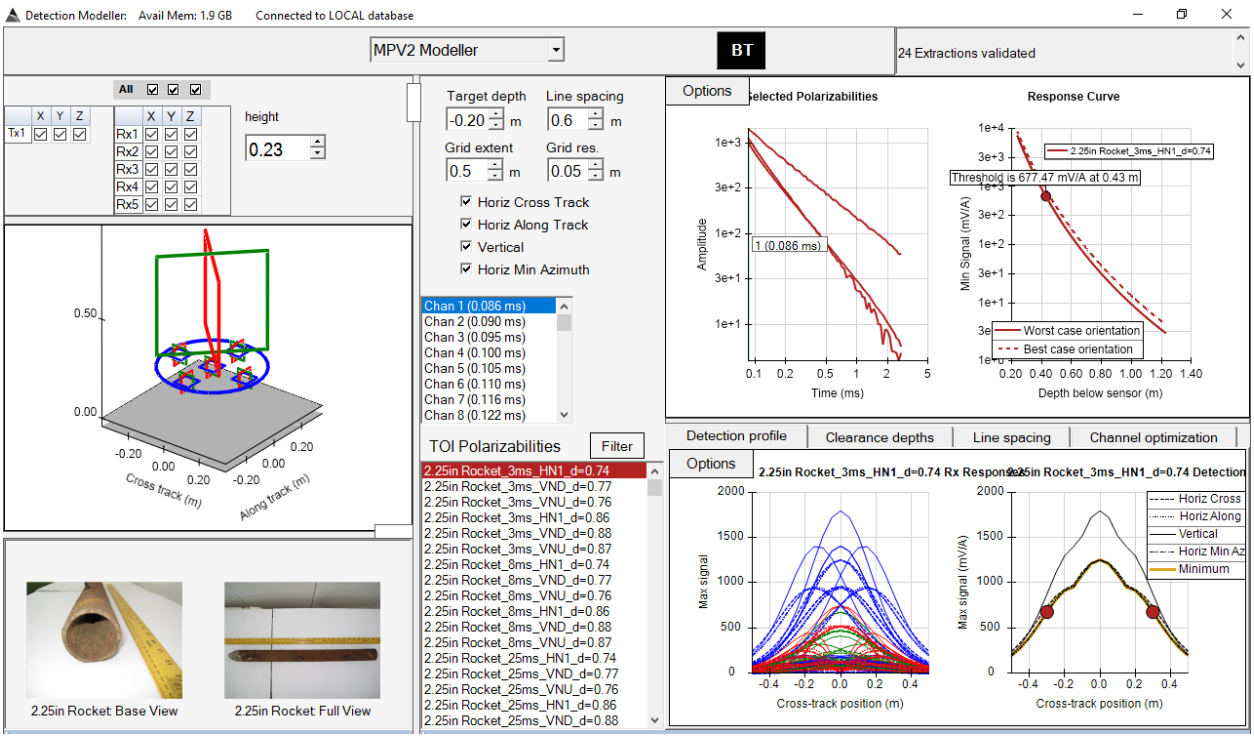

Figure 1. Detection Modeler Interface Showing Threshold Calculations for the MPV Sensor.

2. Tools for checking data quality of AGC data. These tools are described in section 2.1 and formed the basis of the In-Field application (next item in this list).

3. Additional tools for analysis of AGC data (target picking, cluster analysis, etc.), described in section 2.2 and motivated by application of AGC methods to ESTCP demonstrations

4. An In-Field application for checking MQOs (function tests, background validation, etc.) for the MPV sensor. This application is described in detail in section 2.3.

2.1 DATA QUALITY TEST TOOLS

The following set of tools was implemented to review the MPV data quality and ensure correct sensor integration and operation. ESTCP funding was used to improve some of these tools that are used and continuously improved on projects to monitor the data quality of the MPV and other sensors developed within the ESTCP program.

The function test applies to all sensors. The lag and spin tests described herein are more specific to the MPV, for which these tests are critical because of the MPV geometry and of its handheld mode of operation. The MPV data is processed by combining its EMI data with the positional information from the GPS (or RTS) and the AHRS. Each of these three sensors has its own clock that needs to be synchronized with the other ones. The GPS and AHRS data are combined through a rigid body rotation of the MPV sensor head relative to the GPS location, based on the expected sensor geometry (offsets between MPV sensor head and GPS mounting location on MPV handle). These data quality tests are designed to verify correct sensor assembly, lags, biases and repeatability of the signals.

2.1.1 Function test

The function test verifies that the EMI response of a sensor for a given calibration object remains stable. That requirement applies to dynamic and static data. The function test tool described here is used with the MPV, TEMTADS 2x2, MetalMapper 2x2 and the "classic" MetalMapper. For all sensors, the test requires the EMI data collection of a background measurement immediately followed by a measurement with the calibration item. The calibration item is a steel sphere or a steel pipe that is placed in a special holder so that its position relative to the sensor's transmitters and receivers is always the same within one millimeter accuracy.

The background and test measurements are subtracted to remove the environmental noise so that only the EMI response and some second order random noise remains. The test must therefore take place in a relatively quiet location, a location with low metal and low EMI transient disturbance, to avoid causing saturation in any receiver and ensure that the background response remains relatively stable. For static mode the test can be done at a known quiet background location. For dynamic mode, for which a quiet background may have not been identified, the location can be selected by observing the real-time EMI time decays and verifying that the decays do not show any significant response.

The holder location is chosen so that each receiver to be tested receives a signal that is well above the instrument noise; it requires sufficient coupling between the transmitter and calibration item and between the receiver and the item. The "2x2" sensors use the same transmitters for dynamic and static data collection and have therefore the same requirements for the holder location. The holder is located in the center of the array. The MPV and classic MetalMapper use a single vertical-axis transmitter in dynamic mode, and two additional horizontal-axis transmitters in static mode. The holder location can be different for each collection mode as long as it produces sufficient signal in all receivers for the vertical-axis transmitter for the dynamic test, and sufficient signal in all receivers for at least one transmitter, such that all receivers and transmitters can be tested in static mode. In practice we use a different location for the MPV because the optimal location for the dynamic mode interferes with the placement of the detachable static transmitter coils. The holder placement is particularly challenging for the MPV geometry and does not allow for a location that can service both modes without causing saturation in some receivers or too weak a signal in other receivers.

The function test metric is calculated as the maximum percent change, among all receivers and transmitters, of the EMI response of the ongoing function test relative to a reference value. The receiver response is defined as the sum of the EMI decays over a wide range of time channels starting just after transmitter shutoff ringing effects have vanished, and ending not too late to avoid noise. The reference value is a function test measurement provided by the sensor manufacturer or prepared for a project, for example by collecting multiple backgrounds and function test measurements in a very quiet setting, preferably with the sensor significantly raised above the ground, and taking the average value among all these reference tests.

The test is designed to verify proper operation of each receiver and transmitter. Its formulation is straightforward for a single-transmitter system such as dynamic MPV and dynamic classic MetalMapper. For a multi-transmitter system, the test does not need to apply to every receiver-transmitter combination because the receiver and its data acquisition system do not change between different transmitter firings. Moreover, the sensor geometries are such that some receiver-transmitter pairs generate a weak signal that may be too close to the noise to be repeatable. Therefore, the function test metric uses, for each receiver, the response with the smallest deviation relative to the reference response among all transmitter firings.

The test also verifies that each transmitter is being evaluated by selecting, if necessary, one of the receivers with the smallest variation for the transmitter to be tested. The test also verifies that no receiver-transmitter combination produces a response that is dramatically different than the reference. The graphical output of the function test is illustrated in Figure 2 and Figure 3 for MPV dynamic data, and in Figure 4 and Figure 5 for MPV static data.

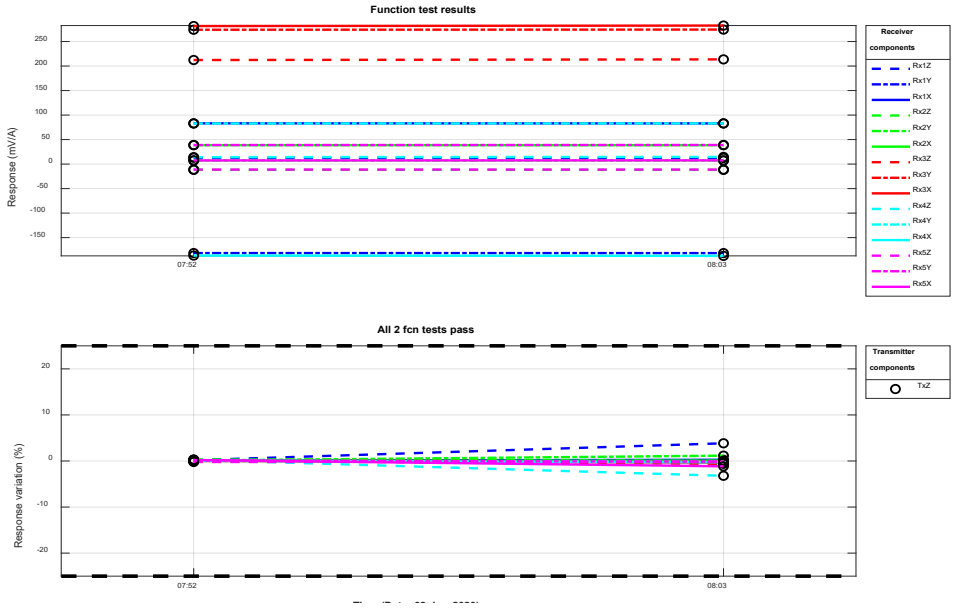

Figure 2. Results for Two Function Tests for MPV Dynamic Data.

The upper panel shows the EMI response for each receiver, after subtracting the test and background measurements and summing the data for multiple time channels. The lower panel shows the percent variation for each receiver within the 25% tolerance range (dashed lines). The second test shows a variation on the order of 5% on the Rx1Z and Rx4Z receivers, which are two of the most strongly coupled receivers and are particularly sensitive to the slightest change in height for the test item.

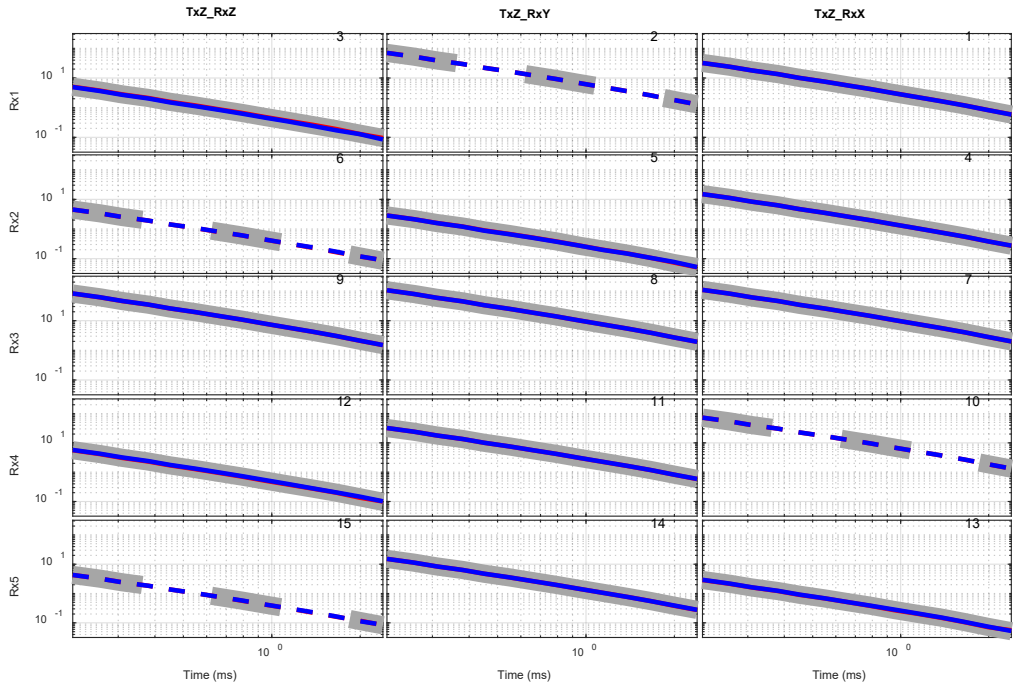

Figure 3. Time Decay of the EMI Response for Each of the Receivers.

The test responses are shown in color (red and blue mostly overlapping) and the reference in grey. Solid lines indicate positive data and dashed lines negative.

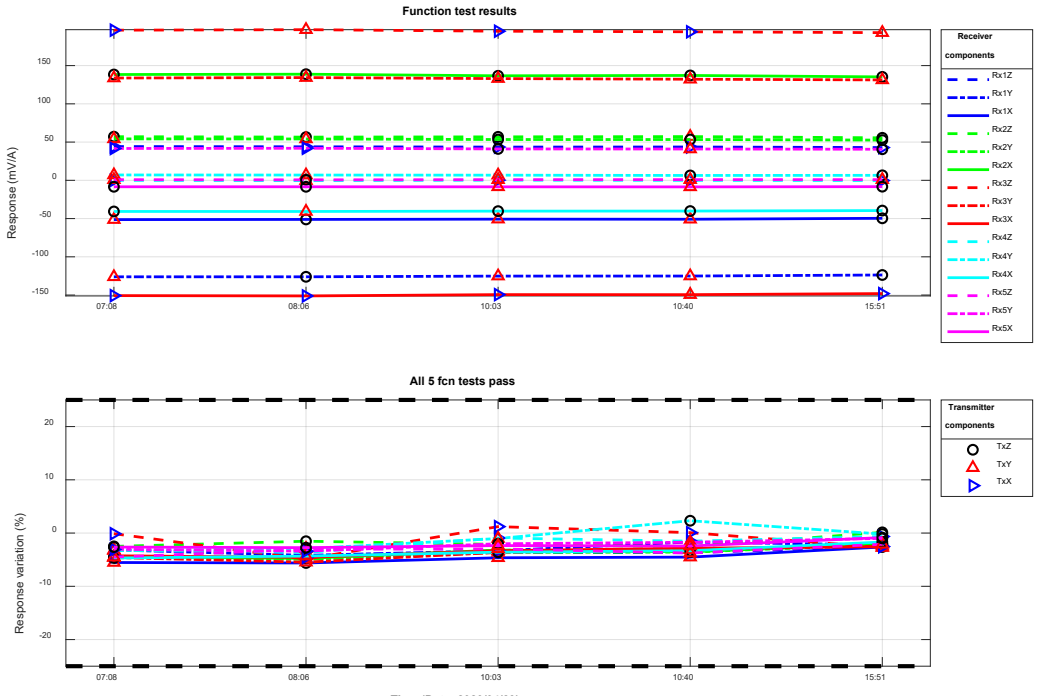

Figure 4. Function Tests Through a Day of Field Data Collection for Static MPV.

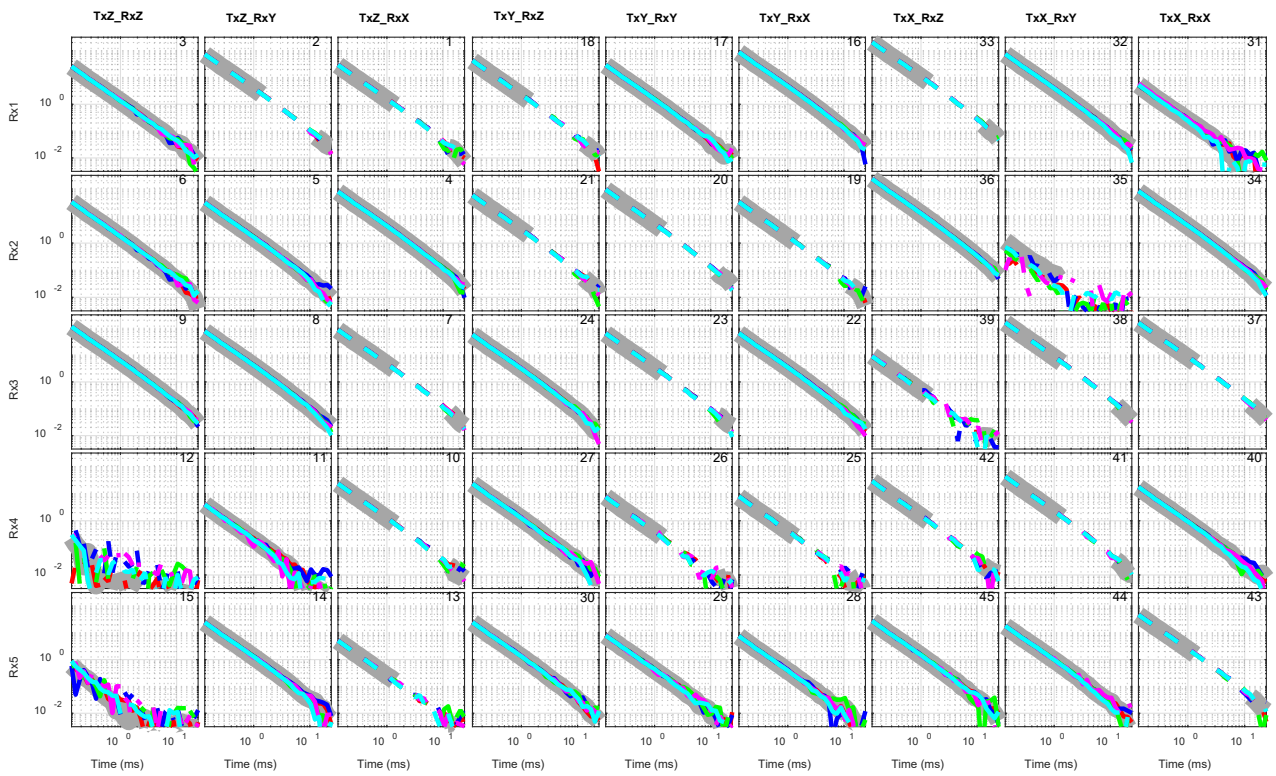

Figure 5. Time Decays for Multiple Function Tests with MPV Static Data.

The decays associated with measurement numbers 12, 15 and 35 (upper right corner of each panel) show weak coupling between the target, receiver and transmitter. For instance, receiver 4Z is evaluated by three transmitters (measurements 12, 27 and 42 for Z, Y and X transmitters, respectively); the best of measurements 27 and 42 can be used to report on receiver 4Z.

2.1.2 Lag test

As part of the daily IVS tests, the center line of the IVS is covered by collecting survey data in two passes in opposite directions (Figure 6). This standard test is performed to estimate and correct for any lag between the positioning sensors (GPS, AHRS) and the EMI sensor by lining up the detection profiles acquired in opposite directions (Figure 7).

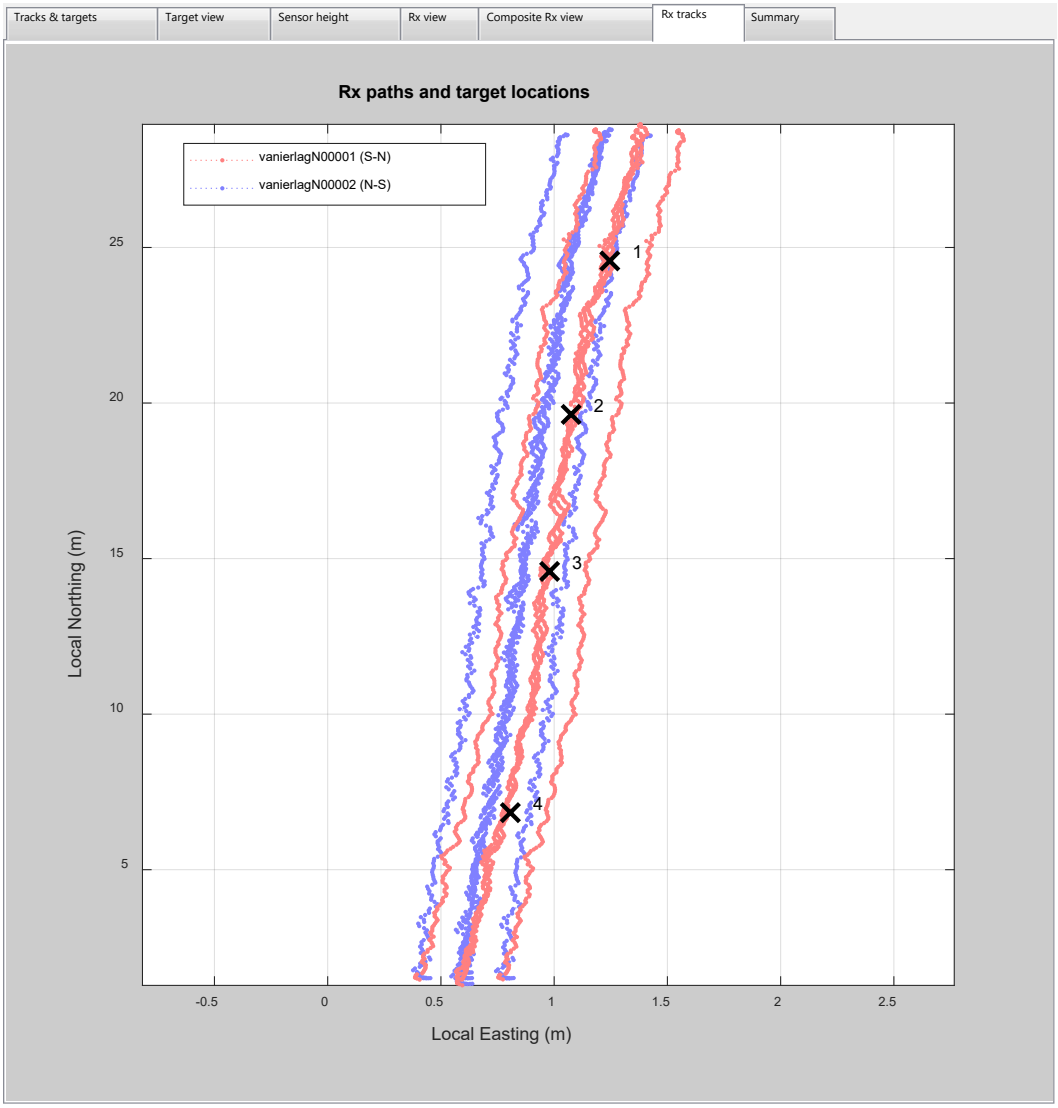

Figure 6. Lag Lines on the IVS.

Two lines are acquired in opposite directions over the IVS targets by collecting dynamic data with the MPV sensor pointing in the direction of travel. The line is physically indicated with a rope to guide the field operator. The receiver locations for the northward line are shown in red and the southward line in blue.

The lag between the GPS and the EMI data is derived by optimization of the correlation coefficient between the detection profiles as a function of the geographic location (position along line). The EMI data for the two passes are expected to differ because of the handheld nature of the survey: the path might differ by up to 5 cm due to ergonomics and parallax effects, given that the operator holds the MPV on the side and his eyes are not lined up with the center of the MPV and the rope on the ground; the EMI signal over the targets can also differ because the operator's walk induces slight pitch, roll and heading rotations, which affect the coupling between the MPV and the targets. A 100% correlation is therefore not expected.

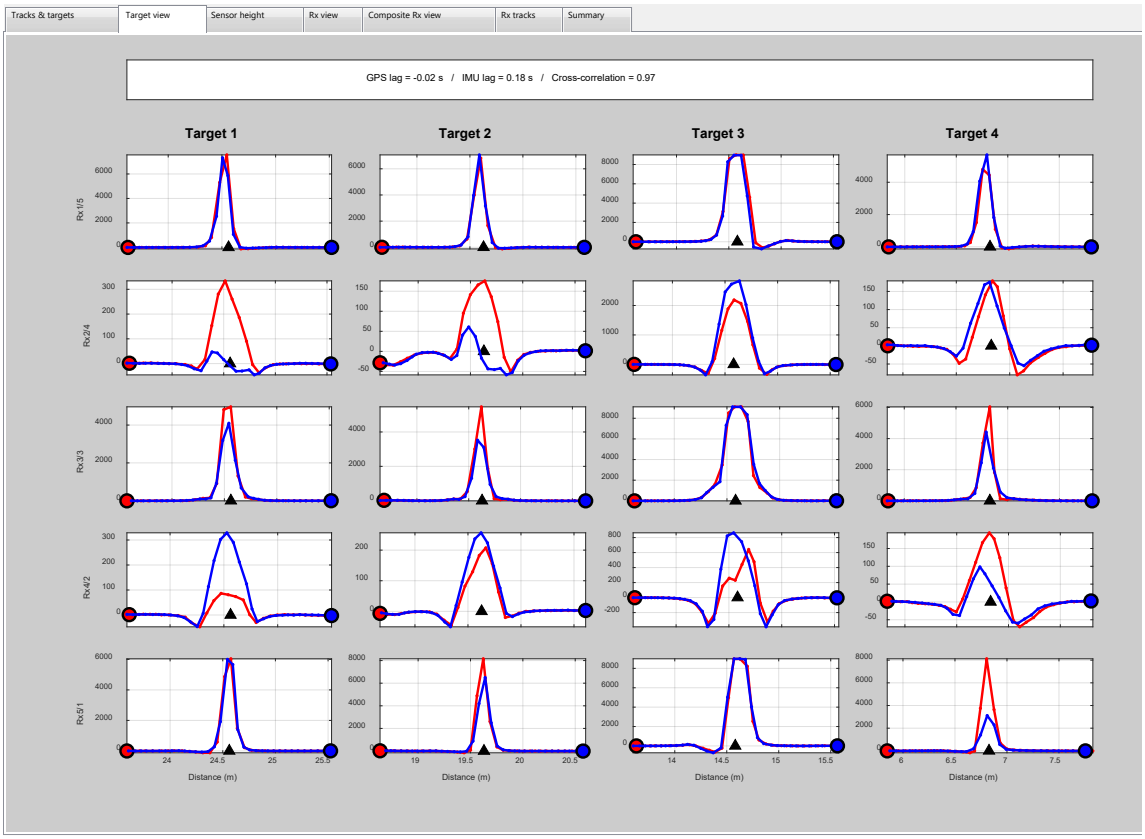

Figure 7. Synchronization of the EMI and Positional Data to Match the Peak Location.

Given the MPV geometry, the receiver pairings for the two opposite passes are 1/5 (front/back), 2/4 (left/right) and 3/3 (center).

Although the operator tries to keep the MPV sensor head along a straight line, the operator's walk itself is recorded by the GPS path and AHRS angles as a wobbly path. The correct combination of the GPS and AHRS to predict the sensor path should result in a straight line in the absence of a lag between the GPS and AHRS sensors, and significant side to side deviations otherwise. The lag between the GPS and AHRS is therefore derived by minimizing the length of the MPV sensor head trajectory.

The lag test is also used to verify whether the sensor is correctly assembled and to identify a heading bias in the AHRS by measuring the lateral offset between the two opposite passes. The paths showed in Figure 6 could suggest that the sensor did not exactly pass over the same locations. However, the EMI data for the 1/5, 5/1 and 3/3 pairings, which correspond to the front, center and back receivers, show in Figure 7 matching signals between the two passes. This suggests that either the actual sensor geometry differs from the expected one, which could happen if there is a rotation within the set of round pipes that constitute the MPV handle, or if there is a bias in the AHRS heading, which would appear as a rotation that moves the predicted MPV head location across track, away from the sensor line. This can occur during the initial mounting of the AHRS if its main direction is not perfectly lined up with the MPV principal direction. This can also occur if there is a bias in the AHRS heading prediction. Given that the GPS is located 1.15 m behind the center of the MPV sensor head, a 1-degree error in the heading corresponds to a 2 cm lateral offset. Given the uncertainties on the actual paths, a bias of 2-3 degrees is acceptable for this test.

The lag test is used on a daily basis to verify the sensor assembly and lags and to track the potential presence of a heading bias. The lag test results are operator-dependent due to the handheld survey mode.

2.1.3 Spin test

Accurate positioning is critical for anomaly mapping and data inversions. As such, the AHRS sensor plays a key role for the MPV because the positioning rover (GPS antenna or RTS prism) are not co-located with the center of the MPV sensor head. The AHRS must provide accurate measurements and be able to track the MPV sensor head motion through straight lines (verified with the lag test) and rotation around obstacles. The spin test is operated by placing the MPV sensor head flat, on the ground and performing a 360-degree rotation in the horizontal plane, walking around the sensor head and keeping the sensor head exactly in the same location while holding the MPV boom near its end, where the rover is mounted. The round MPV sensor head may be simply secured with tent pegs in the ground, or be placed on top of a spin board that holds the sensor head in place. A successful spin test is shown in Figure 8.

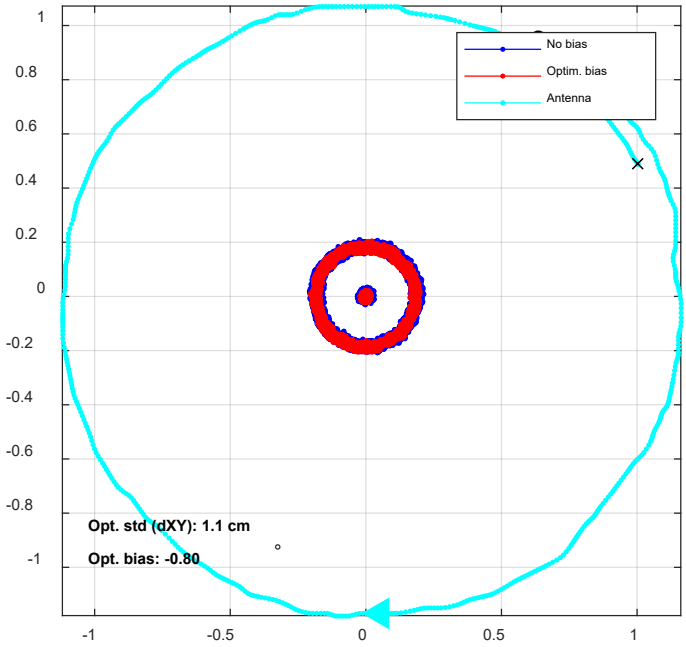

Figure 8. Illustration of the MPV Spin Test.

The MPV is rotated around the center of the head in the horizontal plane. The cyan lines show the path of the RTS prism. The blue and red lines show the paths of the Rx cubes on the MPV head, including the center cube that should remain stationary. The blue lines are based on the raw AHRS data, whereas the red lines are the result of a calculation to find the bias in the AHRS heading that minimizes the motion of the central cube. The lines overlap when the AHRS heading perfectly tracts the rotation. The test shown here indicates that the AHRS unit is well integrated and presents a negligible bias (-0.8 degrees relative to the bias that minimizes motion of the center cube).

The spin test verifies that the predicted sensor head location is independent of the AHRS orientation. It is evaluated by measuring the predicted range of motion of the MPV center cube, which would be at best in the order of 2-3 cm, when taking into account the accuracy of the positioning technologies and the MPV geometry (distance between MPV center and rover mount). The test is used to verify the correct integration and operation of the positioning technologies. It verifies that the rover and the AHRS are turned on, that the effective sensor geometry matches the expected one, the time lag between the GPS (or RTS) and the AHRS clocks, a bias in the AHRS angles (in particular the heading), and the AHRS settings for tracking motion (internal filter/dampening parameters). These can be further characterized by performing the rotation at different speeds and in opposite directions.

The time lag between the GPS/RTS and the AHRS are resolved at the data processing stage. The lag value can be estimated by the lag test described in the previous section. The lag value is needed to interpret the spin test, since a lag would shift the GPS position used with the AHRS angles and lead to an incorrect prediction of the MPV location; the spin test can therefore test that lag. The spin test can also reveal a geometry issue or a heading bias.

The spin tests in Figure 9 illustrates cases where the RTS coordinates were supplied in state-plane feet instead of UTM meters, including a case where the AHRS was also turned off. The tests in Figure 10 illustrate two cases of a heading bias: on the right the magnetic declination was incorrectly specified in the AHRS or in the acquisition system; the left case shows a small bias that could be due to a misalignment when mounting the AHRS on the MPV handle, or a minor lag due to the clock or to the AHRS processing filter, or some temporal drift.

Motion of the center of the MPV head can be interpreted as a heading bias, a lag between the AHRS and the GPS/RTS, and/or a change in the geometry. The magnitude of these effects can be inferred through an optimization problem to identify the value of the parameters that minimizes the motion of the center cube. The minimum motion range and the corresponding optimal heading bias are reported in the figures below and tracked through a day of data collection by collecting spin tests every couple of hours. The AHRS is deemed to operate correctly if the motion range and the variability of the optimal bias remain below some small value. That calculation and monitoring capability is available to the field operator through the BTG Infield App, and it is formally checked in the office with UXOLab, which offers additional tools for troubleshooting and display.

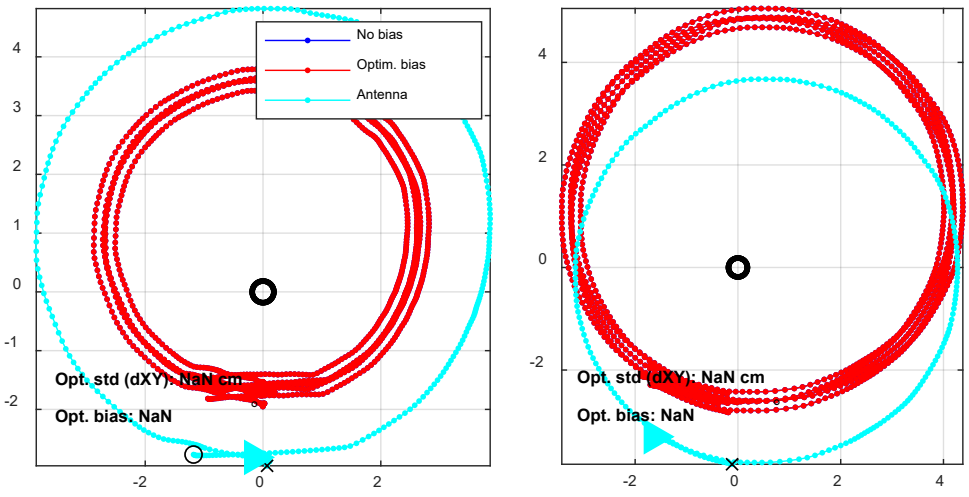

Figure 9 Failed Spin Tests.

The tests fail because the RTS coordinates were provided in state-plane coordinates instead of UTM, causing the diameter of the RTS path to appear to be three times as large. The left panel also fails because the AHRS is not streaming data: the AHRS heading is treated as 0, pointing to the North, the red and cyan circles are offset in the North-South direction by the RTS-mount offset.

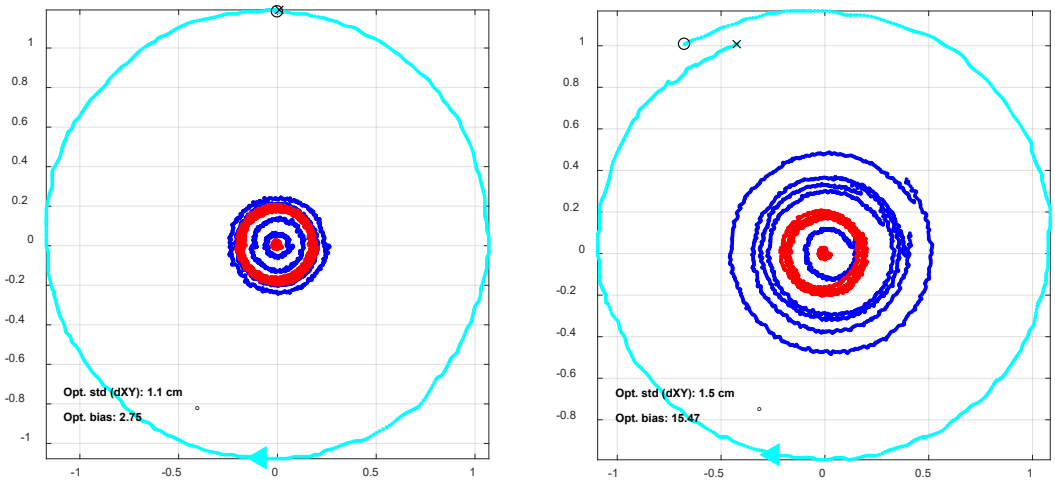

Figure 10. Illustration of Spin Tests with an Azimuth Bias.

The left panel has a small bias that is visible in the dark blue paths that differ from the optimum red paths, for which the receivers track a perfect circle through the rotation. The bias is deemed to be acceptable and corrected when processing dynamic and cued data (value of 2.75 degrees indicated in the graph). The right panel shows a spin test with a severe bias of 15 degrees that could suggest a magnetic declination error or some serious issues with the AHRS unit.

2.2 ADDITIONAL TOOLS FOR ANALYSIS OF AGC DATA

In this section, we list several tools/utilities that were developed under ESTCP 1421 for analysis of AGC data.

Image-based target picking utility added to GridZilla

GridZilla is a UXOLab tool for visualizing dynamic data. We added an image-based target picking utility, which has subsequently been used in several projects as either the primary method for generating target picks, or as a secondary method for checking the target picking results produced by UXOLab's standard line-based target picking utility.

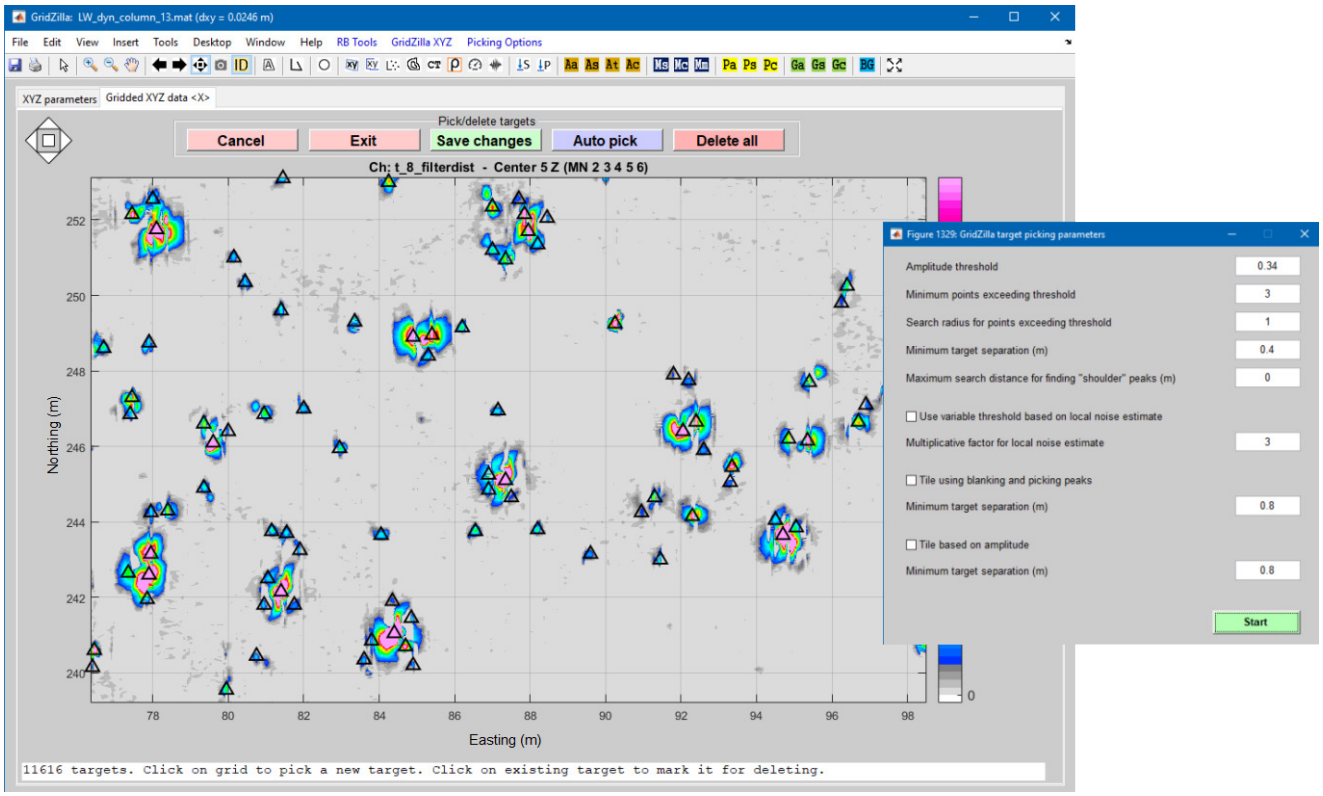

Figure 11. GridZilla in Target Picking Mode Showing Gridded Dynamic Classic MetalMapper Data and the Target Picking Parameter Menu.

Target density map tool

We added a tool to GridZilla for displaying contours of target density (targets per acre). Useful for reporting purposes.

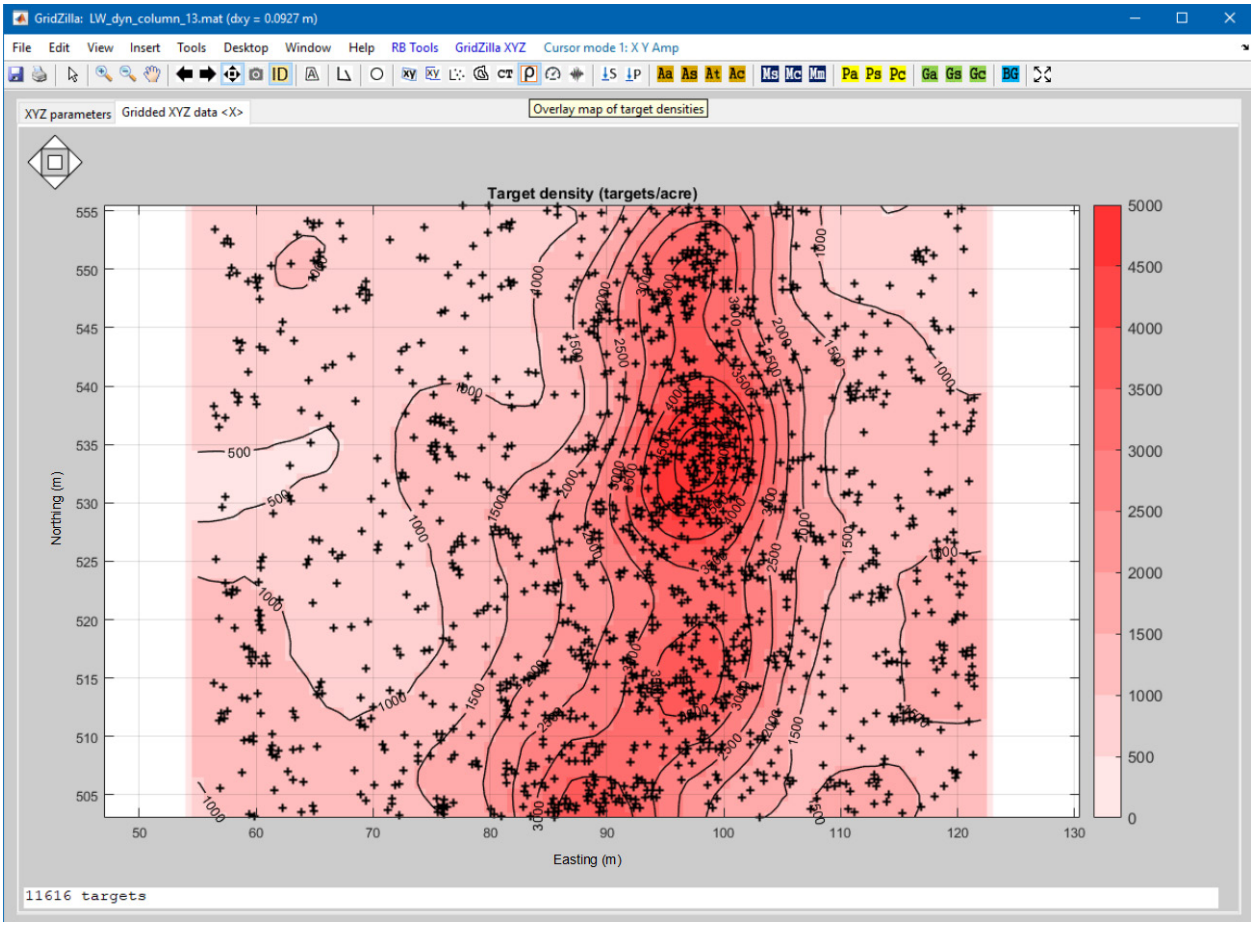

Figure 12. GridZilla Showing an Example Contour Map of Target Density (targets/acre).

Audit tracking for QCZilla QC decisions

QCZilla is UXOLab's primary tool for visualizing the inversion results of cued and dynamic data. It is used routinely for QC of all data types. We added an audit tracking utility that records all QC decisions, such as passing or failing a model or inversion, adding/deleting comments, and setting various flags (e.g., UXO, training, "don't dig"). The utility also records which data cells, specific models, and polarizabilities have been visited. The user ID and computer name is recorded for each entry in the audit tracking log for each data cell.

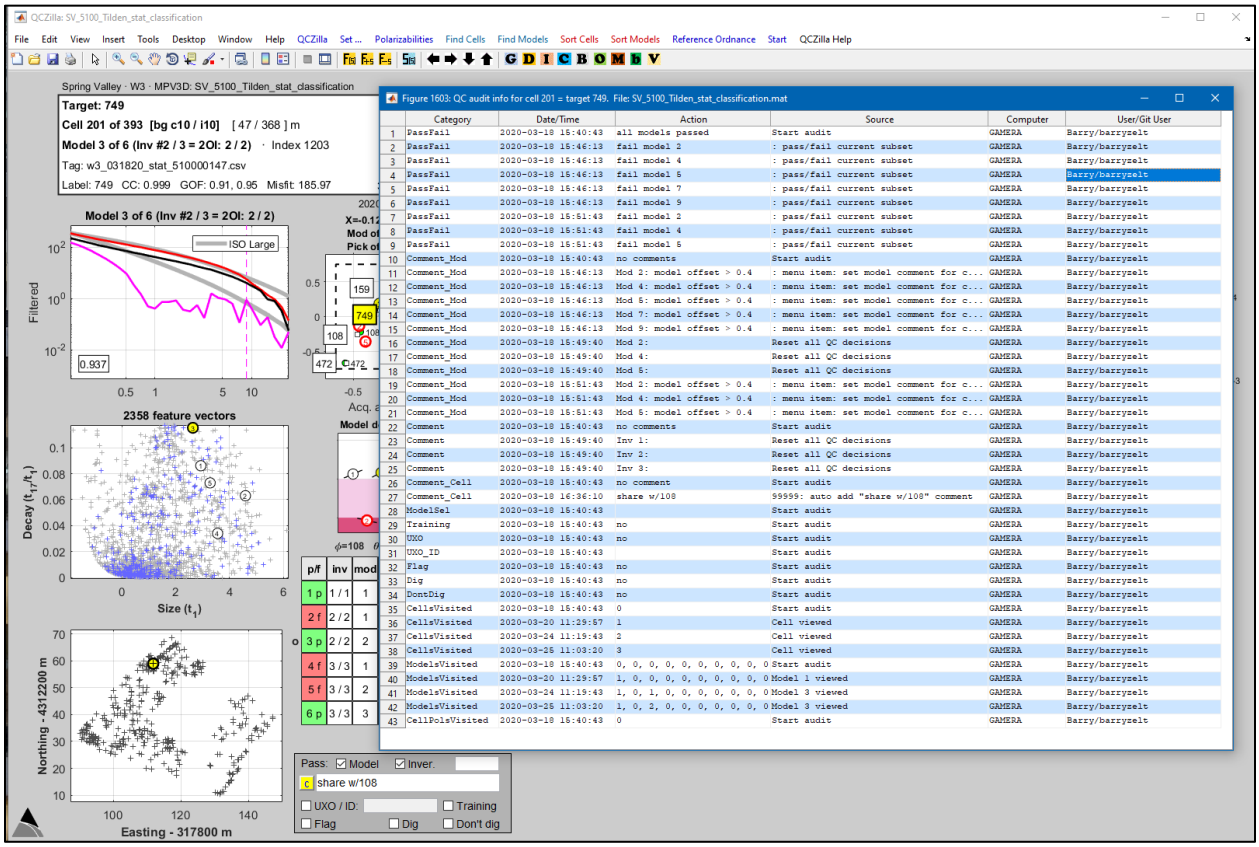

Figure 13. Background: QCZilla Window.

Foreground: QC audit info for the cell of data currently viewed in QCZilla.

New cluster analysis tool

We developed a new simplified cluster analysis tool ("General Cluster") that works with the dataset currently loaded in QCZilla. The three main tabs of the tool comprise: (1) GUI for specifying clustering parameters; (2) display of found clusters showing, for each cluster, the polarizabilities and either the median polarizabilities of the cluster or the best fitting reference polarizabilities; and (3) close up view of cluster polarizabilities. From General Cluster it is easy to view data/inversion results of the members of a cluster in QCZilla. Each cluster can be assigned a name and reports can be generated.

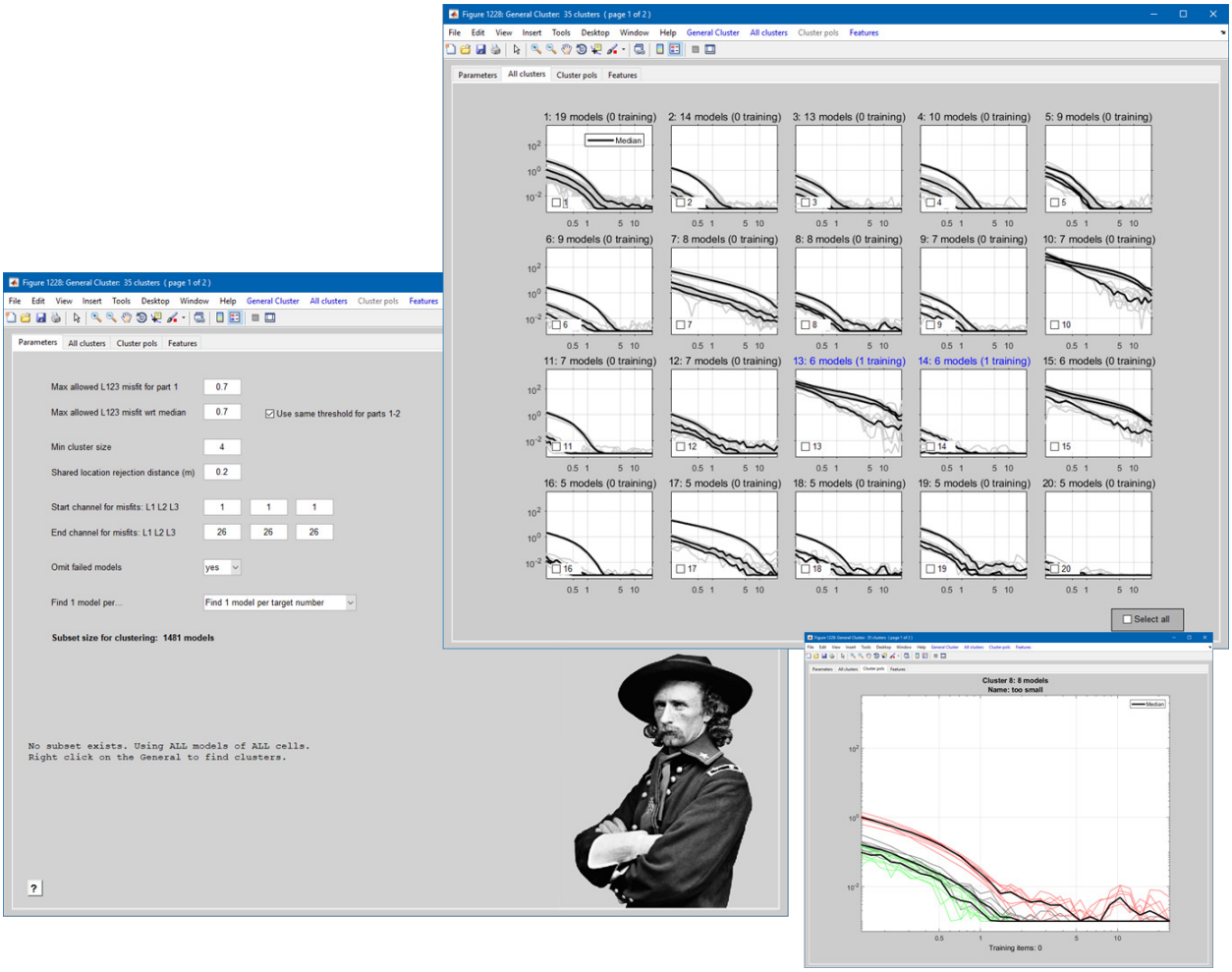

Figure 14. General Cluster Cluster Analysis Tool.

Left: GUI for specifying clustering parameters. Top right: set of found clusters. Each panel shows polarizabilities for each member of the cluster (grey lines) and median set of polarizabilities (black lines). Optionally, the best fitting reference ordnance polarizabilities can be overlain. Bottom right: tab for displaying close-up view of selected cluster polarizabilities.

Added non-ordnance option for DigZilla

DigZilla is the UXOLab utility for classification, i.e., creation of a dig list based on library matching to a set of reference polarizabilities (e.g., DoD library measurements). In some cases, a site may contain cultural or other types of items that are known non-TOI, e.g., horseshoes or spikes etc. If polarizabilities for these items exist they can be included in a "non-ordnance" reference file. We added functionality to DigZilla to allow matching against non-ordnance items. Targets found to have a good match to a non-ordnance item (in both absolute terms and relative to the best match with a library reference ordnance item), are automatically moved to the end of the dig list.

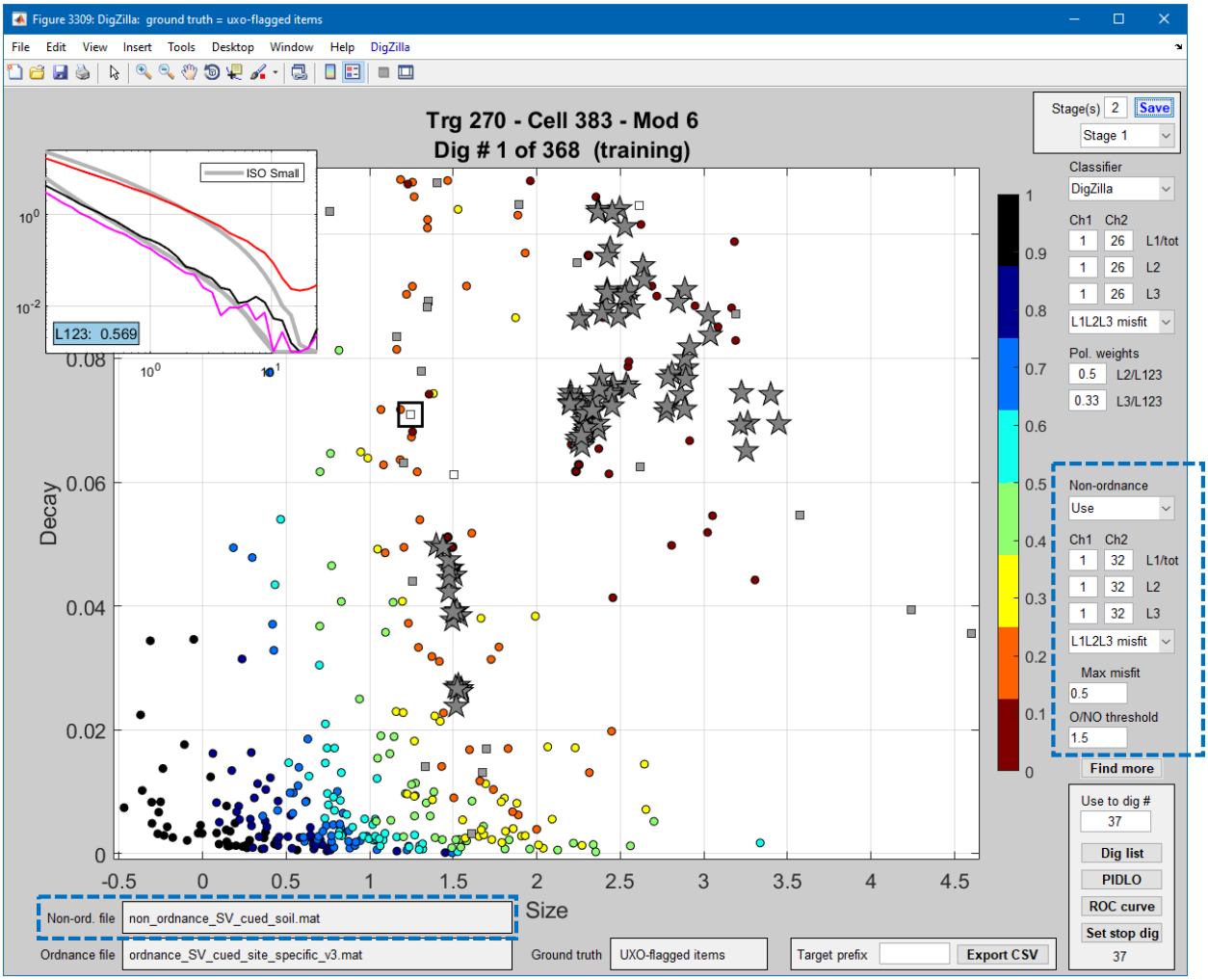

Figure 15. DigZilla Tool for Classification.

Blue boxes indicate elements added for specifying parameters associated with (optional) use of a non-ordnance file for finding items that match known non-TOI items (e.g., cultural features like horseshoes, etc.)

5-point background validation using synthetic seeding/modeling

The standard method specified in the AGC-QAPP for validating new background locations is through a set of five measurements (center measurement plus four measurements offset in each of the cardinal directions), synthetically seeding a target at a specified depth/orientation at each offset location, using the center measurement as a background, modeling the responses and comparing against a specified MQO the modeled polarizabilities with respect to those of the seed target.

The CSV background tool is UXOLab's standard tool for visualizing background response data directly from raw CSV (or H5) files. We added a background validation tool initially for MPV cued data (but subsequently extended it to work with MM2x2 and classic MetalMapper cued data).

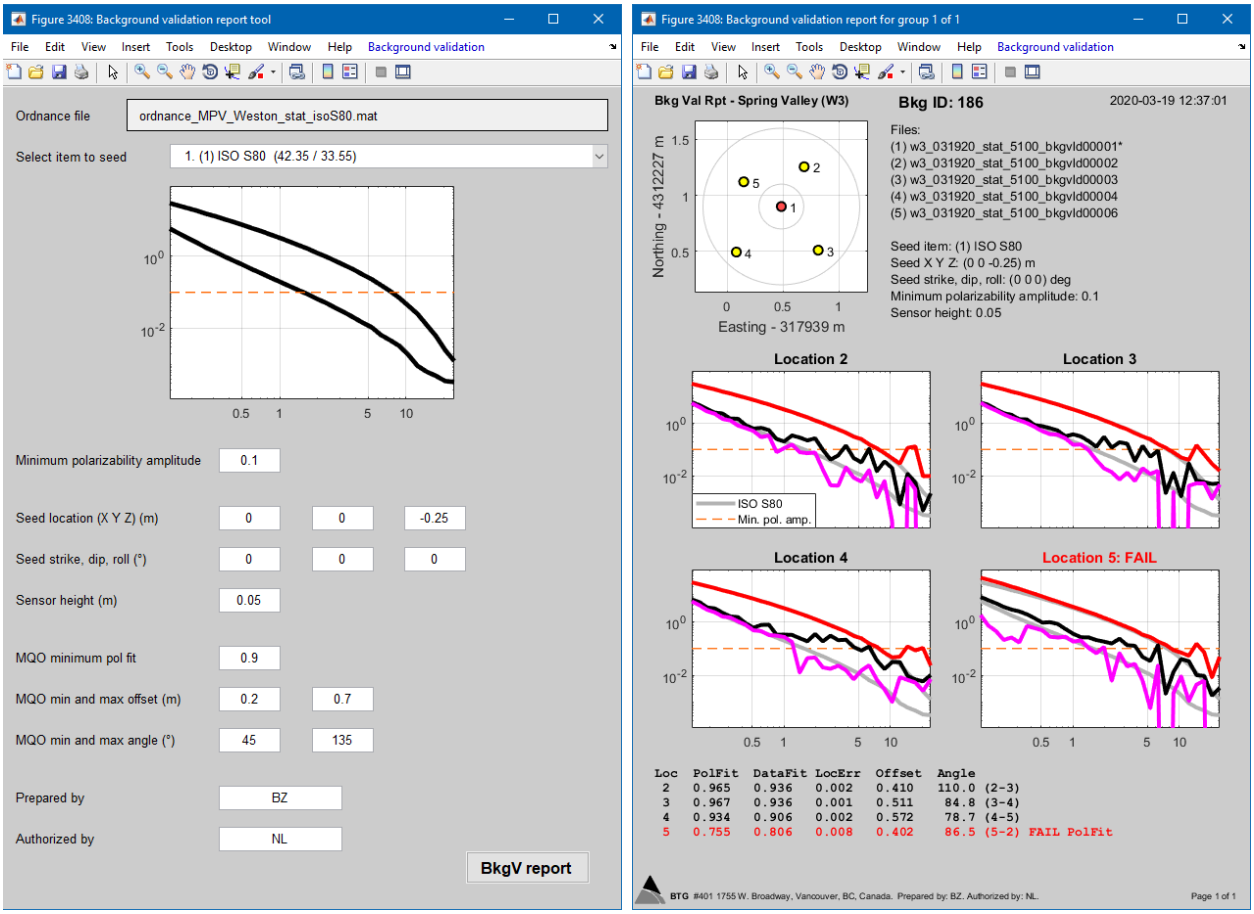

Figure 16. Left: GUI for Specifying Modeling Parameters for Validation of a Background Using a Standard Set of Five Measurements. Right: Five-point Background Validation Report.

In this example one of the offset locations (location 5) fails the polarizability fit MQO.

2-point background validation using synthetic seeding/modeling

We extended the background validation utility to work for validation of ongoing background measurements. For this test the ongoing background measurement is seeded with a specified target and the original 5-point validation center measurement is used as the background. The modeled polarizabilities are compared against a specified MQO.

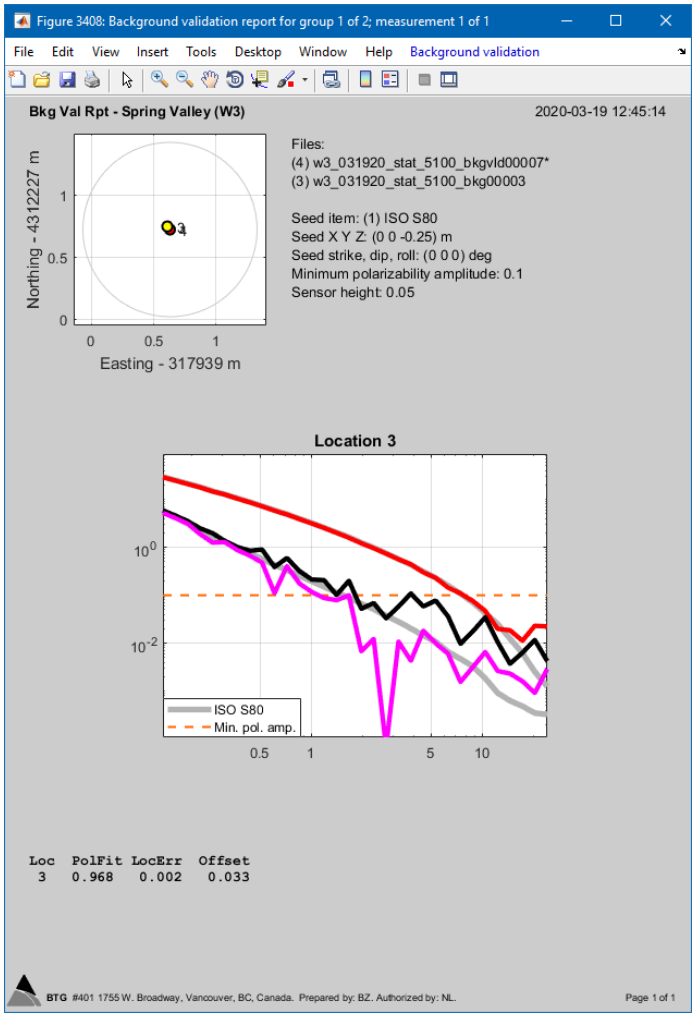

Figure 17. Sample Two-point Background Validation Report.

In this example the ongoing measurement is validated because the polarizability fit MQO and position offset MQO are satisfied.

Utility for converting DoD H5 files to QCZilla-format ordnance file

We developed a tool for converting the DoD library H5 files into a format usable by QCZilla. The tool allows specifying the scale factor to apply and for converting to multiple formats at once.

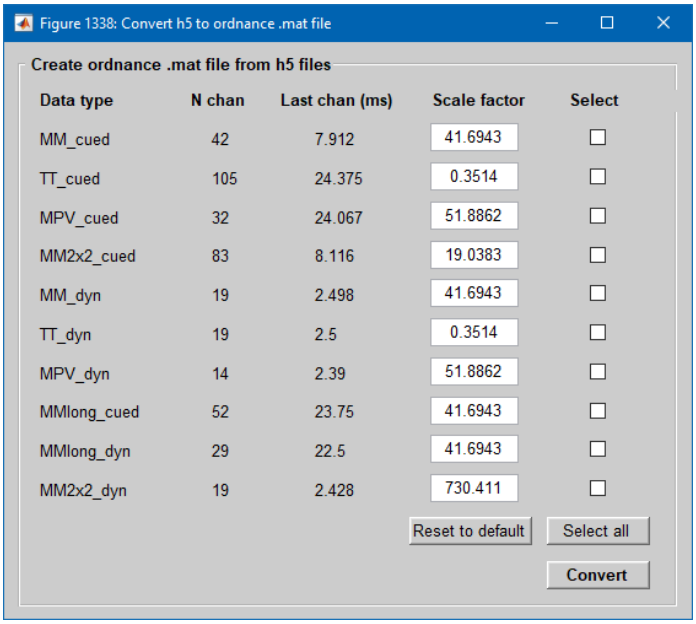

Figure 18. Utility for Converting DoD H5 Library Files to QCZilla Ordnance File Format.

Simple auto QC utility

To increase QC efficiency, we added a simple auto QC utility to QCZilla. The utility can be used to automatically (1) fail all models beyond a specified offset; (2) fail models of inversions with a data fit below a specified value; (3) fail cells of cued data with low GPS quality; (4) fail cells of data with low minimum transmitter current; (5) fail cells of cued data for which the background was not acquired within a specified time limit; (6) fail garbage models (models with non-physical polarizabilities); (7) flag potentially empty cued measurements; (8) fail cells of cued data with data saturation; (8) flag potential UXO based on polarizability misfit; (9) add comments when a target's model location is at the same location and has similar polarizabilities to the model of a different target.

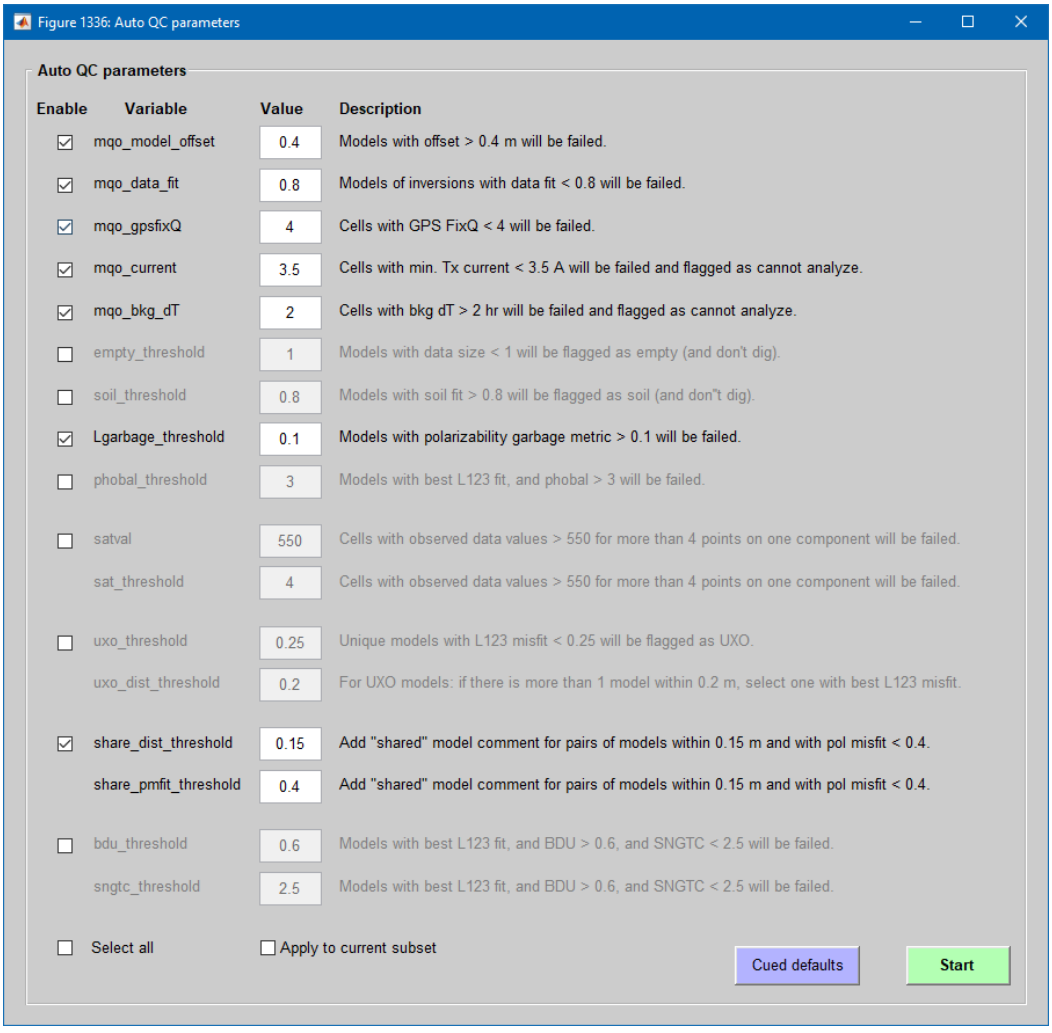

Figure 19. GUI for Setting Auto QC Parameters.

Reporting utility

We developed a reporting utility for (1) generating a standard cover page for a pdf report; (2) generating a standard classification summary page for a pdf report; and (3) overlaying various dig list categories on gridded data within GridZilla. In addition, the reporting utility merges pdf reports to create a single merged pdf report. Parameters can be saved to expedite additional reports.

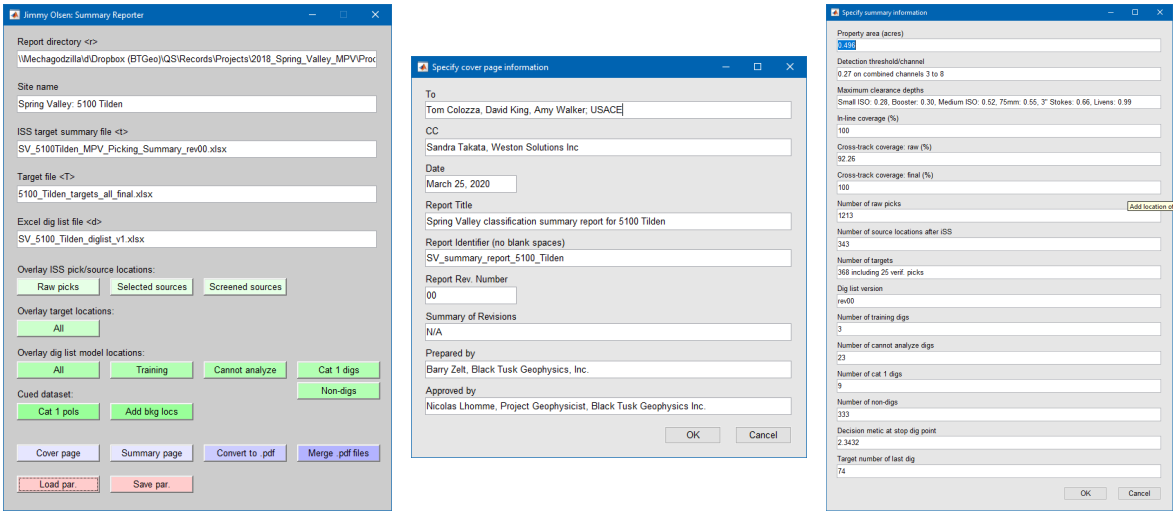

Figure 20. Left: Reporting Tool GUI. On This Screen, Various Relevant Files Are Specified. Various Categories of Targets Can Be Overlain on a GridZilla Display of Gridded Data Using Dedicated Buttons. Middle: GUI for Specifying Cover Page Information. Right: GUI for Specifying Classification Summary Information.

Most of the information on this GUI is retrieved automatically from the files specified on the main GUI.

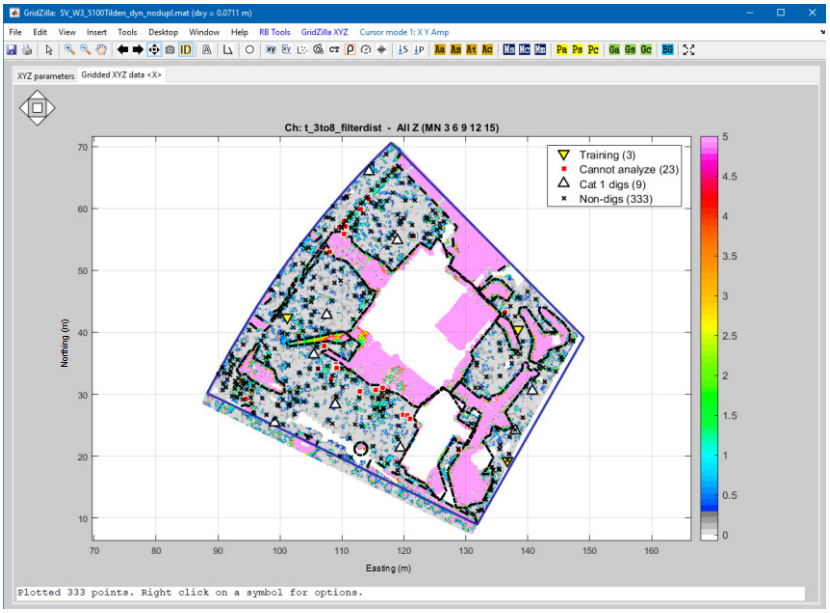

Figure 21. Example GridZilla Display Modified by the Reporting Utility to Show Target Locations Coded Based on Dig List Category.

Google map imagery utility for GridZilla

We added a utility to GridZilla for overlaying gridded dynamic data on google map imagery using the Google Static Maps API. The transparency of the overlain image and intensity of the google map imagery can be adjusted. This utility is useful for creating images for reports.

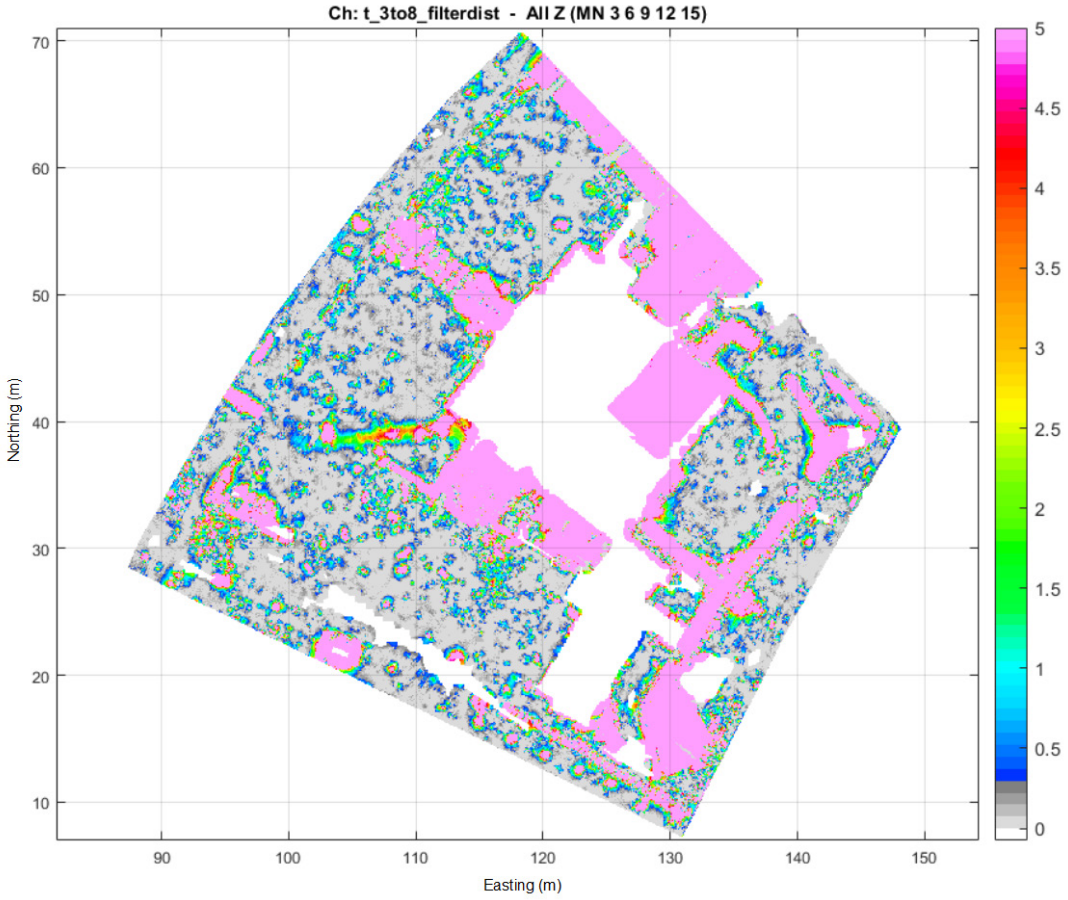

Figure 22. Example MPV Dynamic Data Viewed in GridZilla.

Figure 23. Same Dynamic MPV Data as in Previous Figure, Overlain on Google Map Imagery.

Noise map overlay for GridZilla

This utility overlays a map of estimated noise calculated as the median absolute deviation across a grid of specified size.

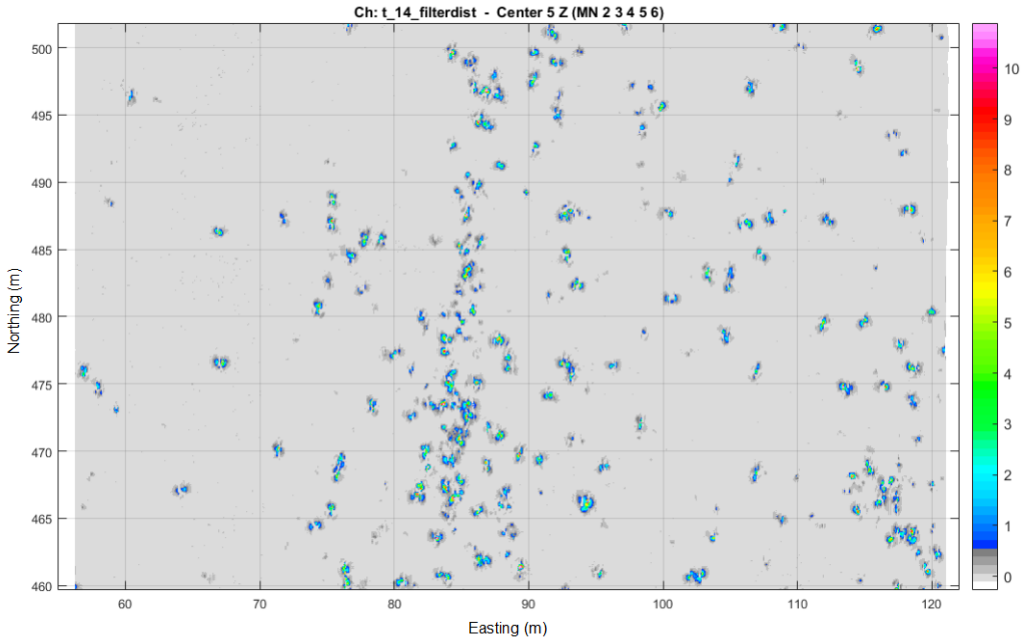

Figure 24. Classic MetalMapper Dynamic Data (Channel 14; 0.818 ms).

Picking threshold was 0.65mV/A.

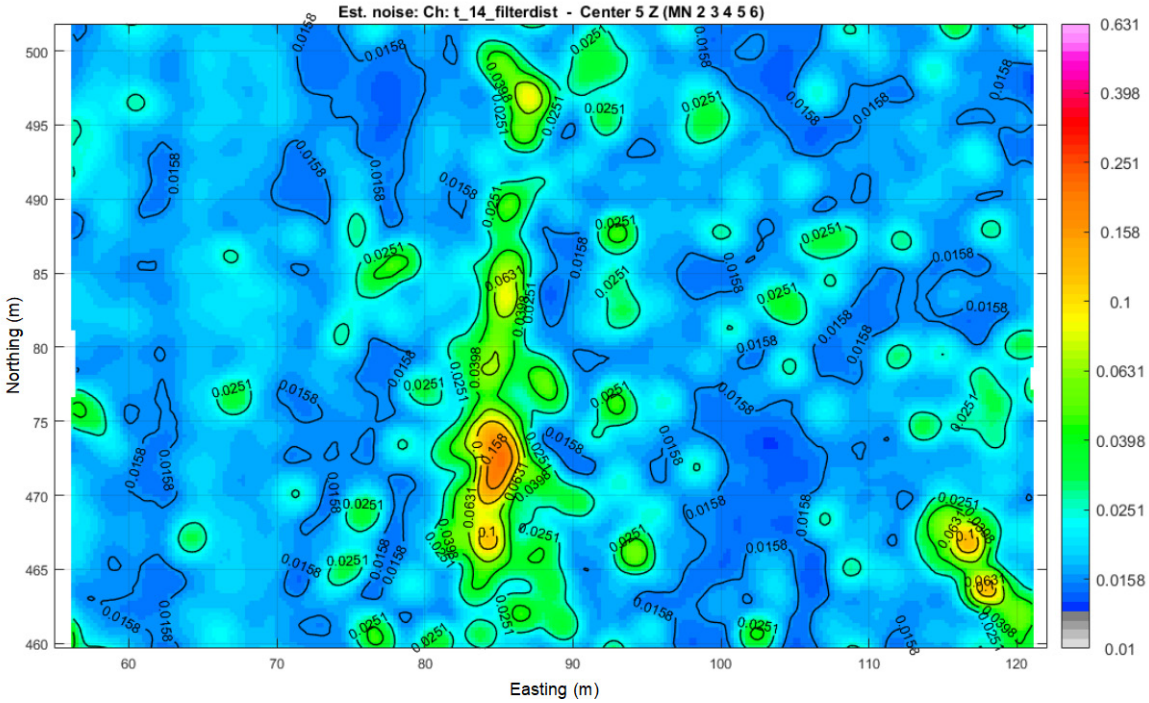

Figure 25. Corresponding Map of Estimated Noise.

Ruler/slice utility for GridZilla

This utility, known as “The Earl of Slice”, allows the user to move or change the length of a line drawn on top of the gridded data. As the line moves a 2-D plot of the data amplitude along the line is continuously updated. The length and azimuth of the line are also reported. Handles at the end of the line can be grabbed to move one end of the line, or the line itself can be grabbed and moved while it maintains its length and orientation.

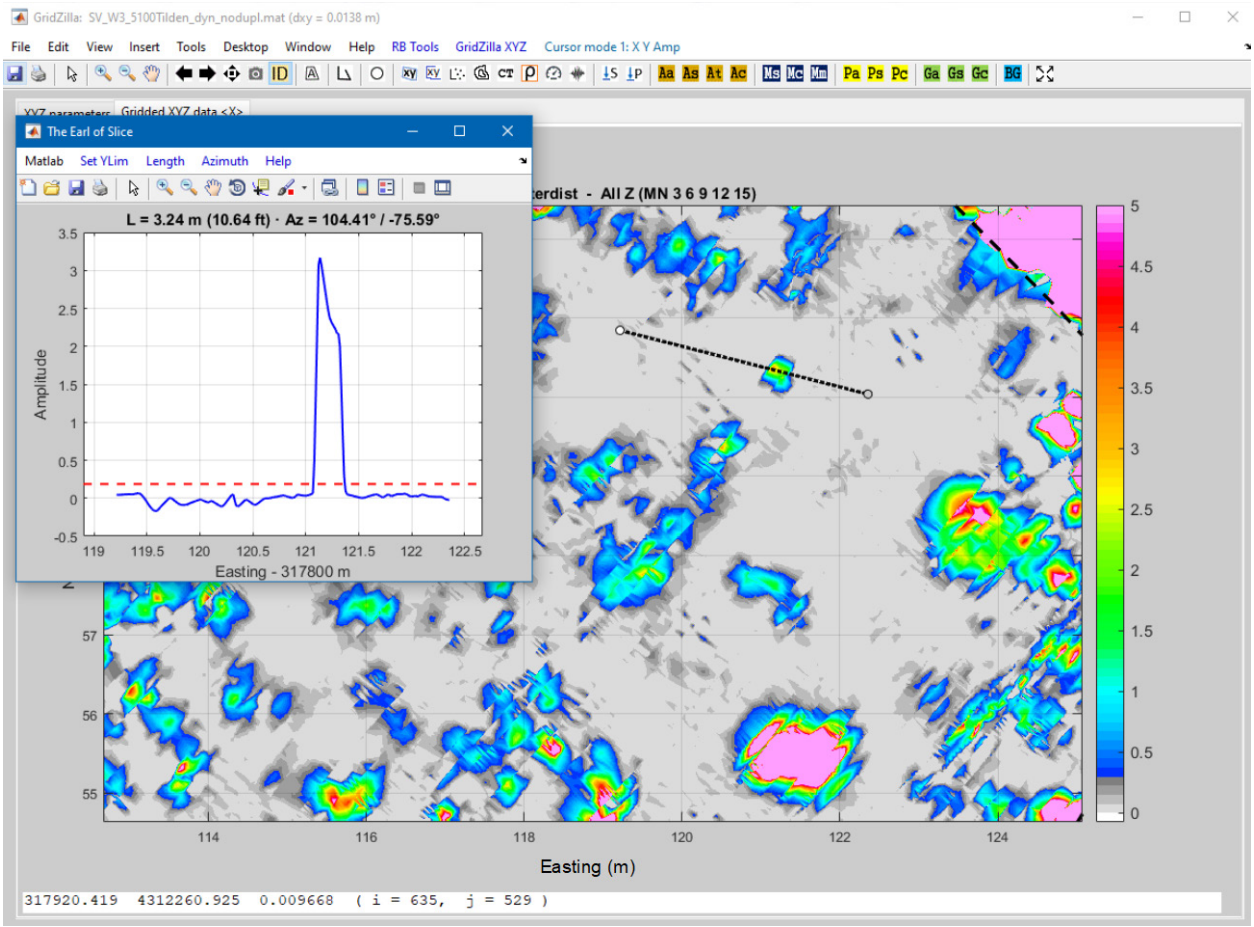

Figure 26. Example of The Earl of Slice in Action.

The inset plot shows data amplitude (blue line) along the dotted line on the GridZilla window relative to the estimated noise of the dataset (broken red line).

Spatial background tool for QCZilla

We added a spatial background tool to QCZilla. For the cued dataset loaded in QCZilla, this tool shows graphically which targets are currently using which background. The tool can be used to show which targets can or cannot use a selected background location. It can also be used to report which cells are currently assigned a background from a non-validated location, or which cells have no validated background available. Finally, backgrounds for a single data cell or subset of cells can be assigned using this utility.

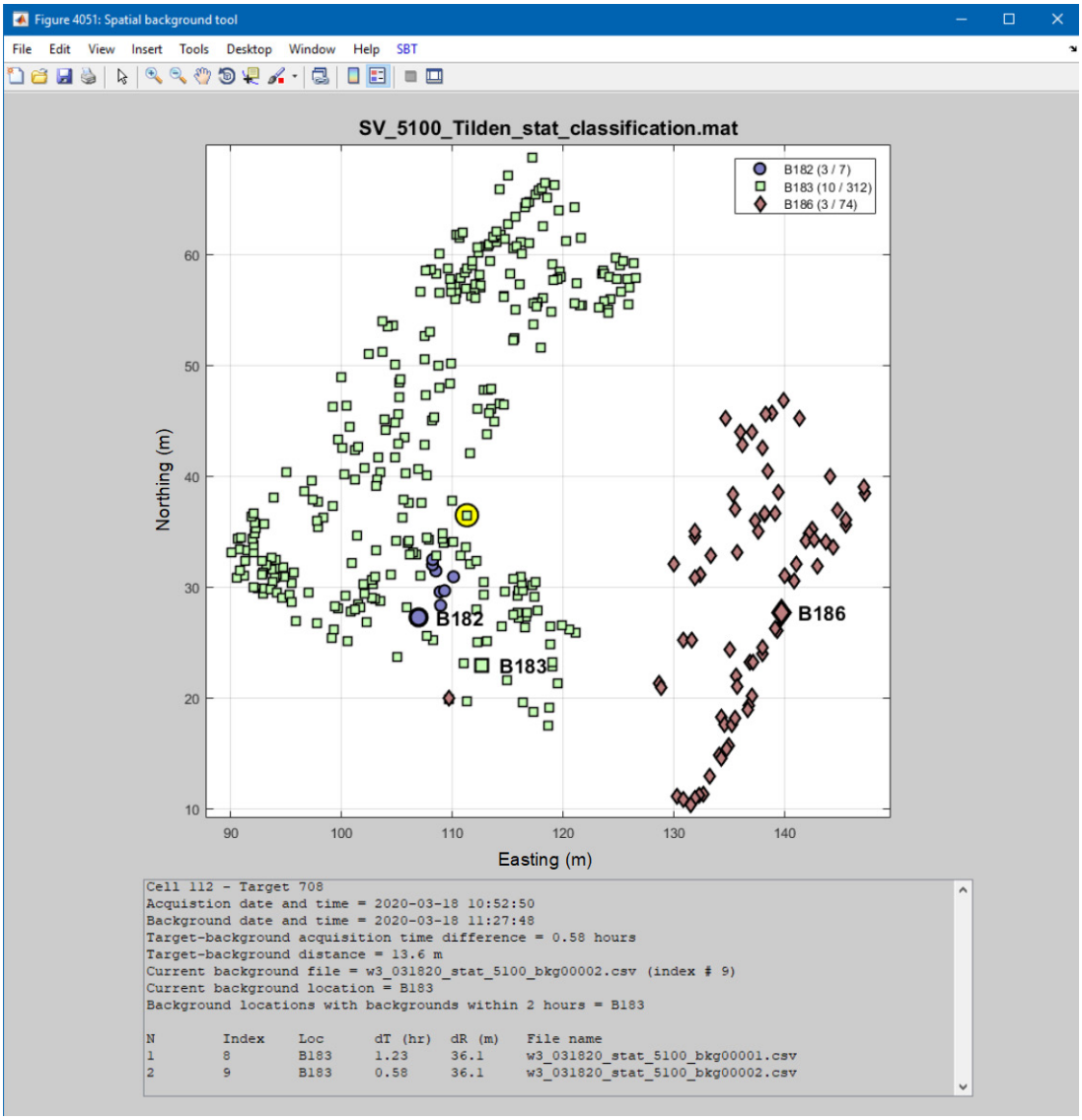

Figure 27. Spatial Background Tool Showing Background Ground Locations (Large Labeled Symbols) and Cued Measurement Locations (Small Symbols).

The symbol for the cued measurement locations indicates the background location used for background data correction. The box at the bottom shows information for a selected (yellow circle) cued measurement, including a list of validated backgrounds taken within two hours of the cued measurement.

"Contour tiling" utility for GridZilla target picker

GridZilla has a basic utility for tiling extended anomalies with target picks. For projects where the MPV would be cueing targets picked from EM61 data, additional tiling features were required. We implemented a "contour tiling" utility which can be used for anomalies of a specified size to (1) add a target at the center of an anomaly; (2) add targets on a circle at specified radius (or radii) and with specified angular offset around the center target; and (3) add additional targets on the anomaly contour (i.e., at the edge of the anomaly).

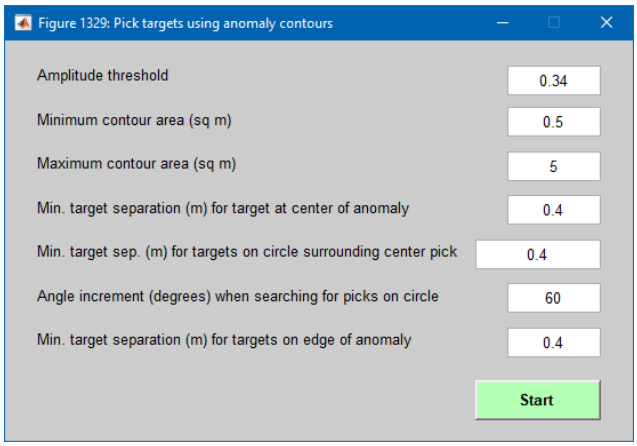

Figure 28. GUI for Specifying Contour Tiling Parameters.

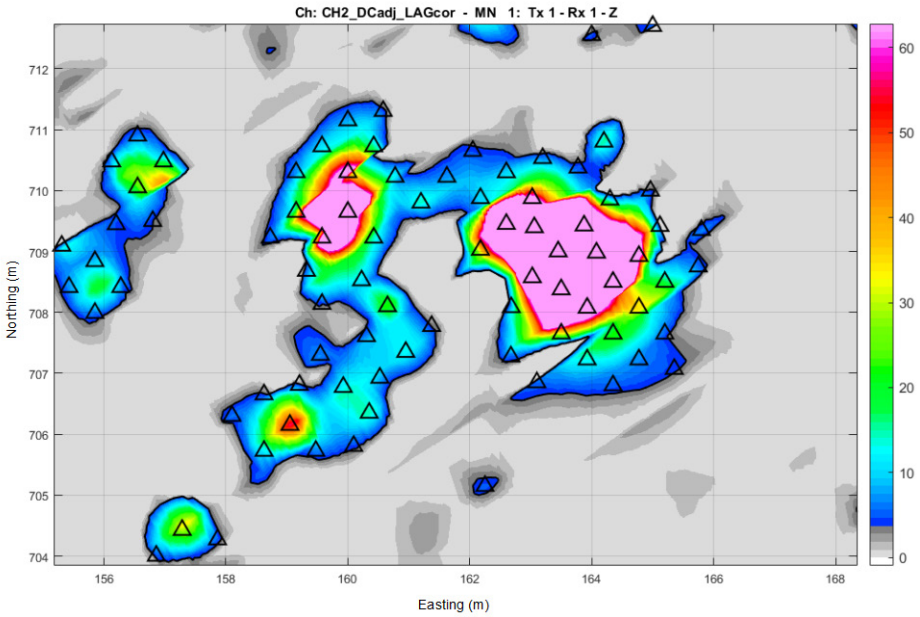

Figure 29. Example of Tiling of a Large EM61 Anomaly.

Sensor speed map overlay for GridZilla

This utility overlays a map of sensor speed in m/s. Checking sensor speed is particularly useful for MPV data where maintaining a constant speed is more difficult, and where increased speeds can lead to data quality issues.

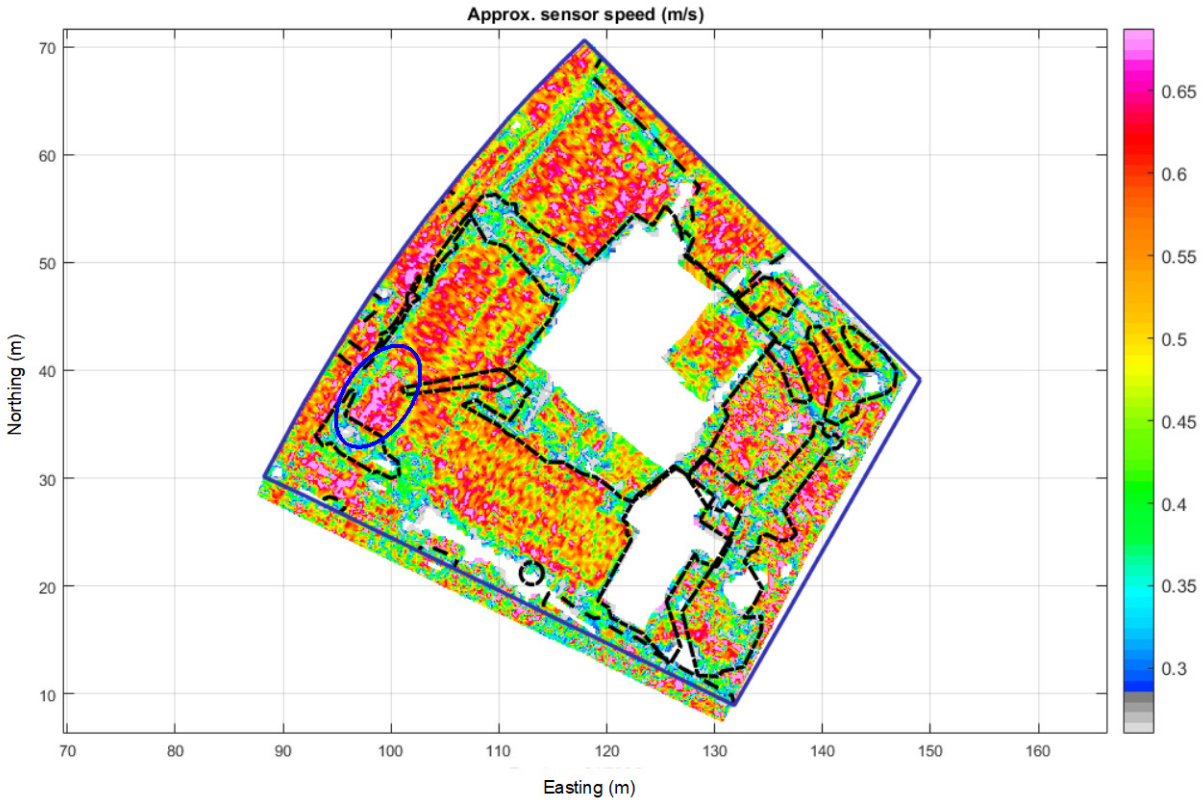

Figure 30. Example Map of MPV Sensor Speed in m/s.

A region of relatively high sensor speed is circled.

2.3 BTG IN-FIELD APP

Until the development of the software described in this report, the MPV lacked the capability to perform necessary quality control (QC) tests in the field. Instead, QC tests were performed off-site after data was collected for the day. This meant that problems with the hardware and software would not be recognized until after a full day of data collection. Ideally these QC tests should be performed in the field directly after acquiring the QC test data, thereby minimizing the risk of collecting unusable data and avoiding the need to recollect a day's worth of data.

With this motivation, BTG has developed the BTG In-Field App. Development began on 09/25/2017, and Version 1.0 was first made available 09/28/2017. The initial release contained the capability to perform the basic sensor function test, described below. Since then, the App has been extended to three separate QC tests and has been improved in for each test's capability and configurability. The objective of this report is to give an overview of the capabilities of the latest version 1.3.3, which was the result of iterative improvement of the original version 1.0.

2.3.1 Overview

In-field quality control tests enhance our ability to make quality geophysical measurements throughout the day. They are designed to test that both the equipment is functioning properly and that the acquired data will be capable of meeting the data and measurement quality objectives (DQOs, MQOs) specified in the project specific QAPP.

The QC tasks are split into three separate tests:

1. **Sensor function test**: designed to ensure the sensor response from a standard object in a consistent location is consistent with the expected/reference response.
2. **Spin test**: designed to test proper functioning and accuracy of the geolocation and attitude sensors.
3. **Background validation and verification**: designed to (1) ensure a new background location is appropriate for use as a background (in a location devoid of metal); and (2) for an ongoing background measurement, ensure that the measured response is consistent with the initial response.

2.3.2 QC tests

In the BTG In-field app, each QC test occupies a separate tab, has similar layout, and the ability to quickly scan for the most recent files for each test (Figure 31, Figure 32 and Figure 33). In addition, each test has its own options UI for configuring settings specific to that test.

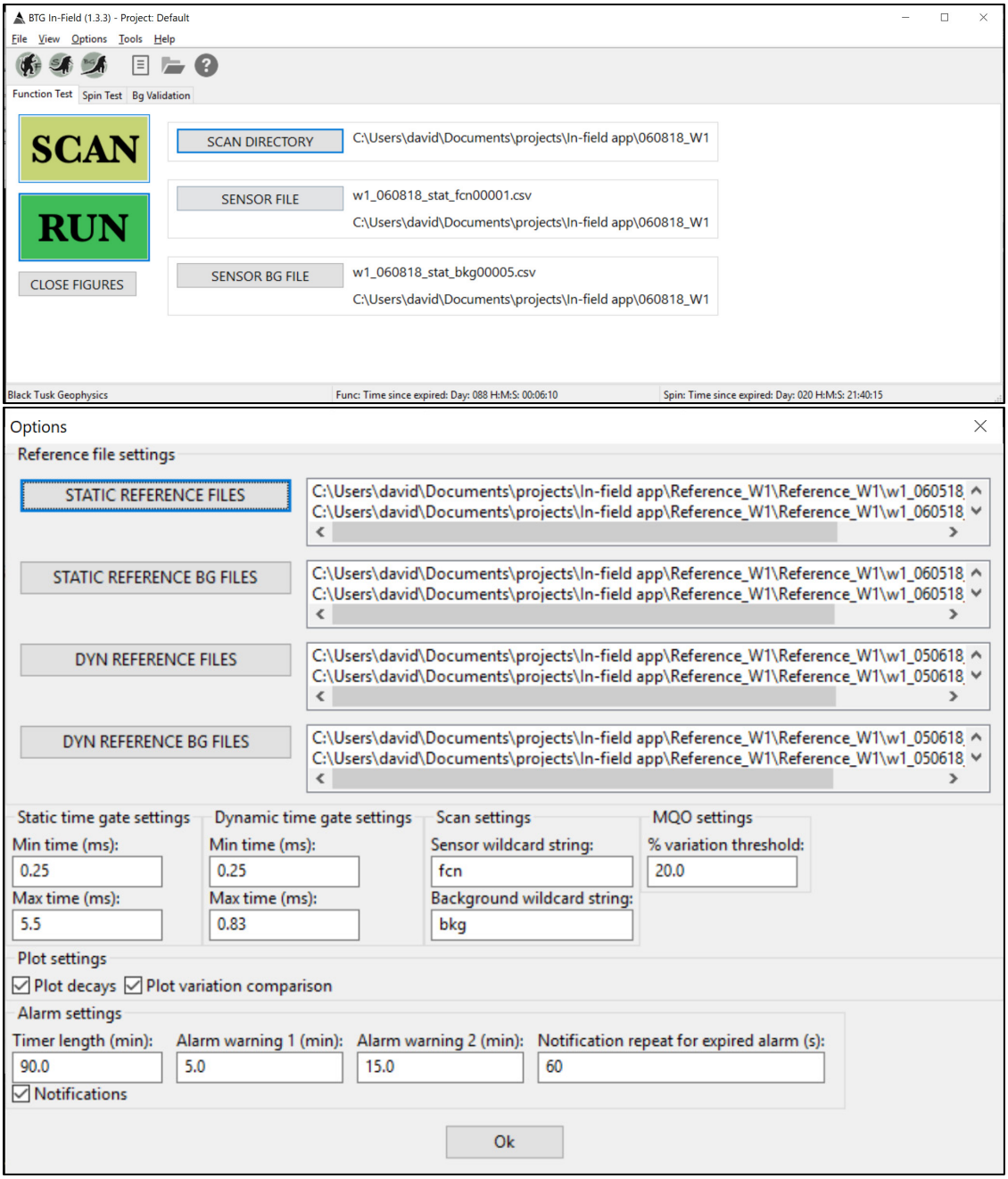

Figure 31. Main Window (Top) and UI Options for the Sensor Function Test (Bottom).

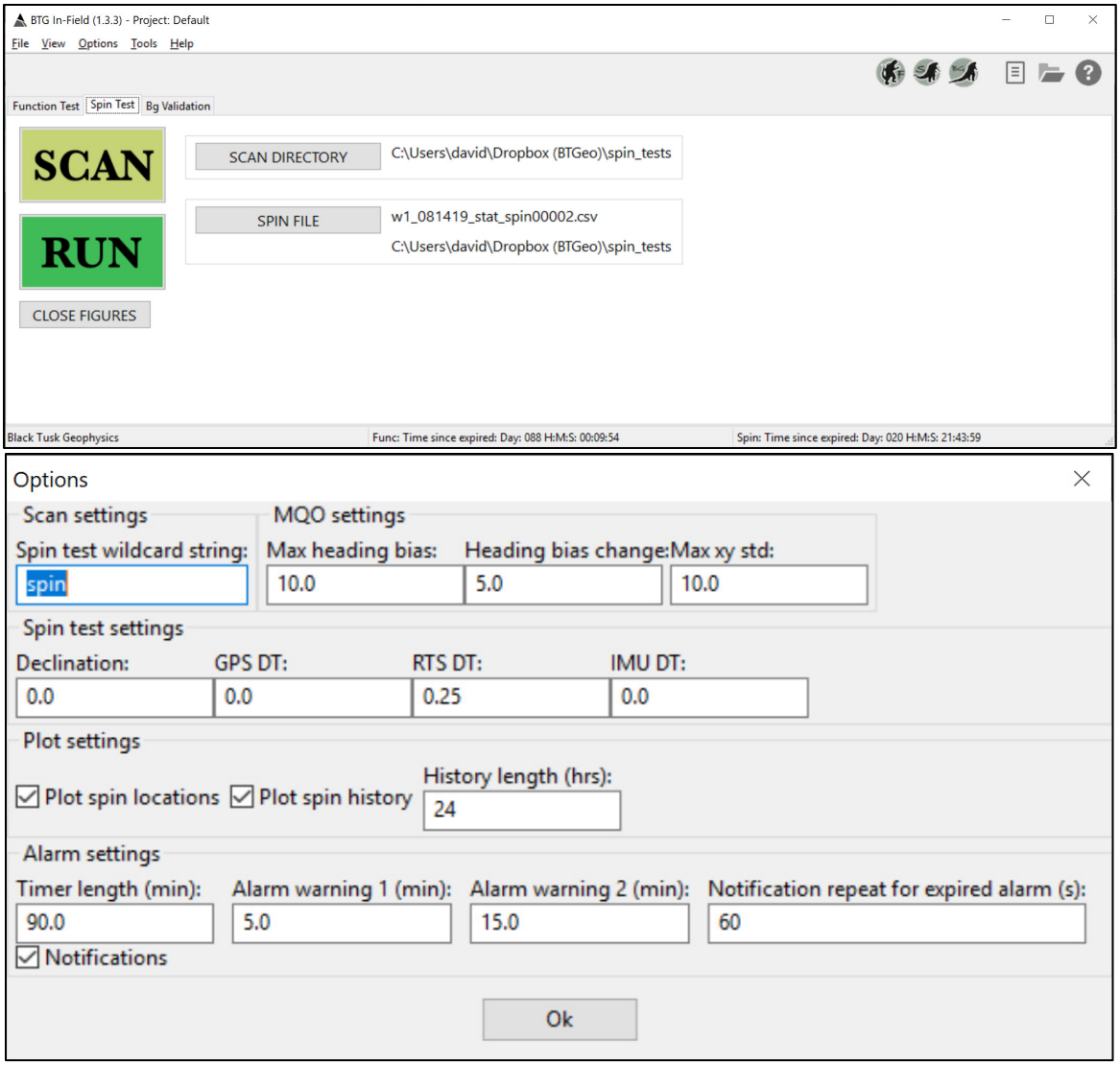

Figure 32. Main Window (Top) and UI Options for the Spin Test (Bottom).

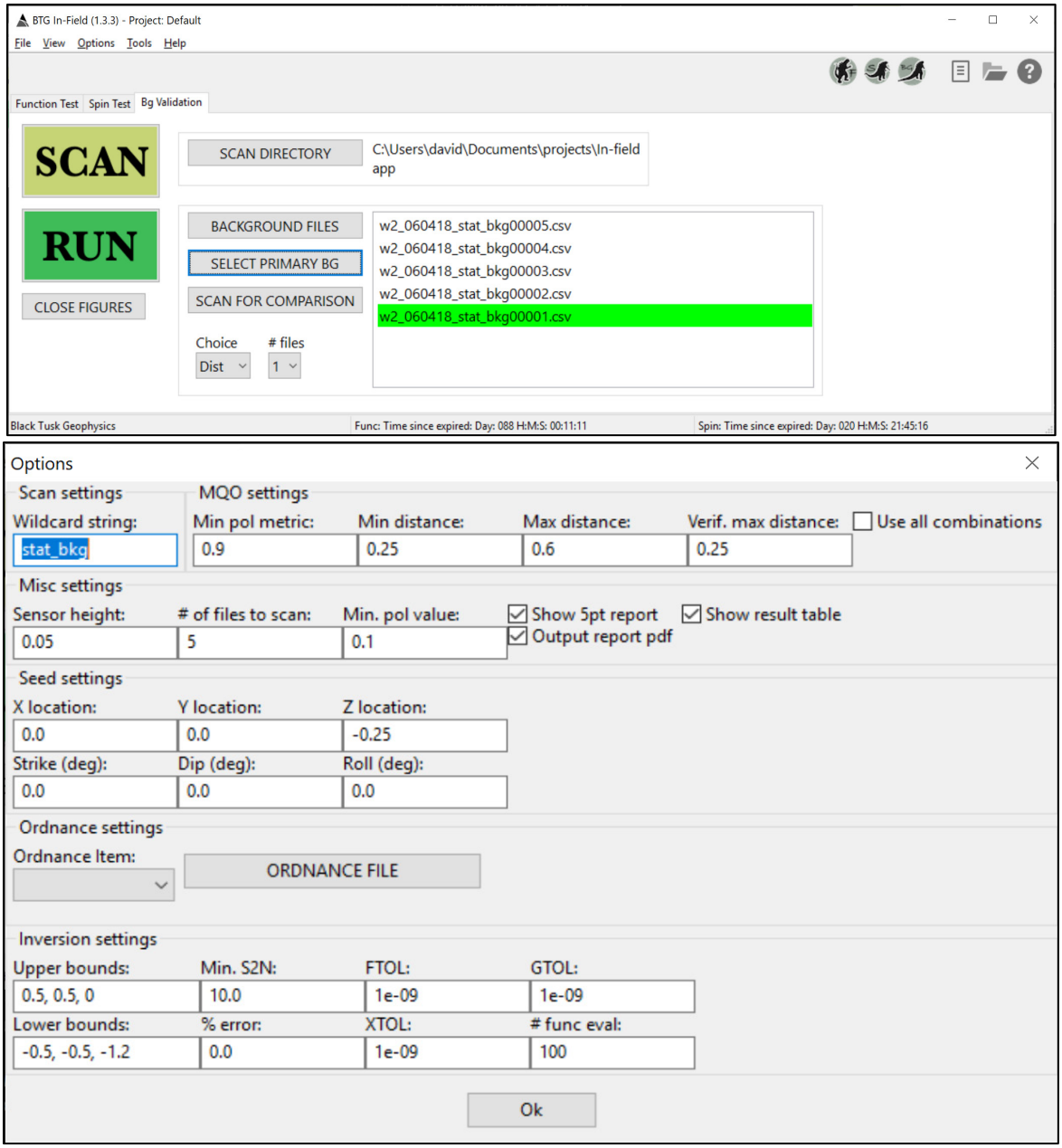

Figure 33. Main Window (Top) and UI Options for the Background Validation and Verification Test (Bottom).

2.3.3 Sensor function test

The sensor function test is used to confirm the reproducibility of the geophysical measurements. Objective validation of the EMI elements is done by taking a measurement with a known item. For the MPV an engraved 1-1/2-inch carbon steel ball bearing is placed at a specified location for both dynamic and cued function tests. Function test measurements are compared to reference values in the field.

To analyze function test data, the user presses the **SCAN** button in the main window of the app (Figure 31-top). This automatically populates boxes for specifying the directory containing the function test, the most recent function test file, and corresponding background file. The user then presses the **RUN** button (Figure 31-top) to run the function test using the specified files and options. Results of the test are logged to a log file and presented to the user with optional plots. In the options UI (Figure 31-bottom) the user can specify parameters such as the time gates to use for the test and the maximum allowed percent variation in the test. An alarm feature allows the user to receive a reminder at a specified interval that it is time to do another function test.

After pressing the **RUN** button, the user is presented with a results window with the MQO and test result values (Figure 34). The table is colored green for a successful result and red for a failed test.

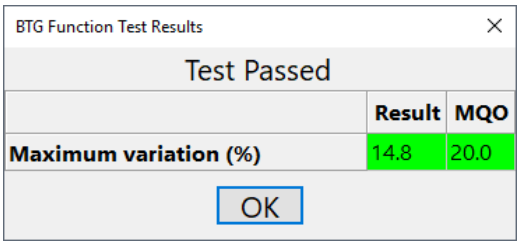

Figure 34. Function Test Results Window.

Optionally, two additional figures can be shown, which can be useful for identifying problems with specific transmitters or receivers:

1. Decay plot: Comparison of the time decays within selected time gates for both the test measurement and reference files (Figure 35).
2. Variation comparison plot: The response variation values for each receiver (Figure 36). The currently set MQO value is indicated by the change in background color: green region indicating pass, red indicating fail.

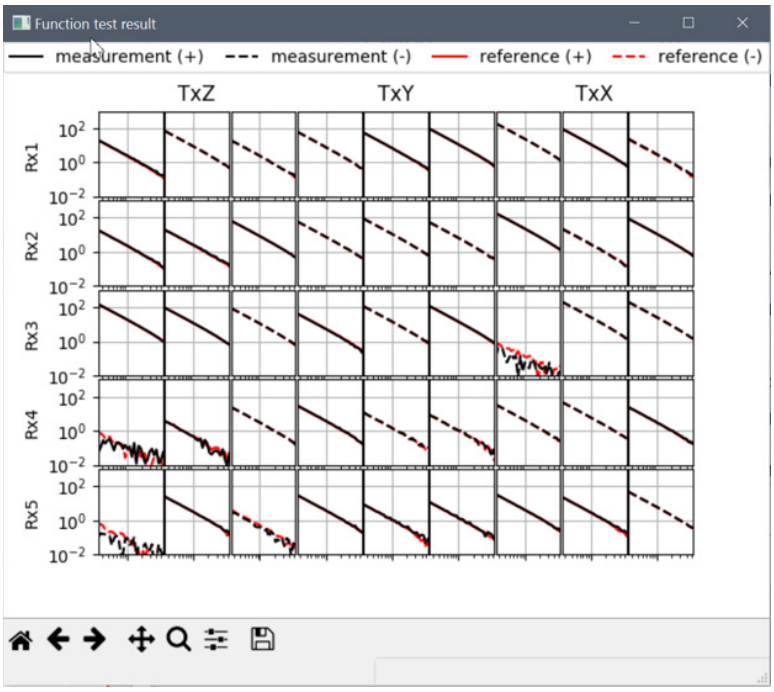

Figure 35. Function Test Decay Plot Comparing Time Decays for the Test Measurement Against the Reference Values.

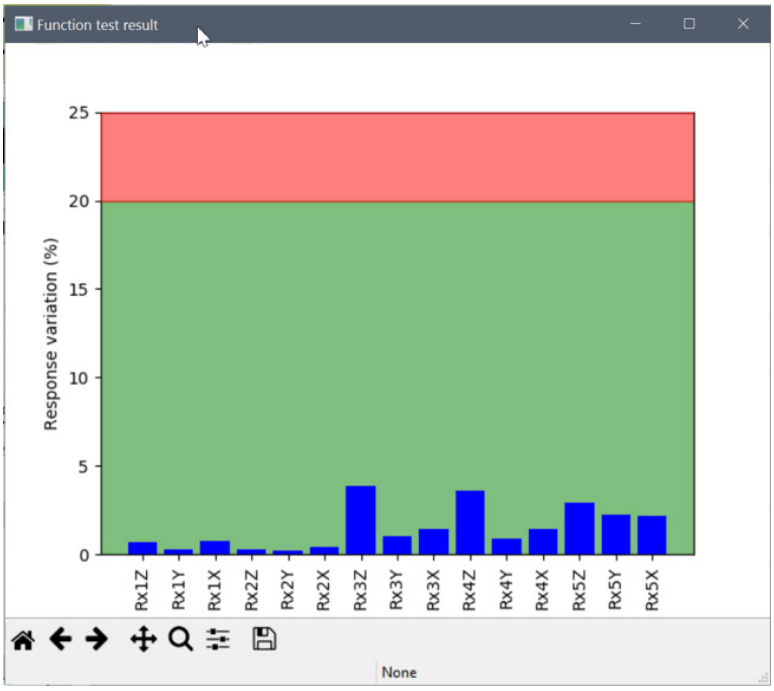

Figure 36. Function Test Variation Comparison Plot Showing the Response Variation Values for Each Receiver.

Green and red areas denote pass/fail regions.

2.3.4 Spin test

The spin test is used to confirm that the sensor's positioning system is configured correctly. Accurate identification of the sensor head's location is critical and requires correct integration of the GPS and AHRS (orientation) units with correct specification of the geometry. This aspect is critical for the MPV since the GPS antenna is more than 1 meter away from the sensor head and the AHRS information is used to translate the MPV sensor head location from the GPS position. This test verifies that the predicted MPV sensor head location is not moving when rotated around a fixed location.

To analyze spin test data, the user presses the **SCAN** button in the main window of the app (Figure 32-top). This automatically populates boxes for specifying the directory containing the spin test. The user then presses the **RUN** button (Figure 32-top) to run the spin test using the specified options. Results of the test are logged to a log file and presented to the user with optional plots. In the options UI (Figure 32-bottom) the user can specify parameters such as MQO threshold values and spin test settings such as lag values used to shift the time values on import. An alarm feature allows the user to receive a reminder at a specified interval that it is time to do another spin test.

After pressing the **RUN** button, the user is presented with a results window with the MQO and test result values (Figure 37). The table's rows will be colored green for a successful result and red for a failed result. The test requires that all results be less than the maximum MQO values.

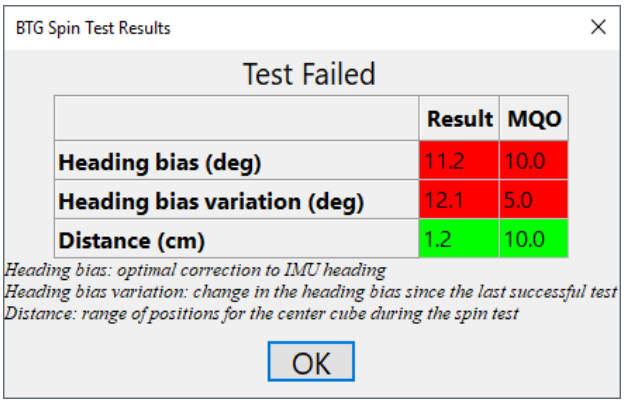

Figure 37. Function Test Results Window.

Optionally, two additional figures can be shown:

1. Location plot: shows the locations of the GPS/RTS sensor head and all receiver positions pre- and post-optimization. The optimum standard deviation of the x-y locations and the optimum bias is shown (Figure 38).
2. History plot: shows the history of successful function test results for the change in IMU bias metric (Figure 39). A failure will be indicated for only the right most point or most recent test, as failed tests are not saved.

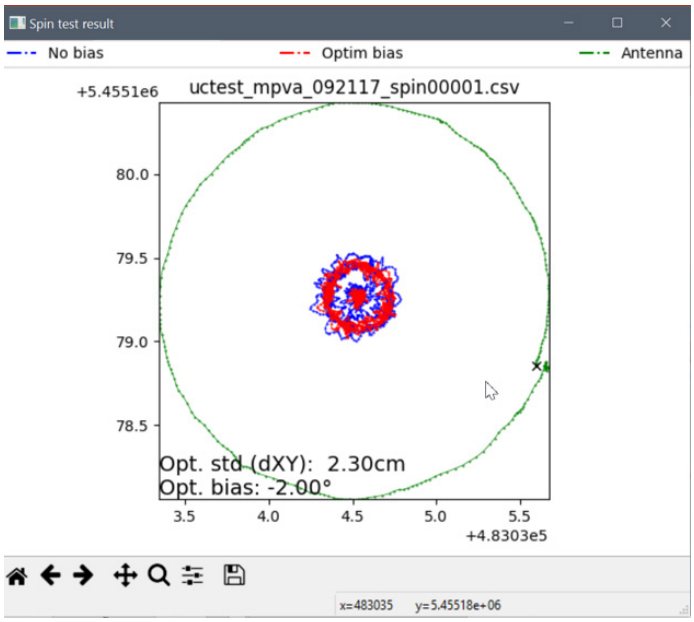

Figure 38. Spin Test Location Plot Showing the Locations of the GPS or RTS Sensor Head (Green Line) and All Receiver Positions Pre-optimization (Blue) and Post-optimization (Red).

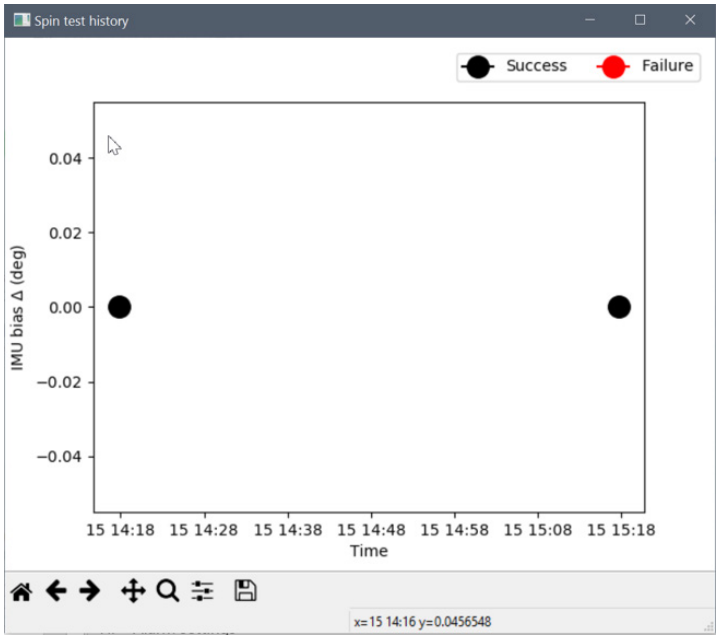

Figure 39. Spin Test History Plot Showing the History of Successful Spin Test Results for the Change in IMU Bias Metric.

A failure will be indicated for only the right most point or most recent test, as failed tests are not saved.

2.3.5 Background validation and verification

The background validation and verification tests use synthetic modeling and are designed to ensure proper background measurements are collected over the course of the day.

1. Background validation (for a new background location): a set of five cued measurements at a proposed background location are acquired, one at the proposed location, and four offset measurements, each separated by approximately 90° and offset from the center measurement by approximately half the sensor width. A seed item at a specified depth/orientation is synthetically added to each offset measurement. Each of these measurements is background corrected using the center measurement. The synthetic data are inverted, and the modeled polarizabilities for each offset measurement are compared to reference polarizabilities.
2. Background verification (for ongoing background measurements at a validated location): a single cued measurement is taken at the validated location. A seed item at a specified depth/orientation is synthetically added to the ongoing background data and synthetic data are background corrected using the original center validation measurement. The synthetic data are inverted, and the modeled polarizabilities are compared to reference polarizabilities.

To perform a background validation or verification, the user presses the **SCAN** button in the main window of the app (Figure 33-top). This automatically populates the list of background files with the five most recently acquired files. The user then presses the **RUN** button (Figure 33-top) to run the validation or verification test using the specified options. Results of the test are logged to a log file and presented to the user in the form of a plot or PDF file. In the options UI (Figure 33-bottom) the user can specify parameters such as MQO settings, seed location and orientation, ordnance file containing the polarizabilities of the seed, and inversion parameters.

After pressing the **RUN** button, the user is presented with a results window with test result values (Figure 40). The table comprises four rows, one for each offset location. The table's rows are colored green for a successful result and red for a failed result.

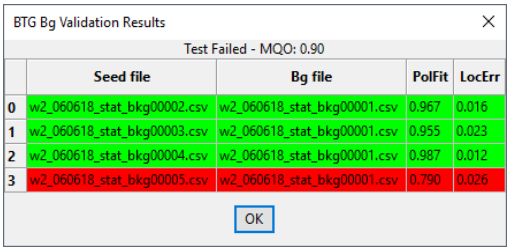

Figure 40. 5-point Background Validation Results Window.

An optional 5-point validation report can be viewed and saved as a PDF file. The report shows the modeled polarizabilities at each offset location compared against the specified reference polarizabilities, a map showing the relative location of the measurements, a table of results, and a display of the key input parameters used for the test. Examples of reports for successful and failed tests are show in Figure 41and Figure 42.

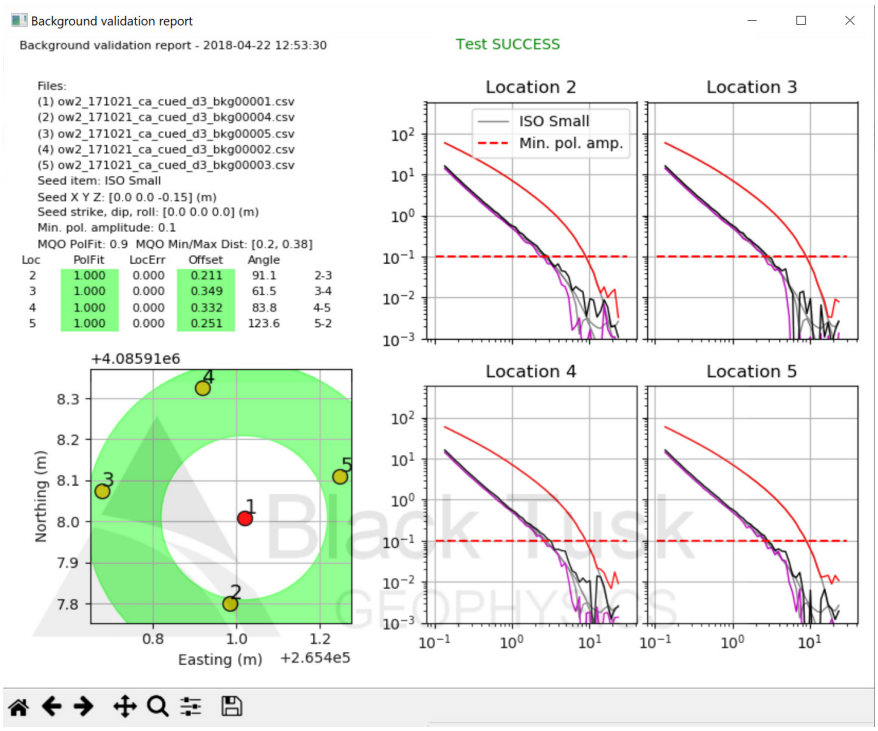

Figure 41. Example of a Successful 5-point Background Validation Report.

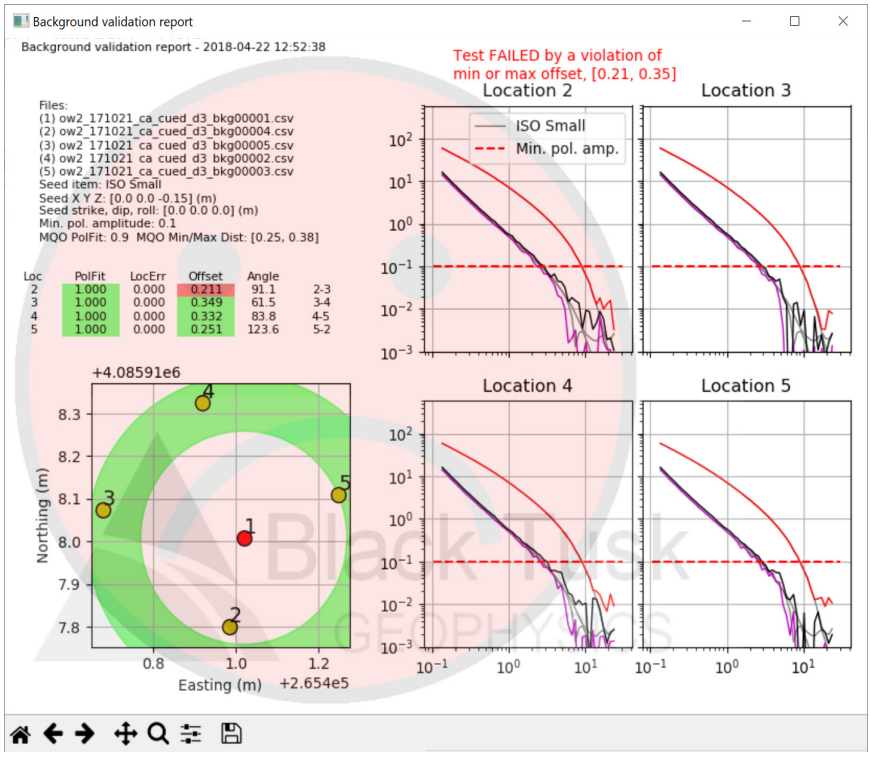

Figure 42. Example of a 5-point Background Validation Report with a Failure Due to Insufficient Offset of One of the Four Offset Measurements.

If there is no GPS or RTS information available, the test ignores MQOs for offset and angular distribution of the offset measurements. An example 5-point validation report when no positioning information is available is show in Figure 43.

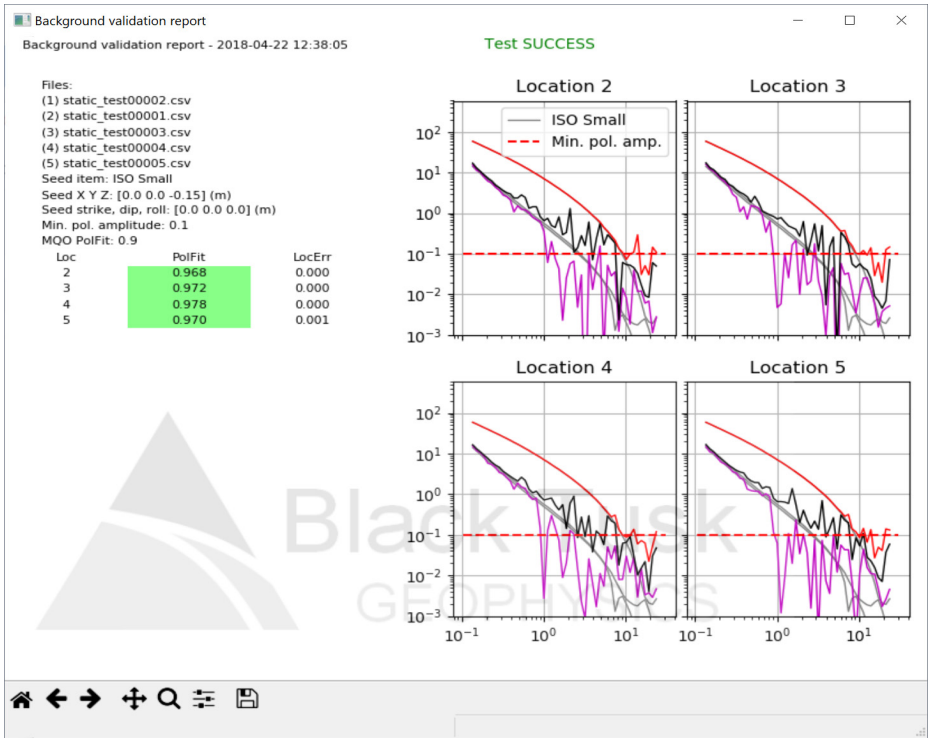

Figure 43. Example of a (Successful) 5-point Background Validation Report When No GPS or RTS Information Is Available.

Ongoing (2-point) background verification

To perform an ongoing (2-point) background verification test, the user presses the SCAN FOR COMPARISON button (Figure 33-top) and the current file list will be populated with the most recent file and the latest file from a successful 5-point validation background test. After pressing the **RUN** button, the user is presented with an optional results window with the MQO and test result values and/or an optional ongoing background verification report.

In the ongoing verification report the distance from the successful 5-point background validation test is shown with a green circle indicating the region where the distance is within the maximum distance offset MQO (Figure 44). A red rectangle indicates a failed MQO (Figure 45).

Figure 44. Example of a Successful 2-point Background Verification Report.

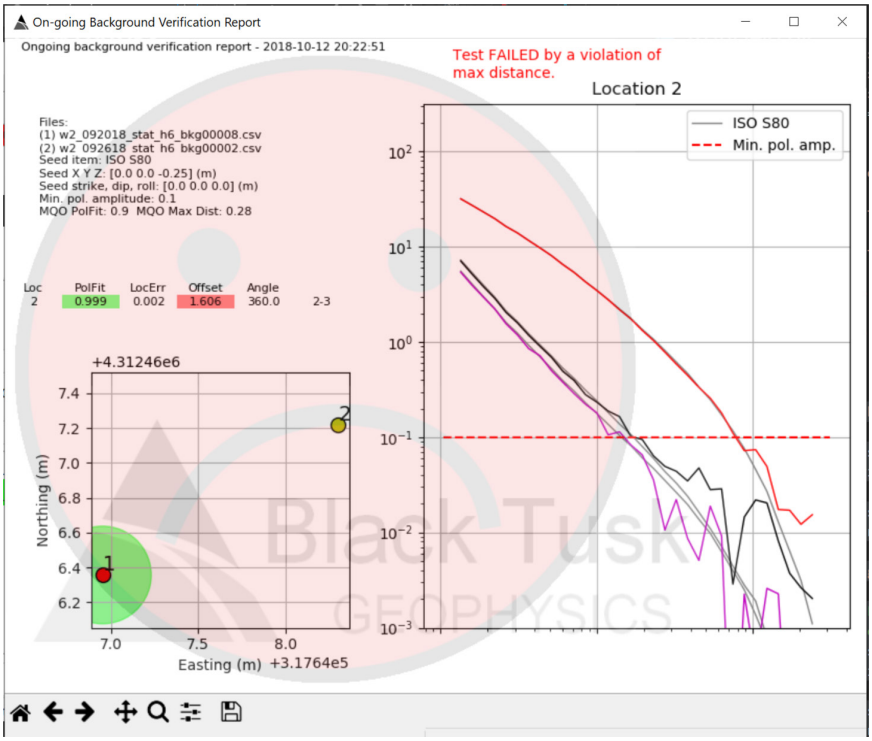

Figure 45. Example of a 2-point Background Verification Report with a Failure Due to Excessive Offset from the Original Validation Measurement Location.

3.0 AHRS TESTING WITH THE LORD MICROSTRAIN 3DM GX4-25 AND GX5-25

In this section, we describe the results of tests carried out with Lord MicroStrain high performance Attitude and Heading Reference Sensors (AHRS). We summarize experiments carried out with the MPV and recommend optimal settings for AGC applications.

The Lord MicroStrain 3DM GX series of high performance Attitude and Heading Reference Sensors (AHRS) have an established reputation for the positioning of AGC sensors. The GX4 and GX5 are the most recent series. Small and lightweight, the GX4-25 has been used by BTG for its Man-Portable Vector sensors (MPV) since 2016. The AHRS has provided accurate and reliable positioning on all projects to date. The GX4s were discontinued in 2017 and replaced by the GX5, which was marketed as a direct drop-in replacement of the GX4 with improved sensitivity. Preliminary field tests revealed severe stability issues with the GX5 that required further investigation and motivated this study.

The GX4-25 and GX5-25 AHRS feature calibrated and temperature compensated tri-axial accelerometer, gyroscope, and magnetometer to measure the dynamic regime and orientation relative to the Earth's gravity and magnetic fields, and fast internal processors designed to provide a stable and accurate estimate of the sensor attitude and heading under all dynamic conditions. The accelerometer measures the acceleration forces (change in speed due to gravity, movement or vibration), the gyroscope the angular velocity, and the magnetometer the local magnetic field.

Figure 46. MicroStrain 3DM GX4-25 and GX5-25.

The azimuth, roll and pitch are predicted by the internal processor by combining the data from the different sensors. When the AHRS is turned on and the sensor moves, the gyroscope and accelerometer detect it and change the pitch/roll/heading outputs. Because the gyroscope and accelerometers are not perfect, these integrated outputs can drift. The magnetic compass for heading and gravity vector for pitch/roll define a reference frame to stabilize the drift in those outputs and to get initial values. The AHRS come with the MIP configuration software to give the user the option to control the filter method for combining these data and to tune the sensitivity and latency of the internal sensors relative to the type of motion for their application.

There are two types of filters. The classic CF filter has the attitude outputs being continuously corrected by feeding back a fraction of the differences between the inertial (gyro) solution and the reference frame. The correction factors determine how quickly these differences are fed back. They act as a low pass filter for the reference frame: the lower the time constant, the quicker the feedback.

The Extended Kalman Filter (EKF) was introduced with the GX4 and is the manufacturer recommended filter. It uses a proprietary algorithm using similar principles as the CF filter. It operates with multiple error states and allows tuning of the sensitivity and time constant of each sensor to effectively dampen variations in the angles by predicting the next values based on the previous ones (via a noise covariance matrix). Our internal tests had better success using the EKF filters in terms of positional accuracy along line and minimal lag during changes in direction and rotation, which are particularly important for the MPV applications.

3.1 APPLICATION OF THE GX4-25 AHRS WITH THE MPV

The MPV is a handheld sensor that is used for the detection and classification of potential munitions. The detection data is collected in dynamic mode to accurately map electromagnetic anomalies associated with buried metal. The classification is achieved by navigating to detected anomalies to perform cued interrogation by collecting the highest quality data in stationary mode right on top of the buried metallic objects. Accurate positioning is critical to correctly map and locate detected anomalies, to invert tiles of dynamic data, to navigate to potential targets and precisely locate the classified objects.

Figure 47. Picture of the MPV, Where the Upper Part of the Handling Boom Has Fixtures for a White Box Containing the AHRS and a Mast Holding the GPS Rover (or a Prism for RTS).

The MPV geometry is illustrated in Figure 47. The GPS and AHRS are attached on the upper end of the MPV sensor handling boom, 1.15 m away from the MPV head to minimize any interference. The GPS antenna location is continuously measured with RTK precision in the order of 1-2 centimeters. The location of the MPV transmitters and receivers are inferred from the GPS by translation and rigid-body rotation using the azimuth, roll and pitch provided by the AHRS. The accuracy of the AHRS measurements is crucial, especially for the azimuth, as a one-degree error in the azimuth amounts to a 2-cm error in the direction perpendicular to the MPV boom (across track).

In dynamic mode the MPV is used to collect data along straight lines. At the end of each line the MPV turns around to survey the next line in the opposite direction. The AHRS has to respond quickly enough to track the 180-degree rotation and adjust to a stable azimuth as soon as the rotation stops. This is particularly important when the MPV is used in an environment with obstacles such as trees and urban features, where the sensor frequently changes course and rotates to avoid obstacles. The AHRS readings must also be relatively immune to instantaneous variations, such as a shock if the MPV hits an obstacle and generates a large acceleration. Finally, the AHRS heading output has to correspond to the azimuth relative to the North. This is a key difference as AHRS are generally used for vehicular applications, where the principal axis of the AHRS matches the direction of travel. This is not the case for the handheld MPV, which might be rotated relative to the direction of travel due to sensor ergonomics, operator morphology, fatigue and convenience, and site conditions such as side slopes or obstacles. The AHRS must be set to rely on the magnetometer to predict the heading, with the accelerometer stabilizing the magnetometer readings without introducing a bias towards the direction of travel.

In cued mode, the AHRS is primarily used to navigate to targets. It must adjust to the change in dynamic regime between navigation to a target, with the operator walking, stopping and changing direction, and cued acquisition mode with the MPV stationary, on the ground, for approximately half a minute while acquiring data over a target. The AHRS should not drift during that stationary period in order to correctly predict the sensor location, which in turn is used to predict the buried target location.

The sensor integration of the GX4-25 AHRS on BTG's MPV was performed by placing the AHRS at the top of the MPV handle and verifying that the AHRS readings were immune to the electromagnetic field from the MPV transmitters. The AHRS was calibrated for soft and hard iron effects according to the manufacturer guidelines. The AHRS filter parameters were established through BTG's internal testing procedures at a local test site. The tests verified accurate, repeatable position and no perceptible drift error over time. One key test was the lag-line test, which consisted in walking back and forth along a straight IVS line and verifying that the paths for the predicted sensor head location were overlapping (the lag test is also used to synchronize the clocks between the EM and positioning sensors). Another test consisted of performing a spin test, where the MPV head is placed on a horizontal board and taken through a 360-degree rotation of the azimuth around the center of the MPV head, in the horizontal plane. The spin test verified that the predicted location of the MPV head remained stable for any heading direction and that the AHRS was not significantly lagging the rotational motion. The tests are described in the next section as standard tests for remediation projects.

3.2 INTEGRATION OF THE GX5-25

Relative to the GX4, the GX5 uses newer, higher performance accelerometers, the same gyroscopes with improved digitization and data conditioning processes, faster internal processors, and new auto-adaptive EKF algorithm with added states to track and correct for more error sources. In principle, this ability allows the GX5 to automatically adjust error thresholds for detecting anomalies in the gravity vector measurement and the magnetic heading measurement. The GX5 also offers the capability to automatically calibrate the magnetometer in-run and in-situ to continuously adapt to changes in the magnetic environment.

The GX5-25 AHRS was tested in the context of using MPVs at the Spring Valley FUDS site with Weston for surveying in a forest and around private properties, using Robotic Total Station (RTS) laser positioning. The factory-new AHRSs were mounted on the MPVs, all calibrations were performed and the MPVs were taken through typical daily data quality assurance tests:

- The spin test results are shown in Figure 48. By predicting the location of the MPV based on the RTS prism location and the AHRS, we verified that the MPV sensor was correctly assembled, that the RTS was providing accurate positioning information and that the AHRS was providing accurate attitude and heading corrections with no significant lag or drift.
- The IVS was surveyed in dynamic mode to perform a lag test. The central line of the IVS was collected in two passes of opposite direction to test the positional accuracy in the cross-track direction and the accuracy of the AHRS heading by verifying that the predicted sensor paths overlap (Figure 50).
- The IVS survey was completed by collecting additional lines on either sides of the central line and inverting the data to confirm that the test targets were correctly predicted in terms of position, depth and polarizabilities.
- The IVS cued data were acquired by using the real-time AHRS and RTS data to navigate to the coordinates of the test targets and record their location, thus further confirming positional accuracy of the MPV system. All these tests were passed before proceeding to production surveys.

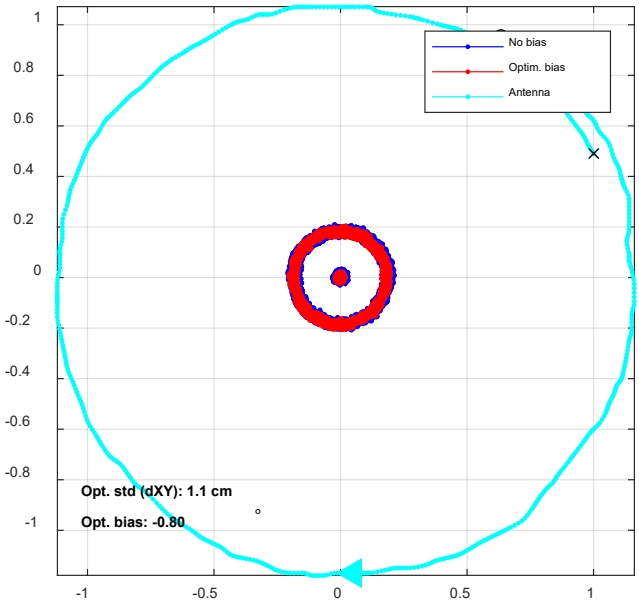

Figure 48. Illustration of the MPV Spin Test.

The MPV is rotated around the center of the head in the horizontal plane. The cyan lines show the path of the RTS prism. The blue and red lines show the paths of the Rx cubes on the MPV head, including the center cube that should remain stationary. The blue lines are based on the raw AHRS data, whereas the red lines are the result of a calculation to find the bias in the AHRS heading that minimizes the motion of the central cube. The lines overlap when the AHRS heading perfectly tracts the rotation. The test shown here indicates that the AHRS unit is well integrated and presents a negligible bias (-0.8 degrees relative to the bias that minimizes motion of the center cube).

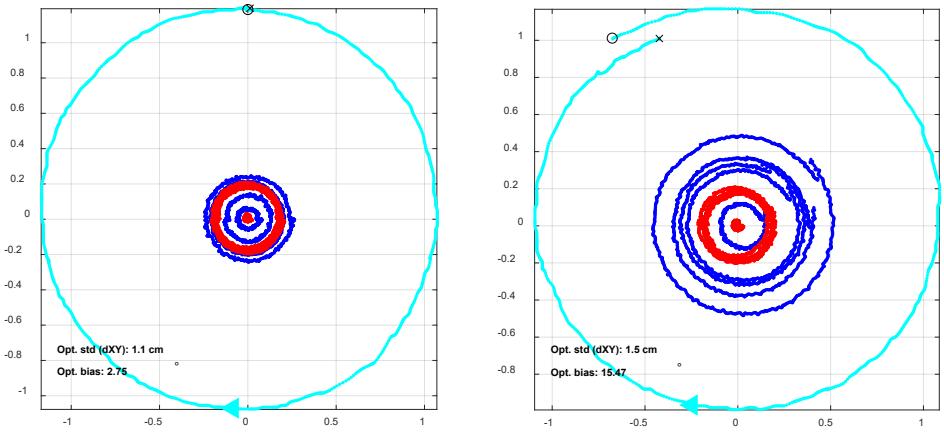

Figure 49. Illustration of Spin Tests with an Azimuth Bias.

The left panel has a small bias that is visible in the dark blue paths that differ from the optimum red paths, for which the receivers track a perfect circle through the rotation. The bias is deemed to be acceptable and corrected when processing dynamic and cued data (value of 2.75 degrees indicated in the graph). The right panel shows a spin test with a severe bias of 15 degrees that could suggest a magnetic declination error or some serious issues with the AHRS unit.

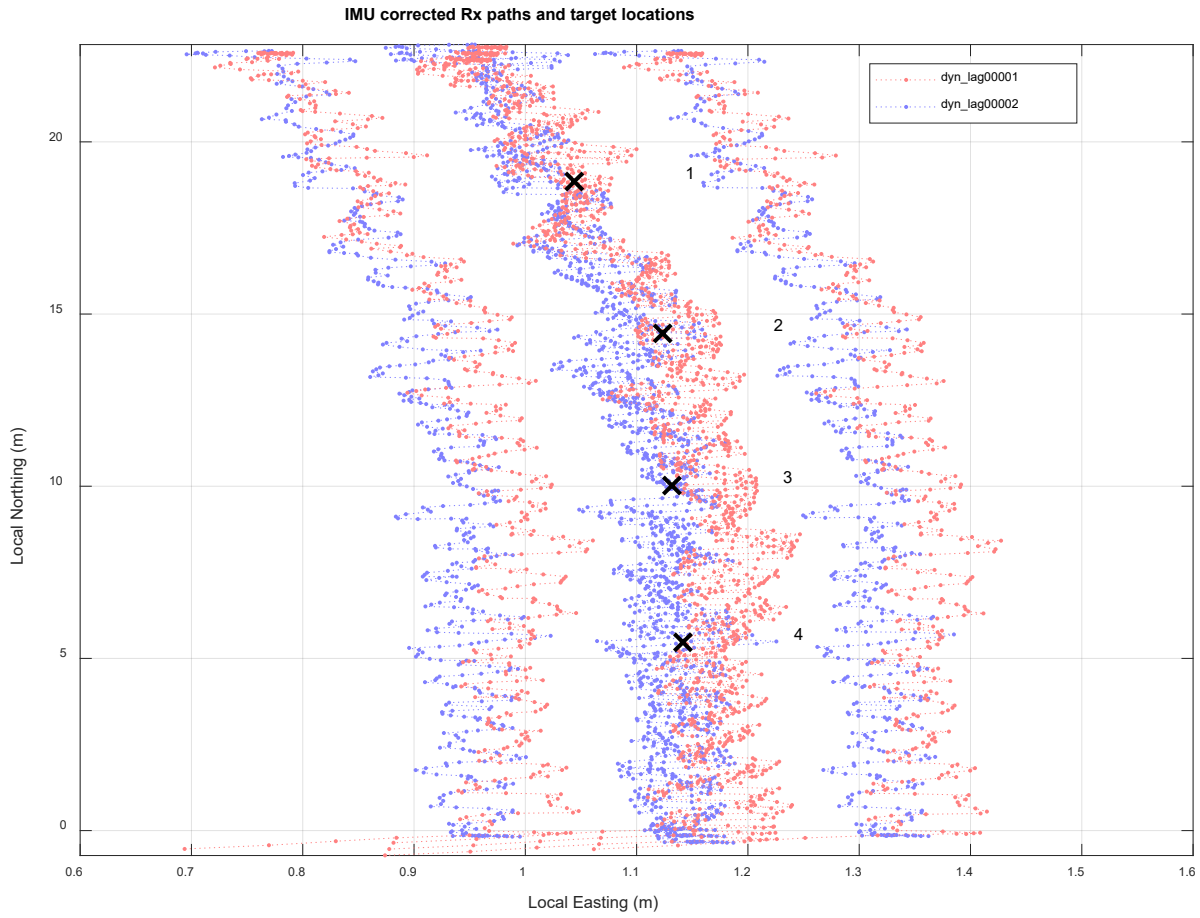

Figure 50. Lag Lines on the IVS.

Two lines are acquired in opposite directions over the IVS targets. The line is physically indicated with a rope to guide the field operator. Lateral deviation from the line is interpreted as positional error that can be due to the GPS/RTS, the AHRS, or a change in the sensor geometry (e.g., handle rotation).

3.3 AZIMUTH BIAS WITH THE GX5-25

The GX5-25 was used in production mode. At the start of a production day, all standard data quality checks were performed at the IVS, including spin tests, and all tests passed. The MPV was then used to collect full-coverage dynamic data with 0.45 m line spacing in a forested survey area. The lines were physically marked on the ground with survey ropes and the field crews were instructed to carefully follow these lines.

The map in Figure 51 shows the receivers path for that area over a day of data collection. The map reveals that there are groups of lines where the line separation is irregular and leaves gaps that exceed the 0.70 m measurement quality objective (MQO, yellow highlights). Given the careful survey setup, the irregular line separation was likely due to a positioning issue. After verifying the MPV assembly to make sure that its geometry had not changed by rotation of the handling boom, we concluded that the AHRS accuracy might have drifted since the morning IVS.

The fact that there are groups of consecutive lines with somewhat regular line spacing (most of the top lines, start of lines on the left and last third to the right for the lower lines) suggest that the bias was temporal in nature. The evening IVS data passed again all MQOs. We found through these tests that positioning accuracy can degrade throughout the day and still meet the morning and evening IVS test requirements. In Figure 52 we show that applying a line by line heading correction can result in full coverage. However, these corrections of 5-10 degrees largely exceed the expected 1-degree error on the AHRS heading output.

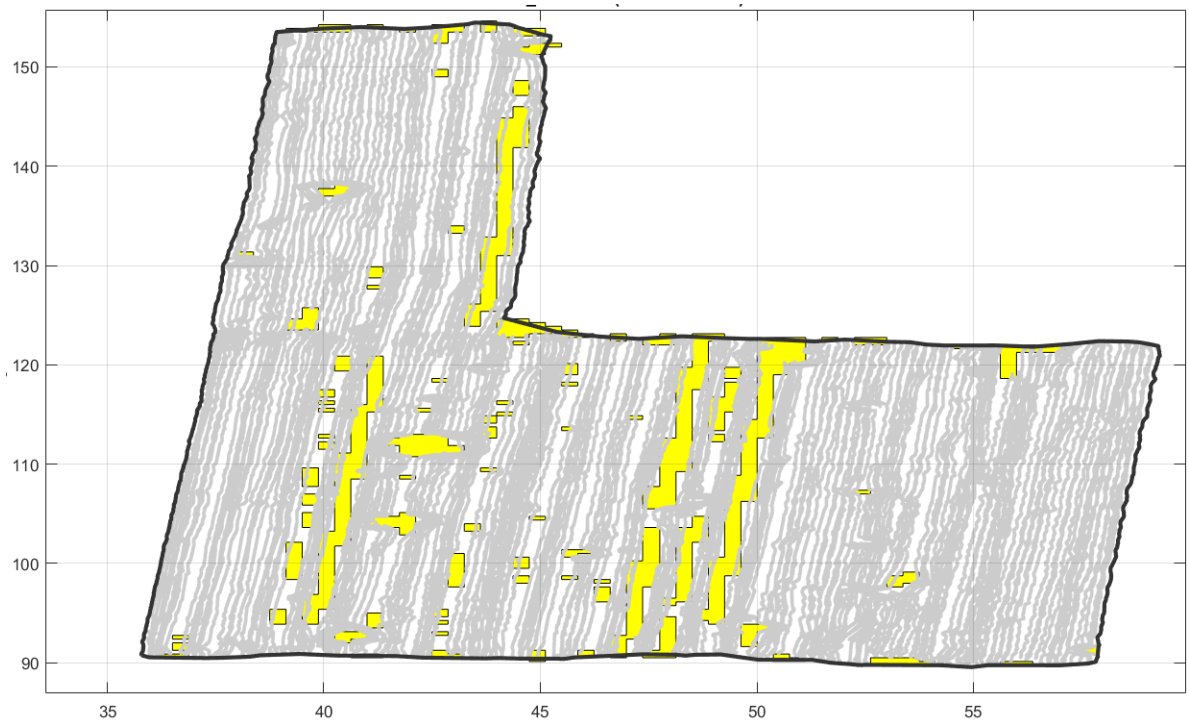

Figure 51. Sensor Path During a Detection Survey.

Grey lines indicate the MPV receiver path. Yellow patches highlight areas where the apparent survey line separation exceeds the line spacing MQO of 0.70 m.

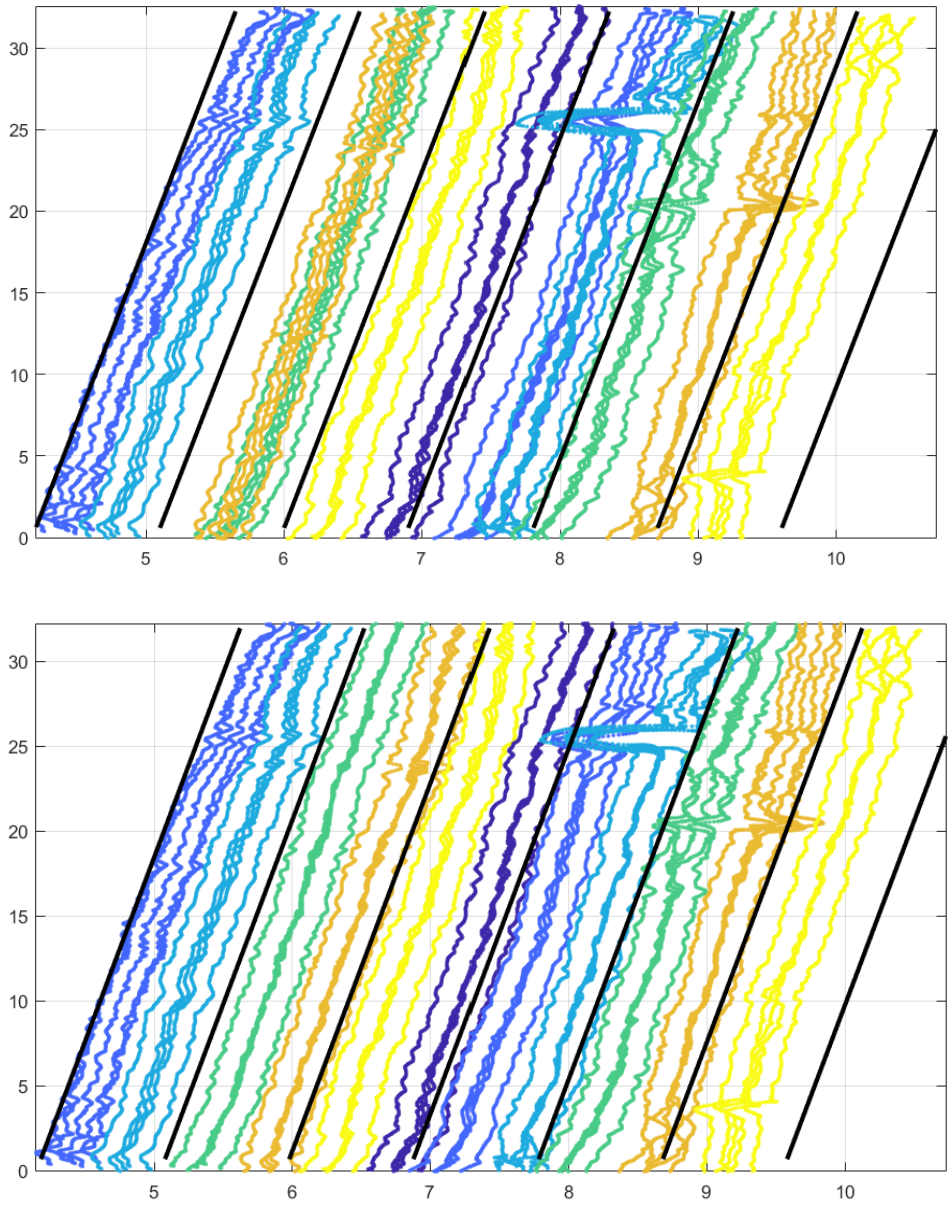

Figure 52. View of a Line Subset with Irregular Line Pattern.

The axes coordinates are local easting and northing expressed in meters. The top panel shows each survey line in a different color: there are 5 tracks for each of the receivers, one on each side and 3 nearly overlapping at the center when the sensor is aligned with the direction of travel. The theoretical survey guide lines with 0.90 m line spacing are indicated in black straight lines. The figure shows, from left to right, overlapping survey lines followed with gaps. The bottom panel shows the same lines after the AHRS azimuth has been corrected by adding a line by line bias to the azimuth to obtain a more even line spacing to match the expected sensor path.

Note that for the 3rd and 4th lines from the left (green and orange), the bias was so large that the order of the lines seems to be flipped between the upper and lower panels; on the lower panel the 3 center tracks overlap, whereas on the upper panel they appear as distinct due to an artificial rotation caused by the bias.

The effect of a bias in the sensor heading on the predicted MPV position is illustrated in Figure 53. The AHRS azimuth, pitch and roll are used to predict the location of the MPV head relative to the positioning rover (GPS rover or RTS prism) through a rigid body rotation. The rover is located 1.15 m behind the sensor head (horizontally) and 1.4 to 2 m above it. A positive bias of 1 degree in the AHRS heading effectively rotates the predicted MPV location and moves it away from the direction of travel, across the track, by 2 cm. Because dynamic surveys cover an area by alternating lines in opposite directions, a constant heading bias shifts alternating lines in opposite directions and thus creates line gaps and overlapping lines.

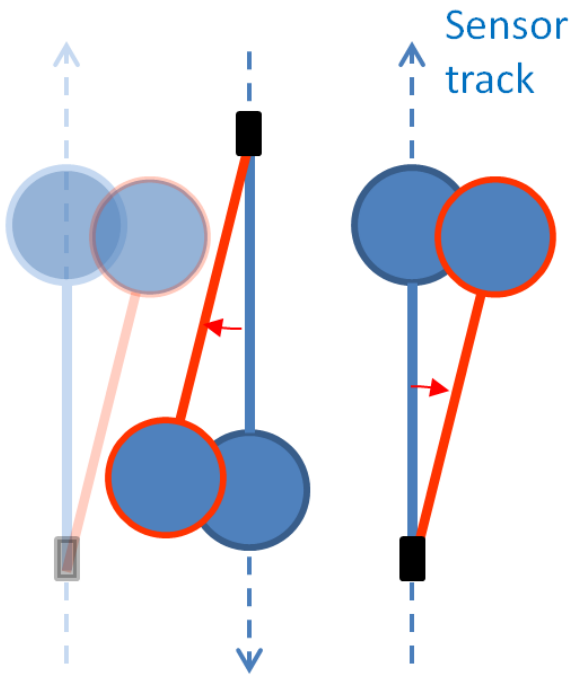

Figure 53. Schematic Illustrating AHRS-related Positional Error.

The dashed lines indicate the real sensor path. The real location of the MPV is indicated with the blue disc, its blue handle and a black box show where the AHRS and GPS rover or RTS prism are located. If the AHRS heading has a positive bias, the predicted MPV head location is rotated clockwise around the location of the GPS/RTS, as shown with the red outlines. When that biased heading is used, the predicted survey lines no longer appear to be regularly spaced; instead they alternate between overlapping lines (left side) and wide gaps (right side).

After finding this issue with the GX5 AHRS the production survey was stopped to investigate the root cause of the error and identify a solution to be able to resume the survey.

3.4 TESTS WITH GX5-25

The SVFUDS remediation project had three GX5 sensors that were tested to confirm that the issue was not limited to a faulty unit. All units were recalibrated, following the manufacturer's instructions for soft and hard iron calibration and gyroscope calibration. A series of tests were conducted to identify a set of filter parameters that would provide stable and accurate positioning. The tests were performed by collecting survey data back and forth along a straight line marked by a rope on the ground and with emplaced targets, similar to an IVS line.

The tests were evaluated by estimating the average lateral offset between the reference line and the MPV sensor track predicted from the positioning data (AHRS and RTS prism). The accuracy of the test required the operator to be very careful with following as close as possible the guideline on the ground with the center cube of the MPV.

The tests tried to identify a set of optimal filter parameters that control the filter modes, parameters and sensitivities to combine the data from the magnetic sensors, gyroscopes and accelerometers on the output heading, pitch and roll. These parameters were chosen based on the recommendations and explanations provided with the user manual. Note that the GX5 and GX4 use different onboard implementations of Kalman Filters, have different sensitivities for most of their internal components, and were provided with different versions of the MIP Monitor software to control the filter parameters. It was therefore not possible to exactly apply BTG's set of working GX4 parameters onto the GX5.

Figure 54 and Figure 55 illustrate some of the guesses on the filter parameters, based on the user manual, correspondence with Lord Microstrain support, and trying to match the GX4's working parameters. In Figure 54 a first set of parameters was used for the first 2 hours. The bias drifted slowly and became too large to be acceptable. Other sets of plausible parameters were tested after 3 hours, but all resulted in rapid drift errors. We found that in all our tests, which spanned multiple days and a large set of parameters, the heading predicted by the GX5 AHRS always drifted over time, sometimes very quickly.

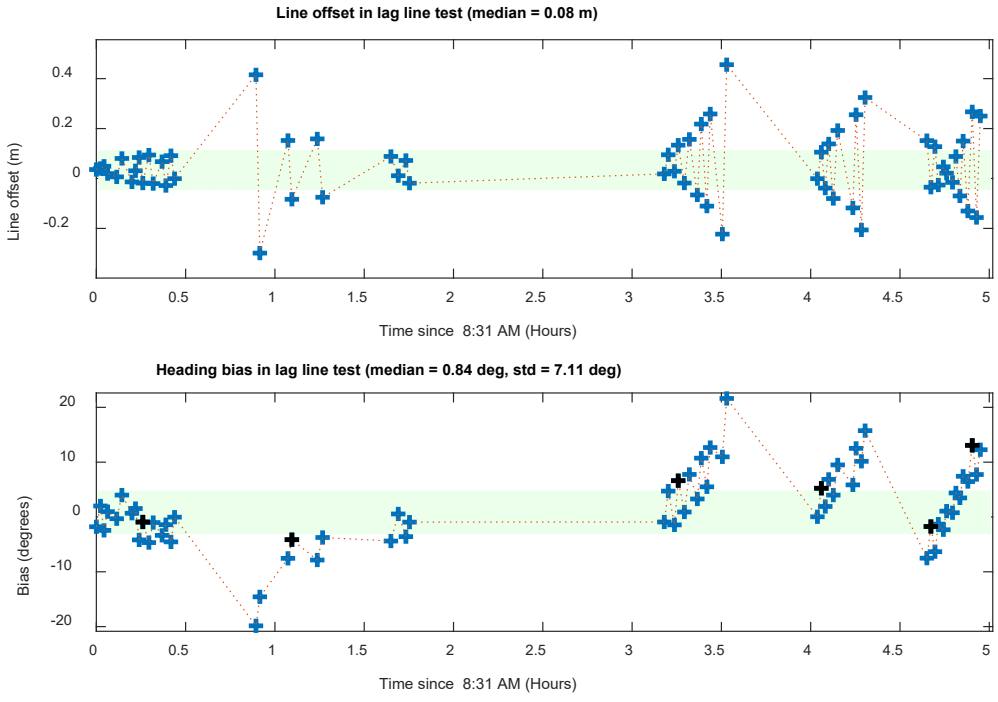

Figure 54. AHRS Test Along a Lag Lines for a Given Set of Filter Parameters.

Data were collected along a straight line in alternating directions. Each marker indicates the lateral offset (top panel) and the corresponding heading error (bottom panel), defined as the correction that would need to be applied to the AHRS heading to predict the MPV head to travel along the center line.

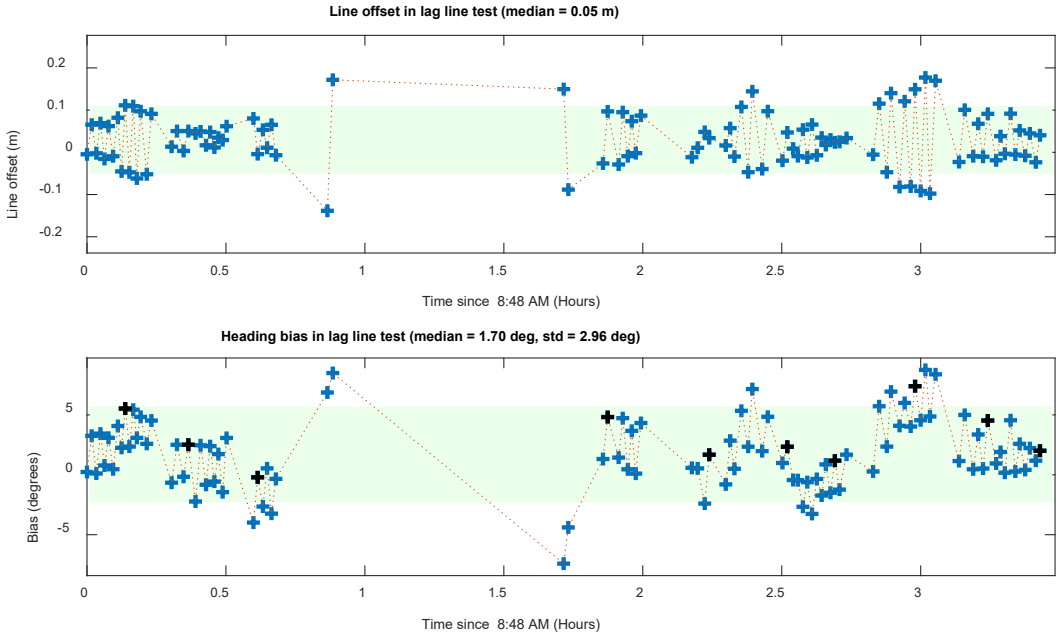

Figure 55. AHRS Testing with Filter Parameters Matching as Close as Possible BTG's GX4 Parameters. The Top Panel Shows the Lateral Offset of the Survey Lines Relative to the Center Line. The Lower Panel Shows the Corresponding Correction that Would Need to Be Applied to the AHRS Heading to Predict the MPV Head to Travel Along the Center Line.

The two lines around the 1 hour mark show a large drift after letting the instrument running in stationary mode. At 1.5 hours the AHRS was power cycled, the first two lines had a large offset, which subsequently reduced, but still drifted over time to values that are too large to provide sufficient accuracy on a survey.

G&G Sciences carried out tests in parallel with the GX5 using the CF filters instead of the Kalman filters, with similar drift issues with the GX5 heading. As a result of the difficulty to stabilize the GX5, it was decided to abandon this type of AHRS for the project and procure the last available GX4s to complete the SVFUDS project.

However, given that there were no other GX4s available to supply the rest of the MMRP industry, BTG and G&G Sciences pursued discussions with Lord MicroStrain to clarify the GX5 AHRS mode of operation and try and identify a working set of parameters for the EKF and the CF filters. The following recommendations were provided by Microstrain: "Do NOT use automatic-magnetic calibration for your system as it will continuously try to calibrate the magnetometer to current conditions. Instead, *decrease* the **magnetometer measurement noise** (default is 0.1, vs 0 for BTG GX4) and *increase* the **gyro process noise** (GX5 default is 5 times larger than GX4). Do it in order of magnitude increments (increase 10 x, decrease 10 x) and see what happens. This should make the heading more responsive to the magnetic field and less stabilized by the Gyro. It is best to set the Mag Adaptive parameter to "Auto-Adaptive". You can also try in using fixed adaptive and increasing the **output uncertainty levels**. Limited tests were done in January 2019 but the drift issue persisted.

3.5 TESTS WITH GX4-25

Multiple GX4-25 AHRS were supplied by NRL and by Lord and tested to verify that this type of AHRS could meet the positioning accuracy requirements for production surveys. The first test consisted of performing lag lines with a fresh, out of the box unit, with factory default settings, without recalibration of the AHRS. The results presented in Figure 56 show that the heading is relatively stable for each set of lines collected in the same direction. The heading bias depends on the direction of travel, it does not show any temporal drift, which is a major progress relative to the GX5, but it is not sufficiently accurate for production survey.

The sensitivity to the direction of travel diminished and the accuracy improved after performing soft and hard iron calibrations with the AHRS mounted on the MPV, as shown in Figure 57. Finally, we applied BTG's standard set of parameters to the EKF filters and confirmed that these provided a stable and accurate heading for lines collected in opposite directions, as illustrated in Figure 58.

We applied BTG's settings to multiple GX4-25 mounted on different MPVs, with different operators, and along different directions of travel, and confirmed that the bias always remained stable and within 2-3 degrees. There might be a slight sensitivity to the direction of travel, although that sensitivity could also be operator specific (the way the MPV is held, and his tracking of the center line), and site specific (especially when testing with an RTS and trying to keep line of sight). In any case this effect remains negligible and would not have an impact for the interpretation of survey data given that most the data is generally collected in continuous blocks of alternating lines, where we know that the same bias applies and results in minimal positioning error between adjacent lines.

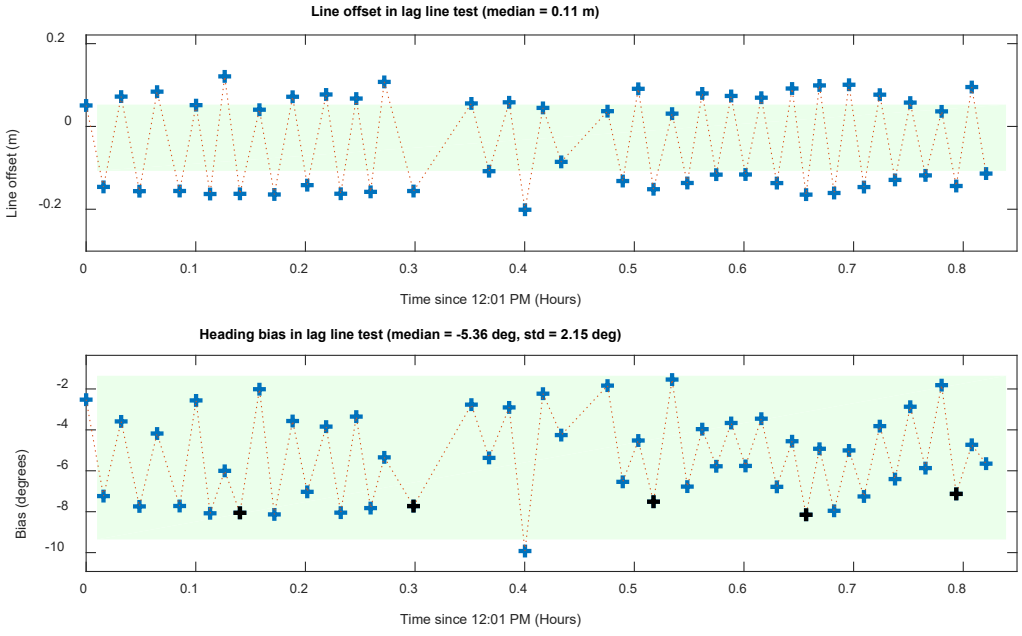

Figure 56. Lag Line Tests with GX4 Out of the Box, Before Calibration.

The direction of travel alternate between each successive marker. In general, lines collected in each direction show a stable bias. The bias is different between the two opposite directions. The bias depends on the direction of travel but there is no temporal drift.

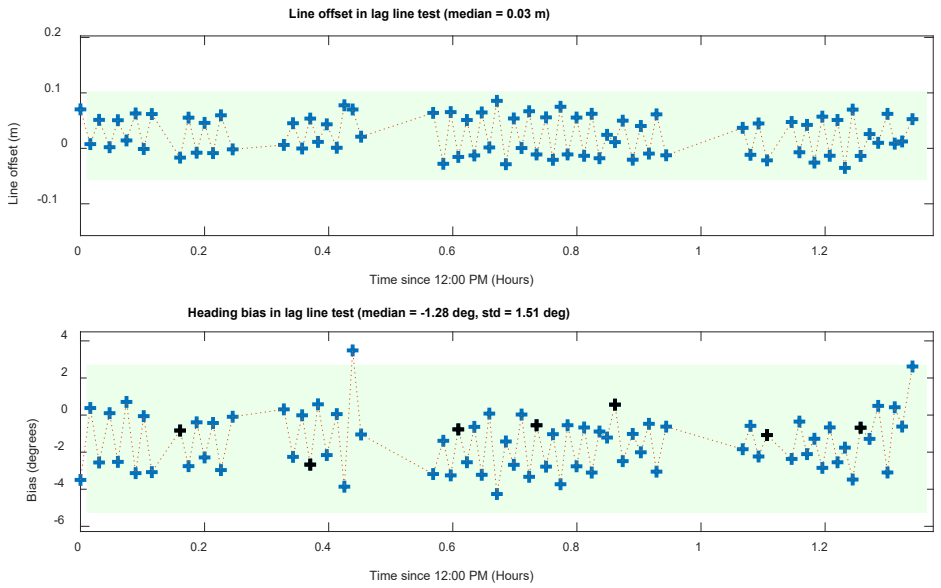

Figure 57. GX4 Lag-Line Test After Soft and Hard Iron Calibration.

The calibration has improved the accuracy of the heading and reduced the directional sensitivity relative to tests without calibration.

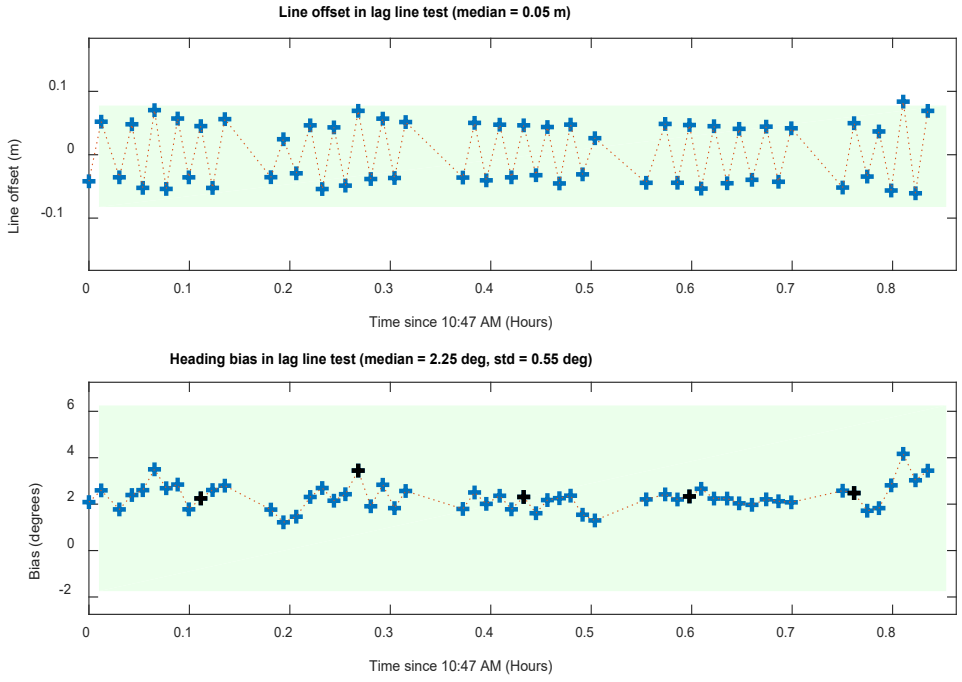

Figure 58. Lag Lines Tests with GX4 using BTG Filter Parameters.

The heading bias is here stable. Its value is not necessarily equal to zero if the AHRS is not perfectly aligned with the MPV sensor boom.

3.6 RECOMMENDED PARAMETERS FOR THE GX4-25

The following picture shows the BTG's parameters in MIP 2016 verified in this study.

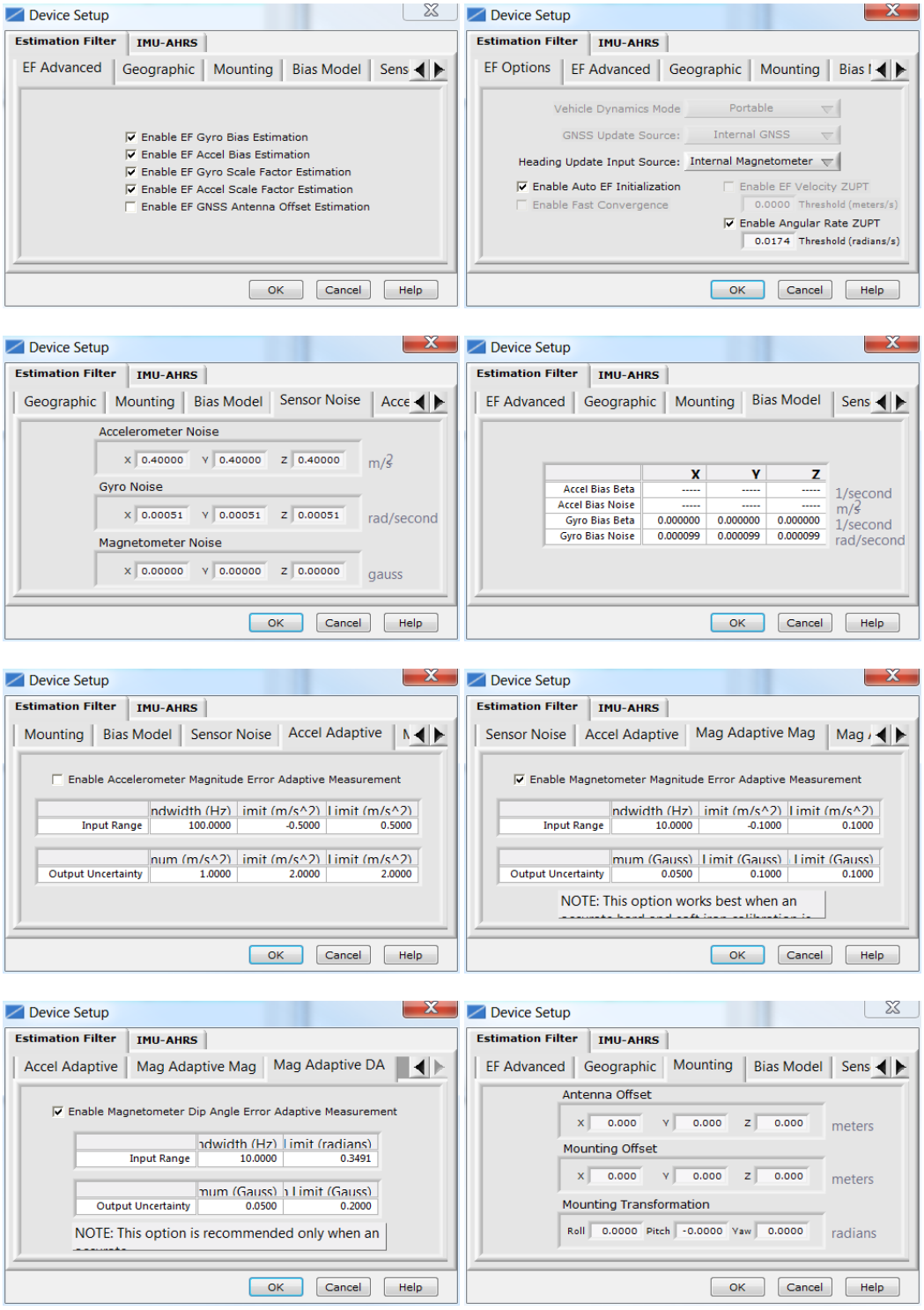

Figure 59. EKF Parameters for the GX4-25 in MIP 2016 Software.

3.7 CONCLUSION

At the time of this report we are not aware of a mode of operation for the Lord Microstrain GX5-25 AHRS that is sufficiently stable for our application, even though the GX5 seems to be satisfactory for other applications. This might be due to the fact that most applications are vehicle-based, where the AHRS is aligned with the direction of travel, and where the heading output is interpreted as the direction of travel, for which it can rely on the accelerometer and gyroscope to be stabilized, whereas for the MPV the heading is the direction to the North, which mostly relies on the magnetometers. Note that G&G Sciences have also performed numerous tests based on CF filters without converging to a satisfactory solution.

We confirmed a set of parameters that make the GX4-25 usable for DGM and AGC with the MPV. The parameters ensure a level of stability and accuracy that is sufficient to perform DGM, processing and informed source selection, and to navigate to targets for cued interrogation and classification, as illustrated by the SVFUDS remediation project, where seeds are routinely predicted within 5-10 cm for dynamic and cued data.

4.0 AGC IN CHALLENGING SCENARIOS

In this section, we present results of investigations into AGC in challenging scenarios that were encountered during this project. In particular, we discuss classification of 20mm projectiles at Former Lowry Bombing and Gunnery Range with the MetalMapper.

4.1 LOWRY 20MM INVESTIGATIONS

4.1.1 Summary

In July-August 2016, BTG conducted a study to assess the ability of the classic (seven-receiver, three-transmitter) MetalMapper (MM) to accurately classify subsurface 20mm projectiles at the 20mm Range Fan Munitions Response Site, Former Lowry Bombing and Gunnery Range (FLBGR), a site containing a significant amount of surface clutter, mostly comprised of .50-caliber small arms casings.

For this study Parsons collected 3 acres of MM dynamic detection data in three separate 1-acre grid blocks of the 20mm Range, with low, medium and high target densities (~400, 700 and 1200 targets/acre, respectively). BTG processed the detection data using similar data processing parameters used for the Center Target at the FLBGR GM (Imperator Captus et Apparatus) MRS. The primary goal of the detection data processing was to identify the locations of any subsurface sources large enough to represent a 20mm projectile.

From the three target lists created by BTG, Parsons selected 298 targets over potential 20mm (as identified by BTG) to cue (148 from the high-density grid blocks, and 75 each from the low- and medium-density grid blocks). BTG processed the cued data and provided an analysis of the ability of both the dynamic and cued data to accurately classify 20mm projectiles.

4.1.2 Results

The project began with Parsons collecting two passes of both dynamic and cued data over a 20mm test line comprising eight holes, with a single 20mm projectile in the first five holes, and two, three and four 20mm projectiles in holes 6, 7 and 8, respectively (Figure 60). All targets were horizontal at 15 cm depth, with a separation of 15 cm between targets for multi-target scenarios. BTG inverted both the dynamic and cued data and analyzed the predicted polarizabilities. Results from the dynamic data showed that for one or two objects, the dynamic polarizabilities could reliably by used for screening based on size. For more than two objects, the dynamic data could generally not constrain reliable primary polarizabilities for all objects. Results from the cued data (Figure 61) showed that excellent polarizabilities could be obtained for both the single and two-target scenarios, so that classification would be successful under these circumstances. For three- and four-target scenarios, it would not be possible to properly classify all targets.

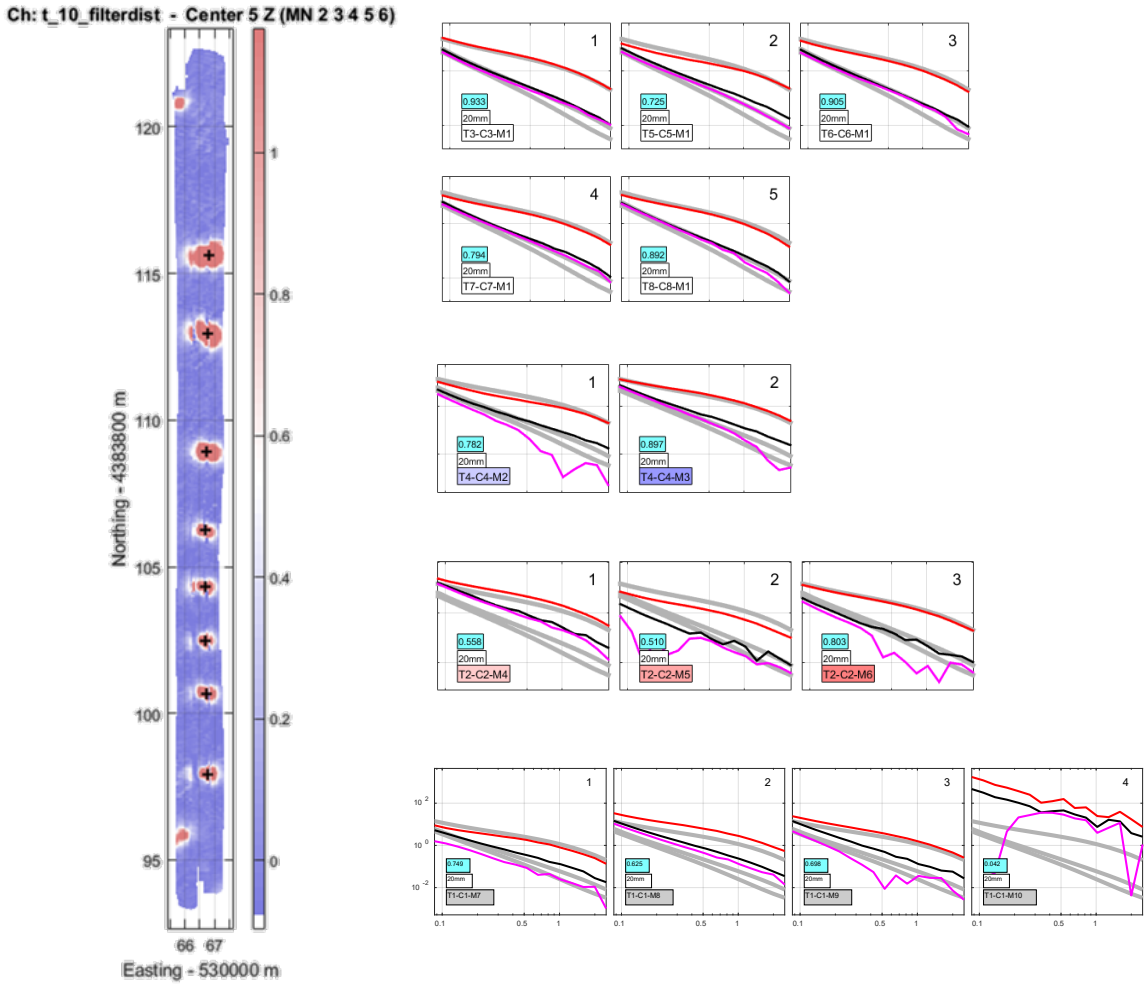

Figure 60. Left: Dynamic Test Line Data Over Eight Holes. Holes 1-5 Each Contain a Single 20mm Projectile. Holes 6, 7 and 8 Contain 2, 3 and 4 20mm Projectiles, Respectively. Right: Dynamic Polarizabilities. (a) Single Source Inversion Polarizbilities from Holes 1-5. (b-d) Two-, Three- and Four- Source Inversion Polarizabilities from Holes 6, 7 and 8, Respectively.

Red, magenta and black lines are predicted polarizbilities. Grey lines are reference 20mm polarizabilities.

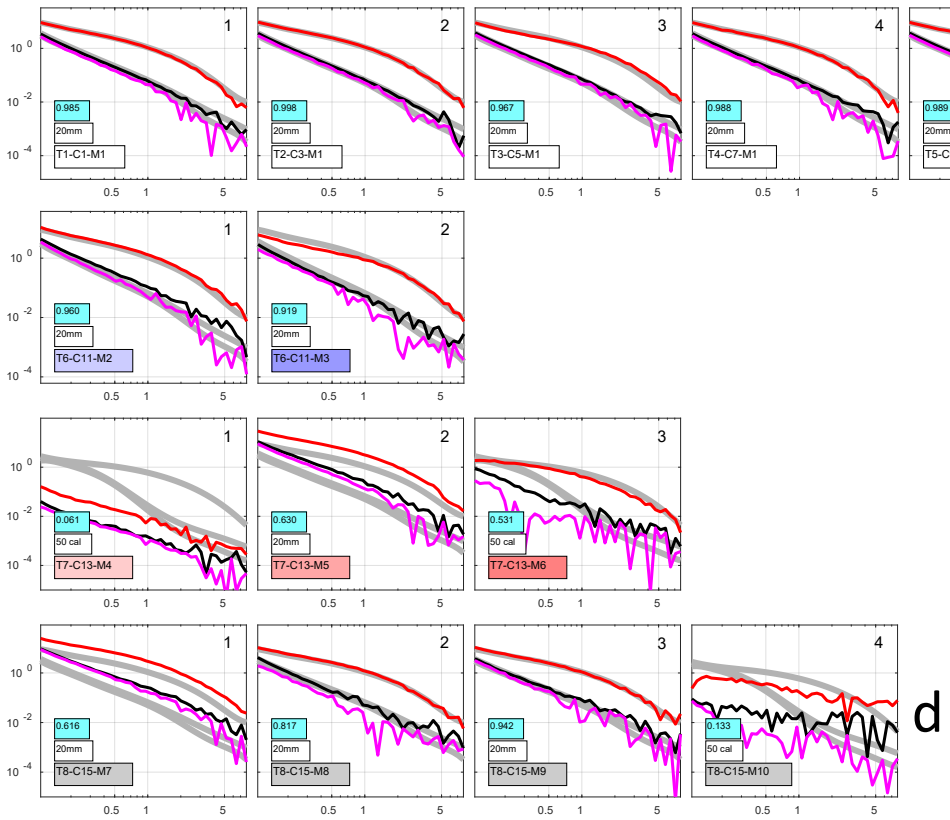

Figure 61. Cued Polarizabilities. (a) Single Source Inversion Polarizbilities from Holes 1-5. (b-d) Two-, Three- and Four- Source Inversion Polarizabilities from Holes 6, 7 and 8, Respectively.

Red, magenta and black lines are predicted polarizbilities. Grey lines are reference 20mm polarizabilities.

Processing of dynamic data from the three grid blocks resulted in 1326, 687 and 403 raw target picks for the high-, medium- and low-density grids, respectively (Figure 62). We inverted the dynamic data using 1-, 2- and 3-source solvers and applied the same informed source selection process used at the GM MRS; however, based on results from the test line data, we did not do any screening because of the inability of the data in multi-target scenarios to adequately constrain the polarizabilities. After merging of nearby source locations, we compiled targets lists for the three grid blocks comprising 1085, 609 and 373 targets, respectively for the high-, medium- and low-density grids. These lists were delivered to Parsons for selection of the 298 locations to cue.

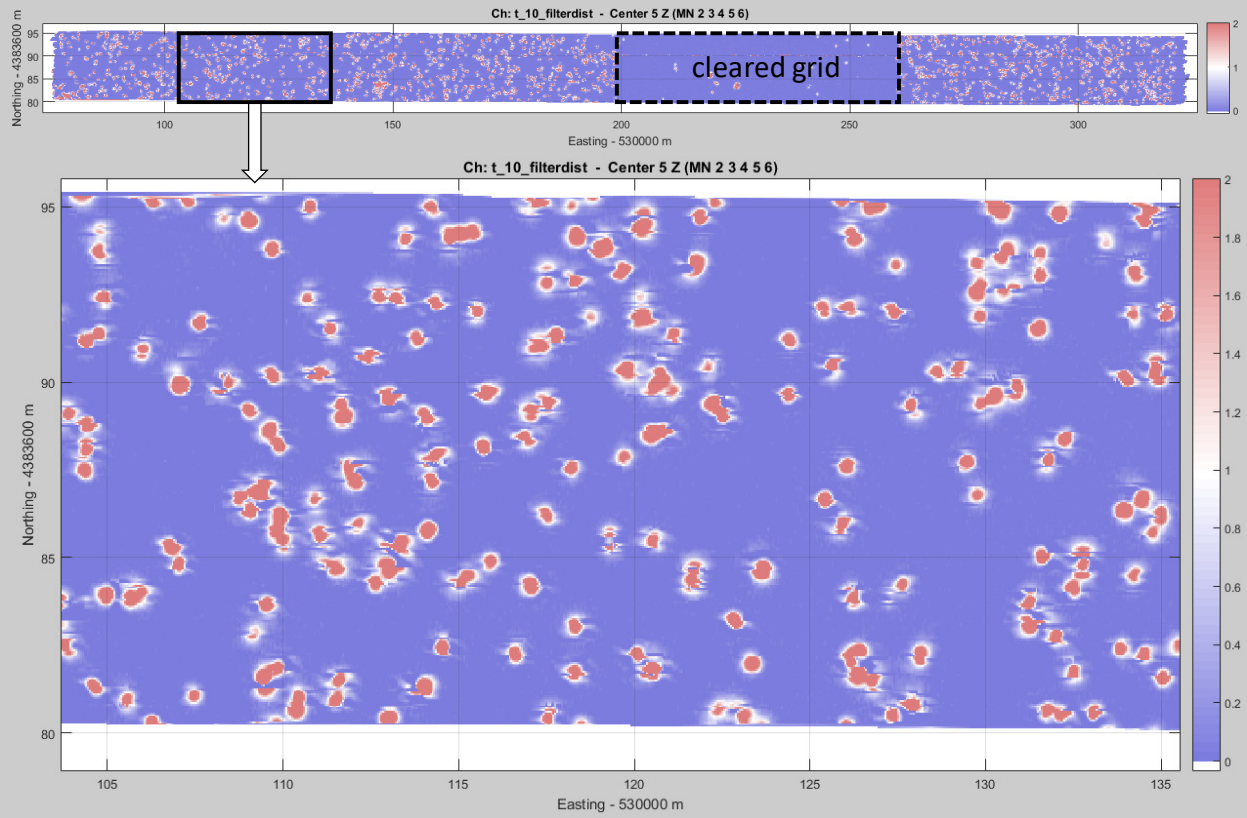

Figure 62. Gridded Dynamic Data (Leveled Channel 10; 0.338 ms) from Row 31 (High Density Area) of the 20mm Range. Top: Entire High-density Grid Block Used in this Study Comprises Four Sub-grids, One of Which is Cleared. Bottom: Close-up of a Portion of the High-density Region Indicated by the Solid-line Rectangle in the Top Panel.

BTG inverted the cued data using 1-, 2- and 3-source solvers. The targets were classified by polarizability matching against a reference library comprising only 20mm projectile and .50 cal polarizabilities. Of the 298 targets, only three did not have a model with a polarizability match (using all polarizabilities, or just the primary) to either a 20mm or .50 cal reference item. There were 126 models with a good match to the 20mm projectile, and 225 models with a good match to the .50 cal (Figure 63). Note that about 50 targets had good matches to more than one distinct item in the reference library. As a deliverable to Parsons we compiled a dig list listing location, depth, decision metric and best matching ordnance type (20mm or .50 cal). In addition, we provided a PDF file showing the polarizabilities of each model (and best matching reference polarizabilities) in dig list order.

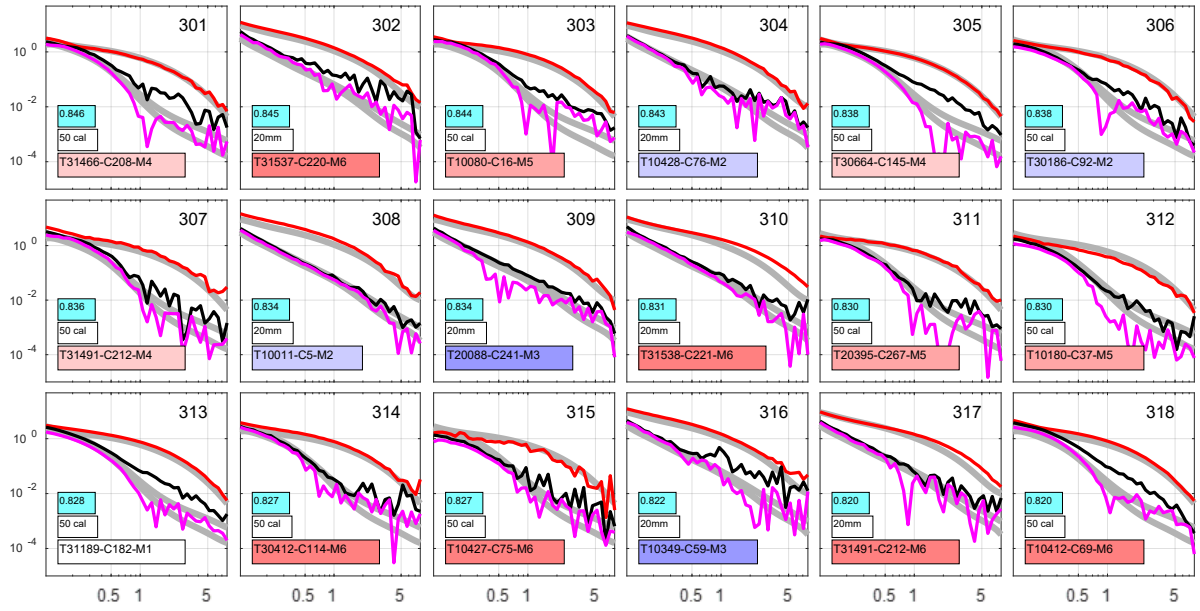

Figure 63. Cued Polarizabilities Sorted by Polarizability Match Metric (Cyan Label at Lower Left in Each Panel). This Set Represents the 301st to 318th Best Matching Polarizabilities Out of the Set of 351 Polarizabilities that Were Identified as a Good Match to Either a 20mm or .50 cal.

Red, magenta and black lines are predicted polarizbilities. Grey lines are reference 20mm polarizabilities. Name of best matching reference item is given in white label at lower left of each panel.

To assess the usability of polarizabilities from the dynamic data for the purposes of making dig/no dig decisions, BTG compiled a PDF report comparing cued versus dynamic polarizabilities for each model in the cued dig list (Figure 64). Of the 298 cued cells, 96% (286) have a primary match metric between cued and dynamic polarizabilities of > 0.8. We concluded that successful screening using dynamic polarizabilities was feasible (i.e., all cued targets have a dynamic measurement with polarizabilities of approximately the same size). The median difference in predicted model depths between dynamic and cued models is 1.3 cm.

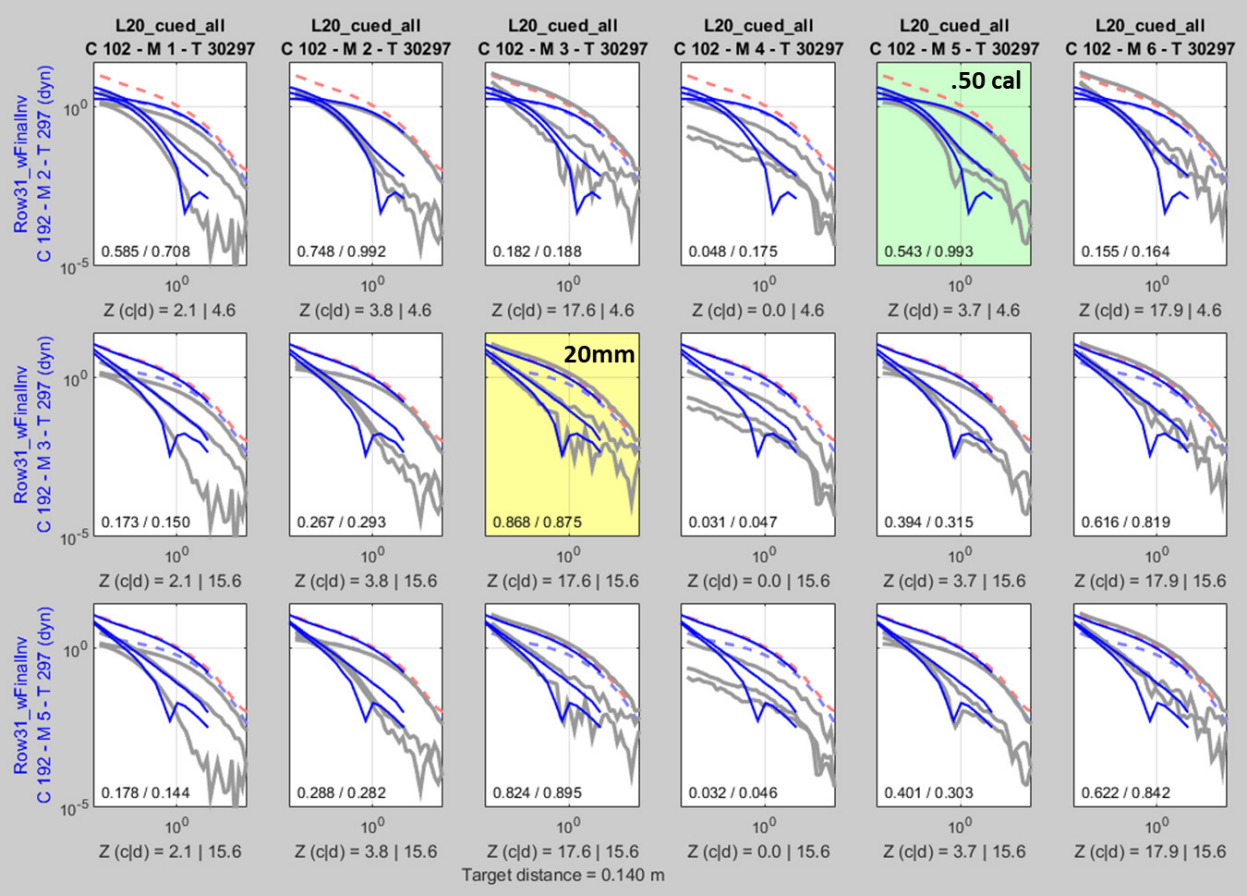

Figure 64. Example of Comparison of Cued (Grey Lines) and Dynamic (Blue Lines) Polarizabilities for One Target.

Each column shows the cued polarizabilities for the six models resulting from single-, two- and three-source inversions, respectively. The dynamic polarizabilities shown in each of the three rows correspond to the three best-matching set of dynamic polarizabilities. The frame highlighted in light yellow has the best overall fit (using all three polarizabilities); the frame highlighted in light green has the best fit to just the primary polarizability. The two numbers in the lower left of each frame are a match metric (between 0 and 1) calculated using all three / primary only polarizabilities. The X label for each frame lists the predicted depths for the cued | dynamic models. In this example, both a 20mm and a .50 cal are located at the target location.

BTG concluded that at the GM MRS the classic MM could be used effectively to accurately classify subsurface 20mm projectiles, despite the large amount of surface clutter (.50 cal). However, because a sizable percentage of the targets at the GM MRS would have to be dug, it was ultimately decided that due to economic considerations AGC methods would not be employed to clear the 20mm Range.

5.0 ULTRATEM SHAKEDOWN TESTING AND VALIDATION

This project included efforts related to testing and evaluation of UltraTEM hardware designed to provide high resolution AGC data at high production rates. The initial 5 transmitter (Tx) UltraTEM Classifier data from the Strathalbyn test plot in Australia was processed under this project to verify data quality and feasibility of informed source selection (ISS) and one pass classification workflows. The project also supported the mobilization of the UltraTEM Classifier and personnel to the Blossom Point test site for a week of shakedown testing and surveying over the Blossom Point UXO test site. The UltraTEM 5Tx Classifier was then taken to the Aberdeen Proving Ground (APG) UXO test site where the sensor successfully passed a formal demonstration of capabilities under the DoD Advanced Geophysical Classification Accreditation Program (DAGCAP).

5.1 PROCESSING OF INITIAL SENSOR DATA ACQUIRED AT STRATHALBYN TEST SITE

Initial data were acquired with two different UltraTEM form factors: the 5Tx UltraTEM Classifier (Figure 65) and the 1Tx UltraTEM Screener (Figure 66). The Classifier was designed to support one pass classification while the Screener was intended for informed source selection (ISS), with the retained source locations requiring subsequent cued measurements as part of a two-pass approach for classification. For sites where ISS screening is particularly effective, it may be more cost effective to dig all retained sources based on UltraTEM Screener data, rather than acquiring and processing cued data.

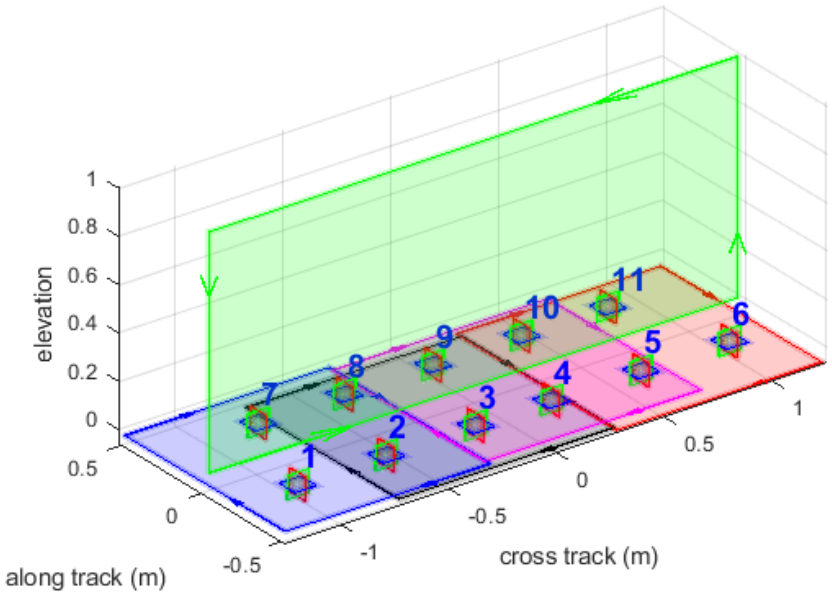

Figure 65. Geometry of the 5Tx UltraTEM Classifier Sensor. The Classifier is Comprised of Four Horizontally Oriented Tx Loops that Each Approximately 1 x 1m Resulting in a Combined 2.5 x 1m Footprint. A fifth vertically oriented Tx Loop (the Green Loop Shown above) Provides Improved Along Line Excitation. There Are Eleven Three Component Rx Cubes Offset to Illuminate Targets from Multiple Angles as the Sensor Passes Over Each Target. Surveys Are Run with a Nominal 1.6m Line Spacing to Ensure Sufficient Data Overlap for Classification.

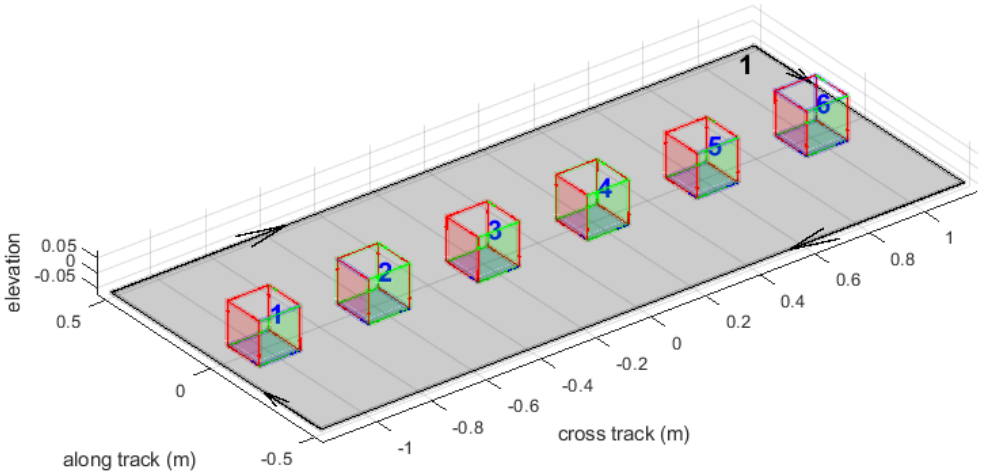

Figure 66. Geometry of the 1Tx UltraTEM Screener Sensor. The Screener is Comprised of a Single 2.35 x 1 m Tx Loop. There Are Six Component Rx Cubes Equally Spaced by 30cm. Surveys Are Run with a Nominal 1.8m Line Spacing.

The primary data processing goal at the Strathalbyn test plot was to assess the data quality of the UltraTEM Classifier under realistic survey conditions at a well characterized test site. The site was observed to have magnetic soils present (see Figure 67) which allowed for the impact of magnetic soil impacts to be investigated. Additional goals of the Strathalbyn processing efforts included a comparison of the recovered polarizabilities for the 1Tx Screener and the 5Tx Classifier over a common set of targets. Both the UltraTEM Classifier and Screener were deployed as towed arrays over the Strathalbyn test site using anticipated survey speeds and line spacings for their respective configurations. A number of multi-object scenarios were also seeded, allowing for an assessment of the ability of both the Classifier and the Screener to resolve multi object scenarios. An image depicting the layout of the Strathalbyn is shown in Figure 68.

Figure 67. UltraTEM Classifier Acquiring Data at the Strathalbyn Test Site.

Note the red soil characteristic of magnetic soils which can impact the performance of EMI sensors

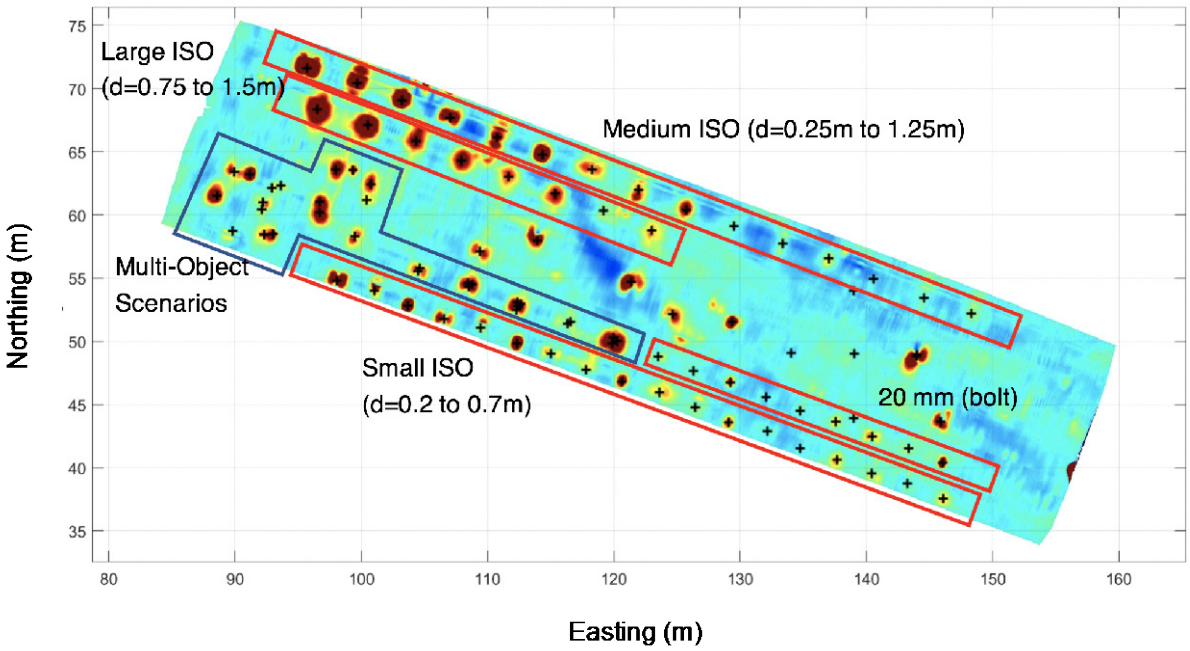

Figure 68. Strathalbyn Test Site Layout.

A summary and comparison of the relative performance of 5Tx UltraTEM Classifier and the 1Tx UltraTEM Screener at the Strathalbyn testplot is presented in a white paper prepared for DAGCAP in Appendix B.

5.2 SHAKEDOWN TESTING AT BLOSSOM POINT

The UltraTEM Classifier was mobilized from Australia to Blossom Point in July 2019. The sensor was assembled and the Blossom Point test site was surveyed. The Blossom point test site has also been surveyed with other AGC sensors.

A comparison of UltraTEM Classifier and TEMTADS 2x2 data acquired over the same set of 60mm mortars in the Blossom Point test plot is shown in Figure 69. The TEMTADS 2x2 was unable to detect the 60mm mortars at 1m while the UltraTEM Classifier does show an elevated response over those targets. The higher transmitter current and larger Tx loops of the UltraTEM combine to provide better performance at depth for the UltraTEM versus other commercially available AGC sensors. The TEMATDS2x2 dataset provided for this comparison did not have coverage over the 75cm deep 60mm mortars.

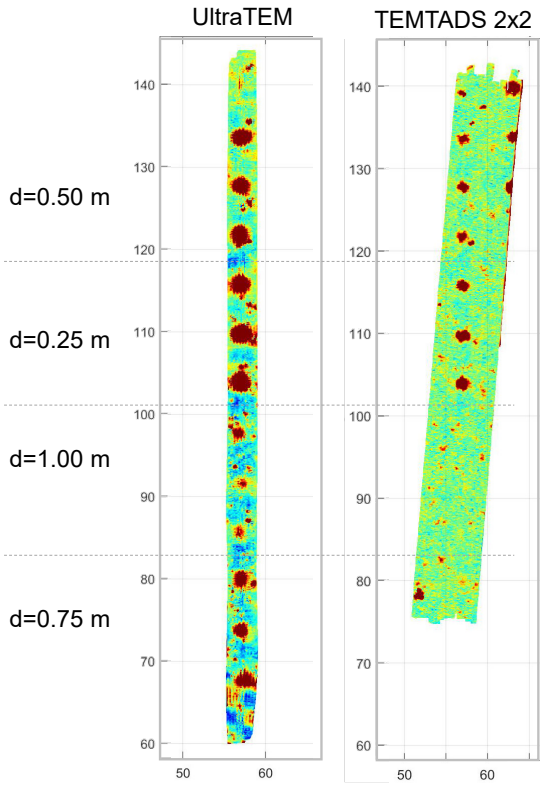

Figure 69. Comparison of UltraTEM and TEMATDS 2x2 Detection Data Over 60mm Mortars at the Blossom Point Test Site.

*The plotting scale for both datasets are from -5*noise to +5*noise with the colour green representing a value of 0 in the common colorscale used for both plotting both sets of data.*

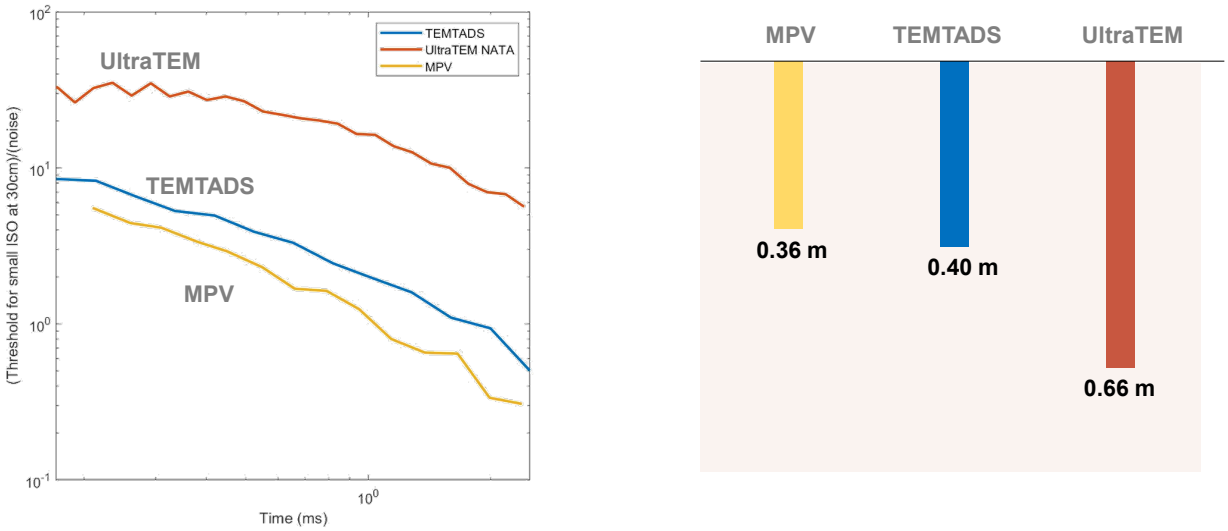

Figure 70. Left: Comparison of the SNR for Small ISO in Worst Case Orientation at 30 cm Depth. Right: Depth of Detection for a Small ISO When the Threshold Is Determined by 3 Times the Noise.

A comparison of sensor performance for deeper targets is provided in Figure 70. A comparison of provided for the threshold for detection of a small ISO at 30cm normalized by the noise profile as well as the depth of detection for a small ISO when the threshold is determined by 3 times the noise. The noise profile used for both the UltraTEM and the TEMTADS 2x2 was derived from the respective Blossom Point datasets while the MPV noise profile was obtained from data acquired at Mt. Owen, a similarly low noise survey environment. It is expected that all three of these sensors can find deeper small ISOs than the depth of detections shown in Figure 70: these depths represent the most difficult orientation and position of the target relative to the sensor.

Successful one pass classification requires not only detection but also the recovery of polarizabilities that match the polarizabilities in the site library well enough that the classification will identify these detected anomalies as TOI. Figure 71 shows the recovered polarizabilities for the 60 mm mortars surveyed with the UltraTEM Classifier. Depths of 25cm and 50cm produce excellent library matches. The polarizabilities recovered for the 60mm mortars at 75cm depth still produce reasonably good matches to the reference library although the secondary polarizabilities are showing some degradation. At a depth of 1m, the secondary polarizabilities are poorly constrained and a classification would be more challenging and likely require reliance on the primarily polarizability only, rather than all three polarizabilities.

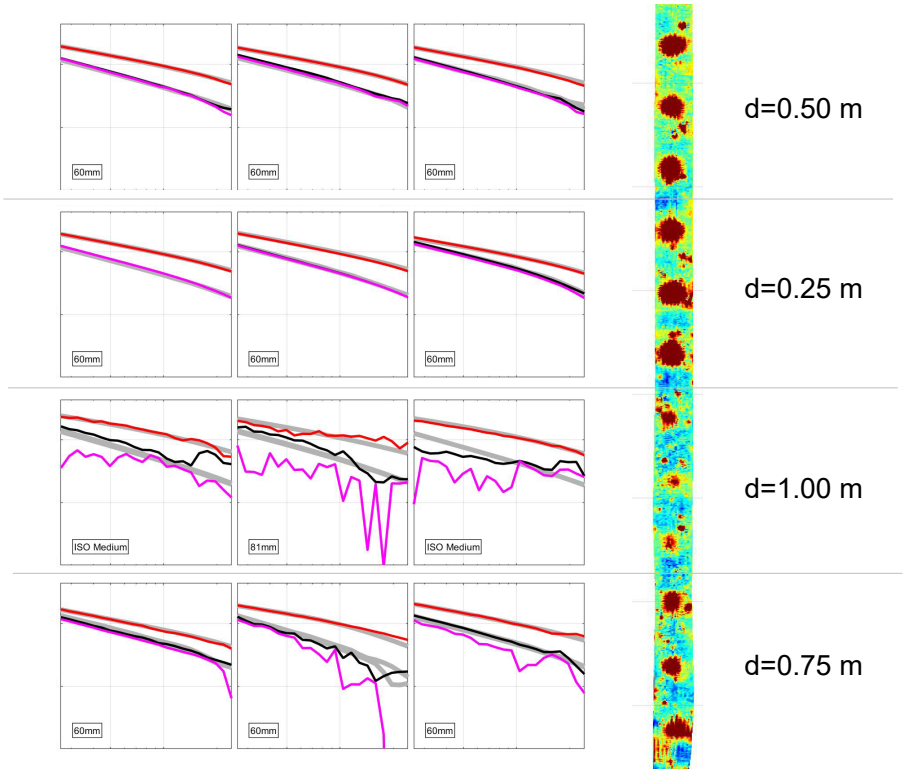

Figure 71. Recovered Polarizabilities for the UltraTEM Classifier Over 60mm Mortar Targets at the Blossom Point Test Site.

A key concern for one pass classification, particularly at high target density sites, is the ability resolve multi object scenarios. The Blossom Point test site also provided an opportunity to bury increasingly complicated multi object scenarios over which UltraTEM Classifier data could then be acquired. Figure 72-Figure 74 show the UltraTEM Classifier's ability to resolve complicated multi object scenarios.

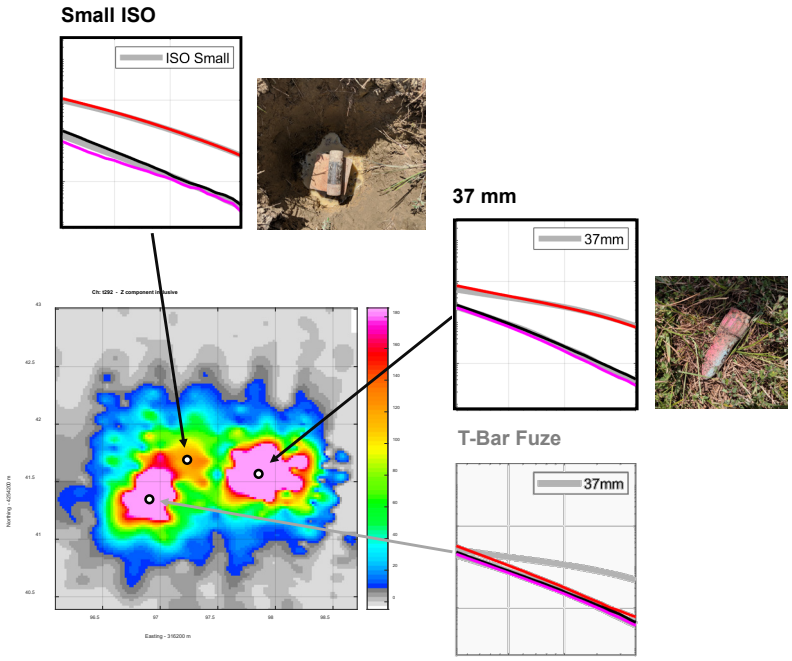

Figure 72. Multi Object Scenario Comprised of Two TOI and One Piece of Clutter Within the Footprint of the UltraTEM Classifier: A Small ISO at Depth and a Near Surface 37mm. Also Present Near Surface is a Fuze Representing a Clutter Target. Inset Plots Show Recovered Polarizabilities (Colored Lines) and Reference Polarizabilities (Grey Lines) for Each Item.

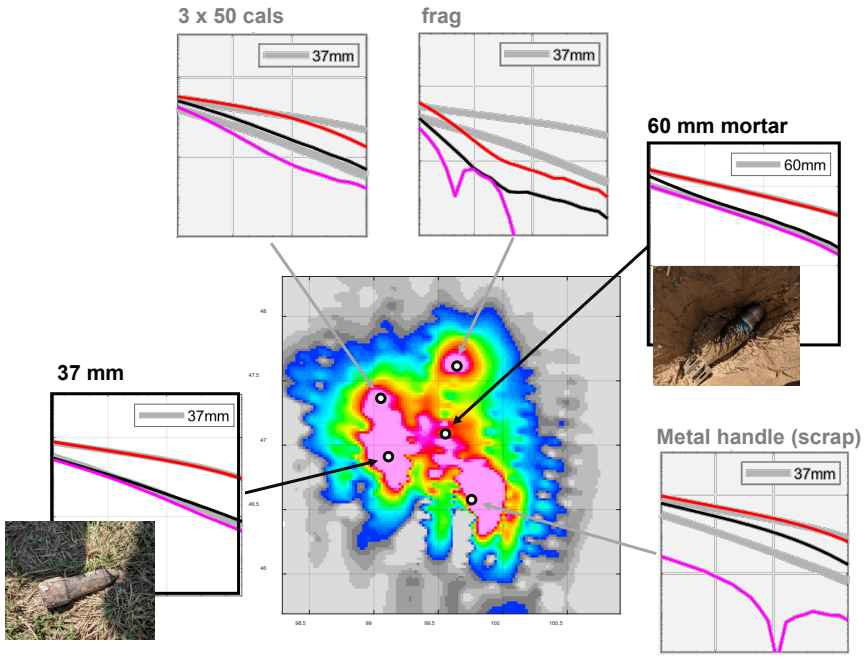

Figure 73. Multi Object Scenario Comprised of Two TOI and Three Pieces of Clutter Within the Footprint of the UltraTEM Classifier: a 60mm Mortar at Depth and a Near Surface 37mm. Also Present Near Surface Are Three Different Clutter Targets.

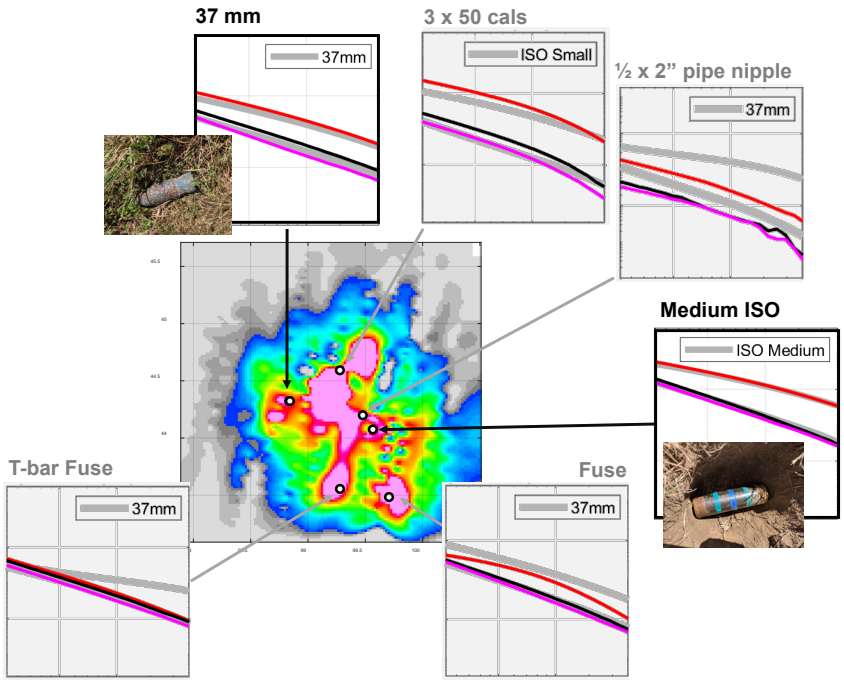

Figure 74. Multi Object Scenario Comprised of Two TOI and Four Pieces of Clutter Within the Footprint of the UltraTEM Classifier: A Medium ISO at Depth and a Near Surface 37mm. Also Present Near Surface Are Four Different Clutter Targets.

5.3 ULTRATEM HARDWARE DEMONSTRATION OF CAPABILITIES AT ABERDEEN PROVING GROUNDS (APG)

After a week of shakedown testing at Blossom Point, the UltraTEM Classifier was transported to APG for surveying on a portion of the UXO test site established for DAGCAP demonstration of capabilities. The sensor was transported from Blossom point on a trailer already assembled. As a result, there was minimal time required for setup with UltraTEM Classifier surveys beginning the first day on site at APG. An L shaped area approximately 1.5 acres was surveyed twice: once at the nominal speed of 0.75m/s recommended for one pass classification and a second time at 1.5 m/s nominally in support of an ISS survey. All UltraTEM data collection was completed midway through the 2nd day on site. In order to maintain the integrity of the ground truth information of the APG test site, DAGCAP only provides a pass/fail status for the demonstration of capabilities so there is little that can be reported on classification performance. The one pass classification diglist successfully met the scoring criteria and the 5Tx UltraTEM Classifier is therefore considered to be validated AGC hardware. A whitepaper submitted to DAGCAP (Appendix B) serves as validation of the Screener system for ISS surveys.

5.4 SYNTHETIC SEEDING A HIGH TARGET DENSITY DATASET FOR TESTING ONE PASS CLASSIFICATION WORKFLOW

High quality AGC data is particularly beneficial to sites with high target densities. The cost of a two-pass classification approach at high density sites is considerably higher as a result of the additional costs of acquiring and processing cued data. High production rate AGC detection surveys with the UltraTEM Screener can reduce the number of cued measurements required (compared with traditional DGM detection surveys) if ISS is viable.

If a one pass classification workflow with UltraTEM Classifier is possible at high target density sites, the need for cued surveys and processing could potentially be eliminated altogether.

The ability to recover multi object scenarios likely to be encountered at high target density sites can be tested on a limited basis through physical seeding of challenging scenarios such as those described at Blossom Point in section 1.13. Synthetic seeding can also be used to allow the processing workflows to be tested on a larger scale.

Because the seeded targets in the test plot at Blossom Point are laid out based on a grid pattern, there are line paths in the regions between the grid centers where there are minimal target responses present in the data. A four-acre UltraTEM 5Tx Classifier data set was constructed by patching together these line paths. Position and IMU information from the original dataset were used to build the dataset.

Synthetic seeding was then used to emplace 10,000 targets randomly distributed over the 4 acre site. Small, medium and large ISOs along with 2 variants of the 20mm projectile were seeded as TOI with scrap being represented by seeding fuzes and 50 cal into the 4-acre site. Figure 75 shows the polarizabilities of TOI and scrap that were used to generate the 4-acre high target density dataset.

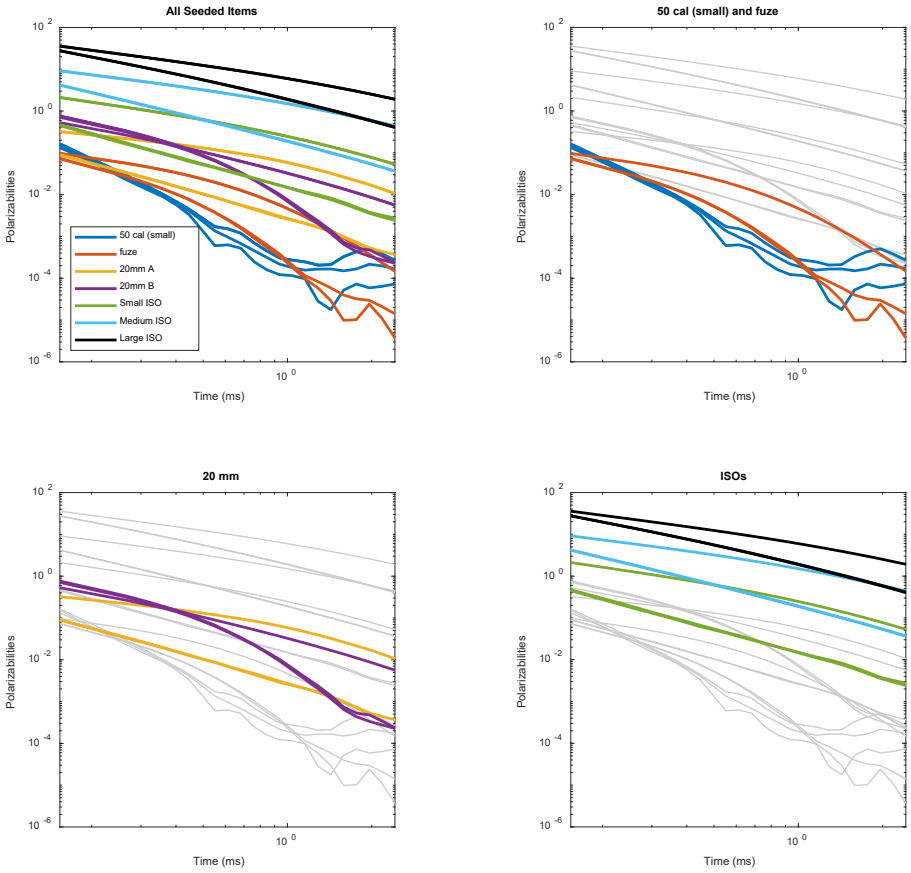

Figure 75. Targets Synthetically Seeded Into the 4 Acre High Target Density Site Constructed for Testing a One Pass Classification Workflow. Top Left: Polarizabilities of All TOI and Scrap Synthetically Seeded. The Other Sets of Plots Highlight Specific Seed Targets in Color: Top Right: Polarizabilities for the Scrap, Bottom Left: Polarizabilities for the Two Types of 20mm Projectiles Used as Small TOI and Bottom Right: ISOs Seeded as TOI.

Table 1 lists the numbers and depth ranges for both TOI and scrap that were synthetically seeded into the four-acre UltraTEM Classifier dataset and Figure 76 shows the spatial distribution of TOI and scrap over the four acres. The noise profile used for generating the synthetic data is approximately the same as Blossom Point. Because the synthetic seeding assumes accurate positioning and orientation information, the resulting analysis represents a best-case scenario for one pass classification.

Table 1. Number and Depth Range of Scrap and TOI Synthetically Seeded to Create the 4-acre High Target Density UltraTEM Classifier Dataset.

Target type	Number	Min. Depth (m)	Max Depth (m)
20 mm	200	0.1	0.25
Large ISO	10	0.6	1.5
Medium ISO	20	0.3	0.9
Small ISO	20	0.2	0.55
Scrap (fuze and 50 cal.)	9750	0.025	0.2

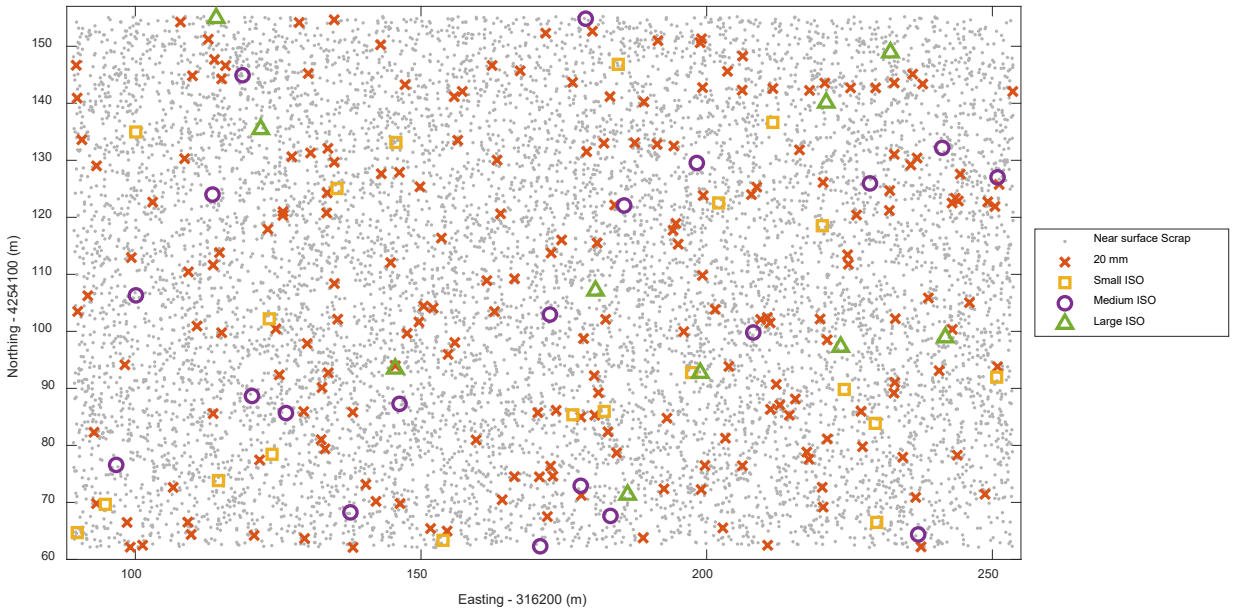

Figure 76. Distribution of TOI and Scrap Synthetically Seeds to Create a High Density 4-acre UltraTEM Classifier Dataset.

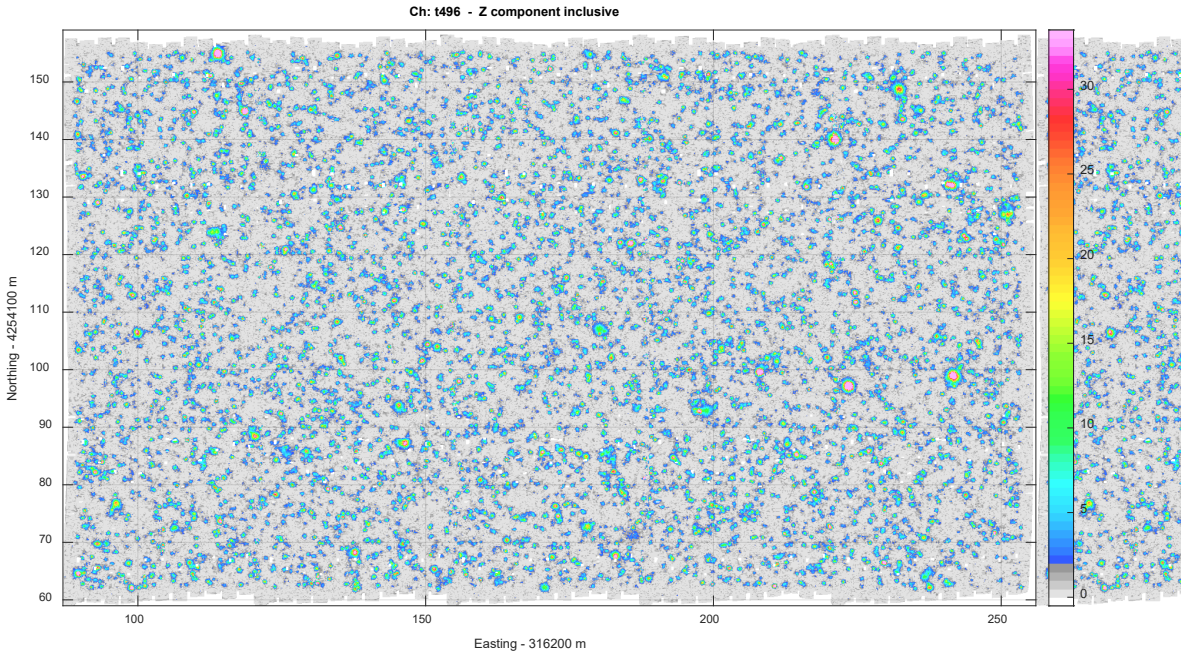

Figure 77. Synthetically Seed Dataset for the Target Distribution Shown in Figure 76.

Target picking was performed on the same t=0.496ms time channel displayed in Figure 77. A threshold was defined as twice the standard deviation to determine a threshold that was used with a profile picker on the Z-component data. A total of 8641 target picks above threshold with the resulting density of detected anomalies exceeding 3000/acre in some areas as depicted in the density map depicted in Figure 78.

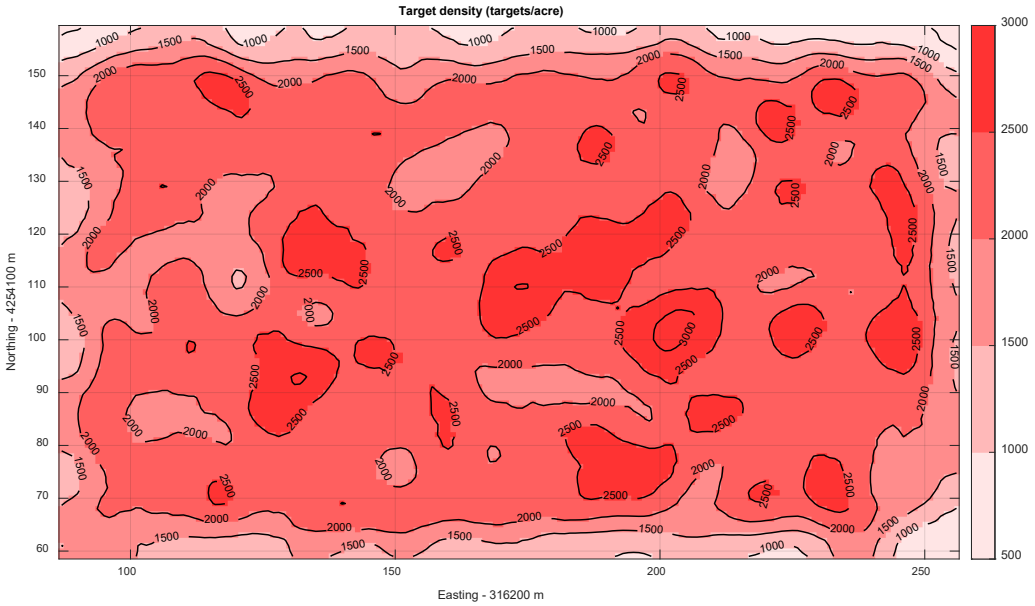

Figure 78. Target Density Map of Detected Anomalies.

Every detected anomaly was inverted using 1, 2 and 3 object inversions. An automated QC, source selection and classification process was applied with no analyst override of the automated decisions. The automated QC consisted of failing models with offsets > 0.6m from the pick location to the estimated source, models where the data fit is < 0.7, and models where the polarizability metric > 0.2. Shared targets were assigned for cases where models were < 0.15m apart and the polarizability misfit < 0.4. There were 388 cannot analyze targets, primarily due to low data fit threshold. Classification was performed using a library matching with a classification library comprised of ISOs and 20mm projectiles.

The automated classification approach with 5Tx UltraTEM Classifer data is able to efficiently find all targets of interest. The receiver operating characteristic (ROC) curve in Figure 79 shows that the automated classification approach identified all 250 TOI with only 329 false positives.

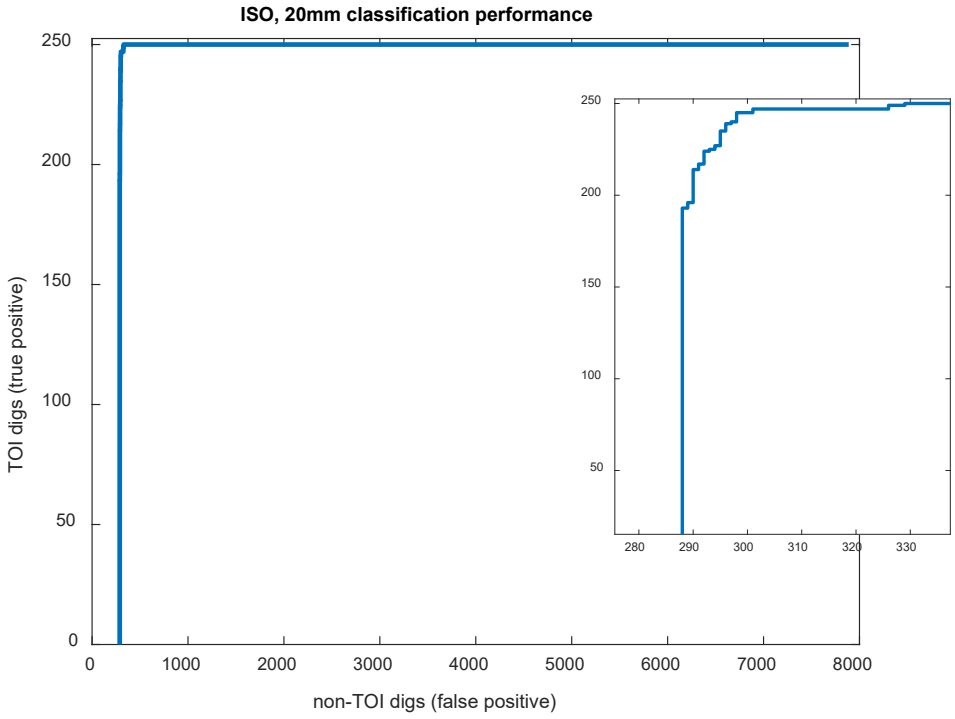

Figure 79. ROC Curve for the Automated Classification Approach Applied to the Synthetically Seed High Target Density Four-acre Site.

Inset shows a close up of the corner of the ROC curve.

While these synthetic seeding results indicate that one pass classification with the UltraTEM Classifier is possible at a relatively high target density site, classification viability and performance will ultimately depend on site specific details such as the types of TOI and clutter present.

6.0 TECHNOLOGY TRANSFER

Technology transfer was a key component of the project, ensuring that advancements in AGC processing workflows and lessons learned from this project could be shared with the MMRP industry. Technology transfer activities included:

- At an ESTCP demonstration at Fort Ord, Black Tusk partnered with CB&I on a survey designed to identify a large range of TOI at a site with very high levels of surface clutter. Details of the Fort Ord demonstration are captured in a standalone report (https://serdp-estcp.org/Program-Areas/Munitions-Response/Land/Live-Site-Demonstrations/MR-201421/MR-201421). Black Tusk was on site at startup to provide training to CB&I on the use of UXOLab. Black Tusk continued providing remote processing support as CB&I independently worked through AGC workflows for the dynamic and cued MetalMapper data from Fort Ord. Black Tusk also processed that data from Ft. Ord and presented those results at a meeting of stakeholders for the site.
- Attendance at the ESTCP symposium over multiple years where posters detailing recent project work and results were presented in the Munitions Response poster sessions.
- Attendance at a public meeting for the Camp George West site was also supported by this project. BTG brought the MPV sensor to the meeting to provide stakeholders an opportunity to see the type of instrument that would be surveying on their properties and to answer technical questions related to AGC.

7.0 PERFORMANCE ASSESSMENT

The software tools developed under this project have been successfully transitioned to a number of production MMRP projects. In particular, the In-Field App has been used for ongoing verification of measurement quality objectives (function tests and background validations) for the MPV sensor. The performance of this app can be measured by minimization of MQO failures that might trigger root cause analyses and corrective actions, which will usually necessitate recollection of data and thereby impact production rates.

The UltraTEM 5Tx Classifier system achieved all performance requirements required for DAGCAP approval as a validated sensor for one-pass classification. The 1Tx Screener UltraTEM described in Appendix B is currently undergoing review by DAGCAP for approval on projects where informed source selection will be used to screen out small, fast decaying targets.

8.0 COST ASSESSMENT

The cost drivers for AGC with the UltraTEM sensor will include:

- Anomaly density: the higher resolution of the UltraTEM relative to conventional DGM sensors will lead to a larger number of target detections and will increase processing costs at sites with high target densities
- Terrain/vegetation: obstacles will reduce production rates for both towed and man-portable UltraTEM form factors and may necessitate recollects or deployment with a robotic total station.
- Site specific TOI: at sites with small TOI (e.g. 20 mm projectiles) that are similar to non-TOI, classification performance will be adversely impacted and more intrusive investigations may be required.

The principal cost benefit of one-pass classification with the UltraTEM is expected to be realized in a higher production rate (~3-4 acres/day for the UltraTEM classifier system) relative to other dynamic AGC sensors, and in elimination of the need for a two-pass approach requiring deployment of a cued sensor. This will reduce survey costs and project timelines, while still ensuring that acquired AGC data can meet project objectives.

9.0 IMPLEMENTATION ISSUES

All technology developed under this project must comply with the requirements of DAGCAP when used by industry for commercial MMRP work:

- UXOLab software tools have been validated for AGC data processing, including processing of UltraTEM data.
- The UltraTEM Classifier system has also been validated for informed source selection and one-pass classification. DAGCAP approval of the 1Tx UltraTEM for ISS is still pending.

APPENDIX A POINTS OF CONTACT

POINT OF CONTACT Name	ORGANIZATION Name Address	Phone Fax E-mail	Role in Project
Kevin Kingdon	Black Tusk Geophysics #401 -1755 Broadway W, Vancouver BC V6J4S5	(604) 428 3382 kevin.kingdon@btgeophysics.com	Principal Investigator

APPENDIX B WHITE PAPER: VALIDATION OF ULTRATEM SCREENER FOR INFORMED SOURCE SELECTION

B.1 INTRODUCTION

The purpose of this white paper is to provide an overview of the UltraTEM Screener AGC sensor and to provide objective evidence that this system can reliably achieve performance requirements for Informed Source Selection (ISS) under the DoD AGC Accreditation Program (DAGCAP).

The UltraTEM Classifier, designed for one-pass AGC surveys, was validated at Aberdeen Proving Ground (APG) in 2019. Our SOPs for UltraTEM assembly, data acquisition and data processing have been updated to apply to both the Classifier and Screener arrays.

This white paper has been prepared with the understanding that review and approval of this white paper by DAGCAP will serve as validation of the UltraTEM Screener for ISS.

B.2 ULTRATEM SCREENER

The UltraTEM Screener is a single transmitter AGC array that can be deployed in man-portable, pushcart or towed array form factors (Figure 80). For all form factors, six receiver cubes are evenly spaced in the cross-track direction within a horizontal transmitter. The two portable form factors use a 1.8 m x 0.9 m transmitter coil with the sensor cubes spaced 30 cm apart. The towed-array uses a large 2.35 m x 1.0 m transmitter coil with the sensor cubes spaced 40 cm apart.

The system is designed to acquire data that supports target picking, inversion, and informed selection of sources on the basis of simple criteria (e.g. amplitude and decay of estimated polarizabilities). The Screener system is not intended for one-pass classification surveys where a ranked dig list is generated on the basis of polarizability matching with the DoD library.

An UltraTEM Screener system is assembled using the following base components:

i. UltraTEM-IV Receiver Bank (Figure 81) containing six receiver cards.

ii. Six 3-component receiver cubes. Receiver cubes consist of three orthogonal coils with dimensions of 15 cm x 15 cm x 15 cm each with an effective area of 104.5 m2 (Figure 81).

iii. An EODTx50 high current geophysical transmitter.

iv. A Real-Time-Kinematic Global Positioning System (RTK-GPS) and Attitude Heading and Reference System (AHRS) for position and orientation of the sensor frame.

v. A data acquisition system running BTField software.

Figure 80. UltraTEM Screener Form Factors (Top to Bottom): Man-portable, Pushcart, and Towed Array.

Figure 81. Left: UltraTEM-III Receiver Bank. Right: UltraTEM-III Sensor (Receiver Cube).

B.3 POSITIONING

A Trimble R10 GPS operating in Real-Time Kinematic mode is used for accurate tracking of the position of the receiver system. The Trimble R10 GPS provide the capability to track both the standard GPS constellation of satellites as well as other constellations such as GLONASS, Galileo and Beidou. The increased number of satellites minimizes the chance that insufficient satellites are available to compute an accurate position in those areas with occluded sky view.

We use the Lord Microstrain 3DM-GX5-25 as an AHRS for the UltraTEM system which produces typical orientation accuracies of better than 0.3 degrees in pitch, roll and heading. The Lord Microstrain is housed in the FLaG (Fluxgate Lord MicroStrain and GPS) Box. This is positioned on the GPS pole below the GPS.

An Applied Physics Model 533 Fluxgate magnetometer is also included in the FLAG box to provide a redundant method to compute the magnetic heading of the UltraTEM system. The Fluxgate magnetometer measurements occur during the off-time of the UltraTEM transmitter and in principle are more accurate than the heading estimates from the Microstrain. In practice, we have found that there is little difference between the accuracy of the Microstrain and fluxgate headings so that either can be used

B.4 DATA ACQUISITION

UltraTEM data are acquired using Black Tusk Geophysics' BTField software package. During data acquisition BTField displays gridded raw data, GPS quality, data profiles, transmitter information and raw EM decays in real time (Figure 82).

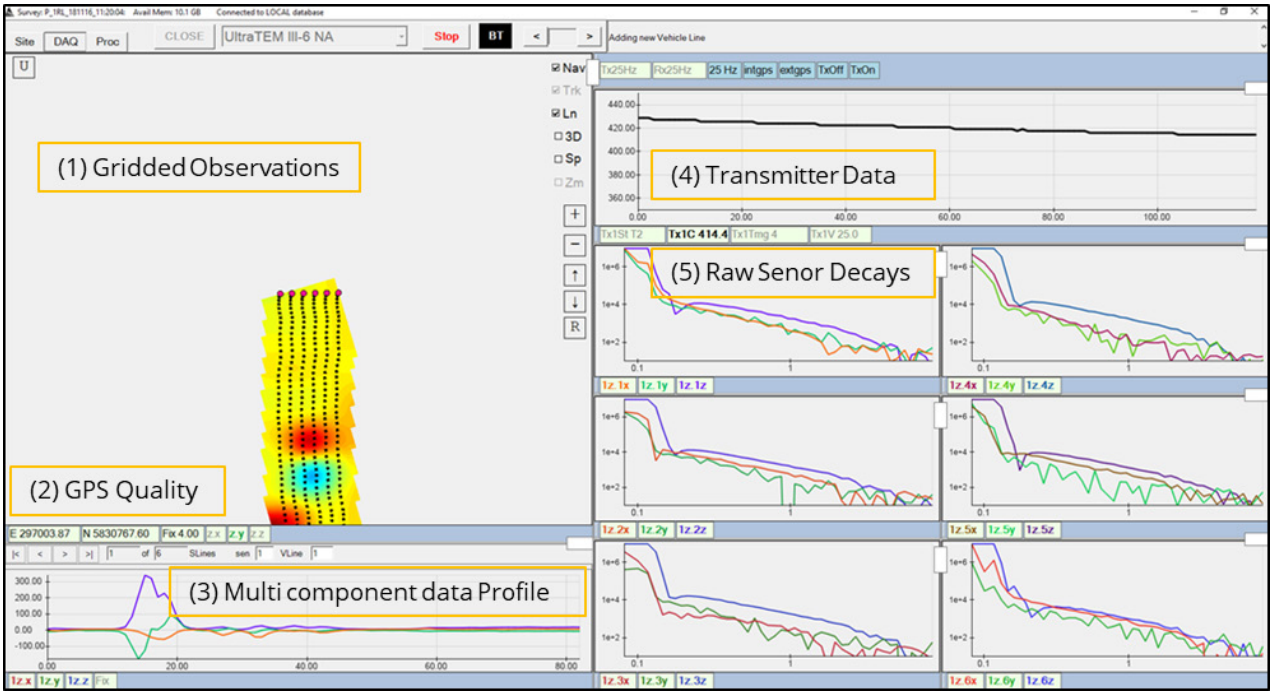

Figure 82. BTField Data Acquisition View for UltraTEM Screener.

B.5 DATA ANALYSIS

Inversion and ISS results presented in this document were carried out using BTG's DAGCAP-validated UXOLab software. We are currently working on development of informed source selection in BTField. We intend to validate this package for informed source selection, and it will be made commercially available to other companies who wish to self-perform UltraTEM Screener data processing on MMRP projects.

B.6 INFORMED SOURCE SELECTION WITH ULTRATEM SCREENER DATA

B.6.1 Location and polarizability accuracy

In this section, we use UltraTEM data collected at the Stathalbyn test site, South Australia to characterize recovery of target locations and polarizabilities from UltraTEM Screener data. The site was surveyed with both UltraTEM Classifier and Screener towed arrays in 2019, prior to validation of the Classifier system at APG. Figure 83 shows the site and Figure 84 shows a gridded image of the UltraTEM data showing ground truth for seeded items.

Figure 83. UltraTEM Classifier Collecting Data at Strathalbyn Test Site.

Red soils are diagnostic of magnetic background response observed in the UltraTEM data.

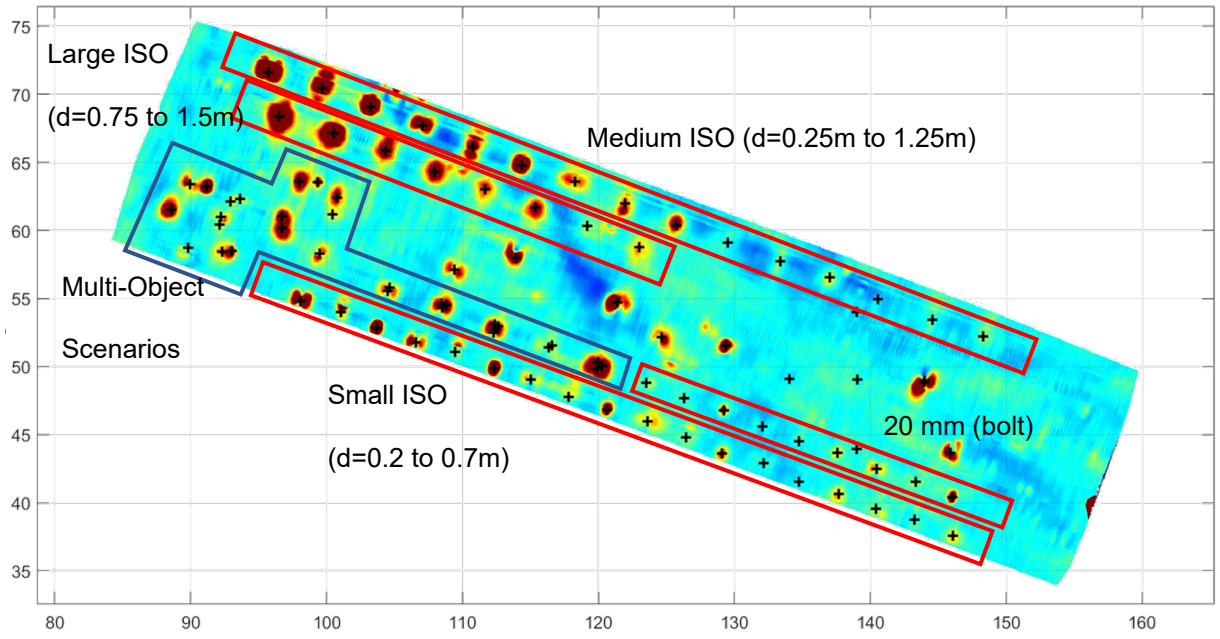

Figure 84. Strathalbyn Test Site Data.

Figure 85 shows a comparison of polarizabilities estimated from UltraTEM Screener and Classifier for medium ISOs seeded at the Strathalbyn test site. The Screener system achieves excellent matches to the library for shallow (0.25 m) medium ISOs. However, the estimated secondary polarizabilities start to deviate from the library polarizabilities for the deeper (≥0.5 m) medium ISOs. This is because recovery of secondary polarizabilities from Screener data typically depends on lower SNR data and/or data from adjacent passes that may be affected by positional errors. In contrast, the 5-transmitter UltraTEM Classifier acquires multiple target excitations in a single pass, resulting in well-constrained secondary polarizabilities in most cases.

Figure 86 and Figure 87 summarize recovery of polarizabilities and locations for ISOs detected with Screener and Classifier datB. Mean and maximum deviations of recovered locations from ground truth locations are comparable for Screener and Classifier systems (Table 2).

Table 2. Mean and Maximum Offsets of Estimated Locations from Ground Truth Locations for ISOs Seeded at Strathalbyn Test Site.

System	Mean offset (m)	Maximum offset (m)
Screener	0.09	0.19
Classifier	0.09	0.22

As expected, there is slightly more variability in the estimated polarizabilities for the Screener data. We demonstrate in the next section that polarizabilities estimated from Screener data can be used to reliably select sources.

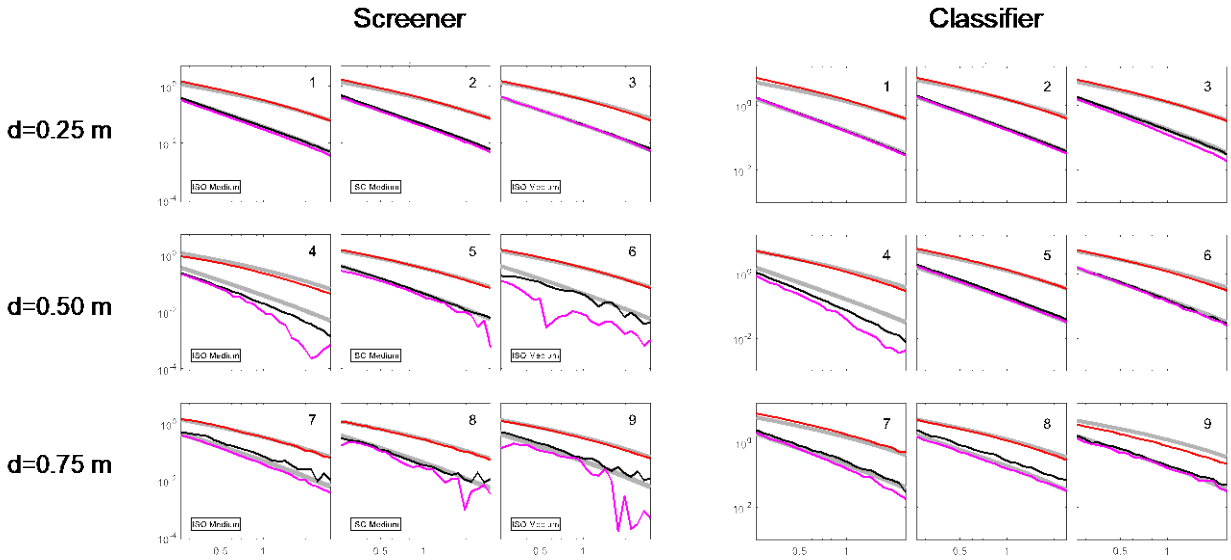

Figure 85. Comparison of Polarizabilities Estimated from UltraTEM Screener (Left) and Classifier (Right) for Medium ISOs Seeded at the Strathalbyn Test Site.

Grey lines are DoD library polarizabilities for the Medium ISO. Numbers at top right of plots indicate the same item.

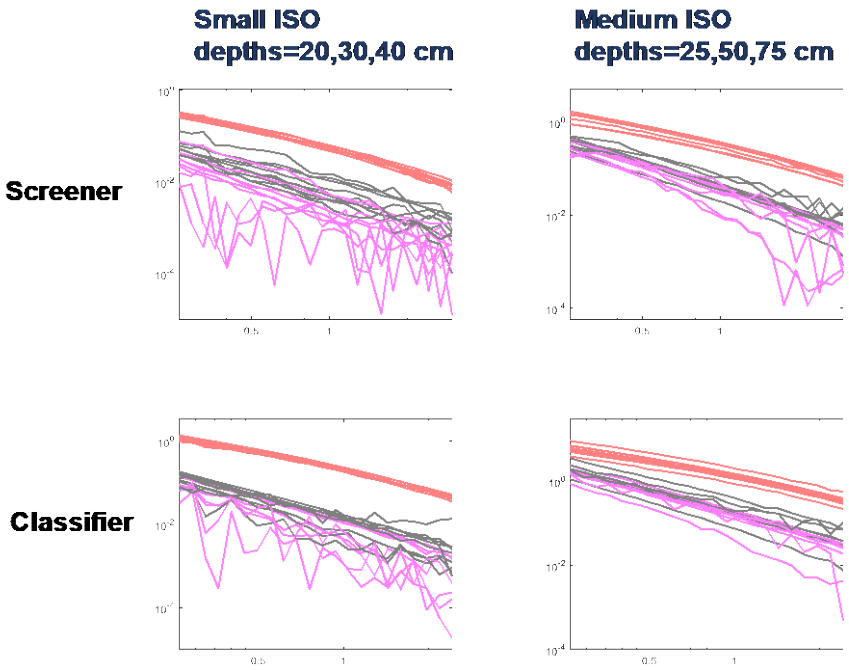

Figure 86. Comparison of Polarizabilities Estimated from UltraTEM Screener and Classifier for Small and Medium ISOs Seeded at the Strathalbyn Test Site.

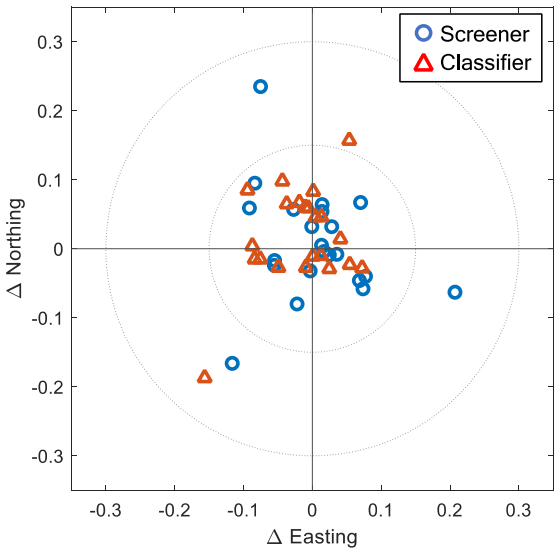

Figure 87. Deviation of Estimated Locations from Ground Truth Locations for ISOs Seeded at Strathalbyn Test Site.

B.6.2 Informed Source Selection: Strathalbyn Test data

Using our data processing SOP and DAGCAP-validated UXOLab software, ISS was applied to the UltraTEM Screener data acquired at the Strathalbyn test site. For this test, we choose the smallest TOI to be a small ISO at a maximum depth of 30 cm. To study our ability to screen small targets, we treat the seeded 20mm simulants at the site as non-TOI.

For the UltraTEM Screener, a threshold based on a small ISO at a clearance depth of 30 cm results in predicted clearance depths for the medium ISO of approx. 70cm and a clearance depth of 1.25m for the large ISO. The Strathalbyn test site has 26 ISO that are shallower than their respective maximum clearance depths (see Table 1). These include 11 medium ISOs seeded at depths up to 0.8m and 4 large ISOs seeded up to a depth of 1.07 m. There are 14 20mm simulants seeded at depths up to the predicted clearance depth of 0.25 m for this target. Both the ISOs and 20mm simulants include examples of multi-target scenarios.

A grid-based target picker applied to channel t=0.292 ms was used to detect data anomalies. A threshold based on 4 times an estimate of the noise was chosen (7.6 mV/A). This threshold resulted in 210 anomaly picks. Figure 89 plots the locations of the anomaly picks and locations of emplaced targets. We note that due to magnetic soil noise, several geology-related anomalies were picked. Each of the 210 anomalies were inverted for 1, 2, and 3 dipole source models. This results in 6 models for each anomaly and 1260 dipole sources in total (Figure 90). Assuming 0.4 m horizontal offset MQO, there are dipole sources related to all detected ISOs, and there are dipole sources for 13 of the 14 20mm simulants. The one undetected 20 mm simulant is due to variation in the background caused by magnetic soil response.

The Informed Source Selection parameters used to screen the 1260 dipole sources are shown in Figure 88. For this example, the sources were screened according to polarizability size, but not decay. At sites with high levels of noise, the decay metric can be less robust than the size parameter. The Informed Source Selection process results in 126 sources selected (Figure 91). All ISOs within the specified clearance depth were selected. We note that many of the ISO deeper than the maximum clearance depth also had selected source locations. Table 3 lists the 26 ISOs within the max clearance depth along with their closest selected source. The median offset between TOI and closest selected source was 0.08m, and all the selected sources for the ISOs have offsets less than 0.2 m (see Figure 92).

Table 4 shows screening results for 20 mm simulants. All but one of the isolated 20 mm's were screened out. The data fit and polarizabilities for the isolated 20 mm that was not screened are shown in Figure 93. The inversion overestimated the depth of the source, resulting in an overestimate of the size (i.e. -0.96, which is slightly greater than the size threshold of -1). For the 6 20mm simulants that were part of multi-target scenarios, there are sources selected that are related to 3 of the 20mm. The ISS parameters were conservative, and it is not surprising that some of the 20mm would not be screened – in particular 20mm simulants that are part of multi-target scenarios.

In summary, the informed source selection process was able to screen out the majority of 20mm simulants, while selecting all ISOs within the specified clearance depths. The ISS reduced the initial 210 anomaly picks to 126 selected sources.

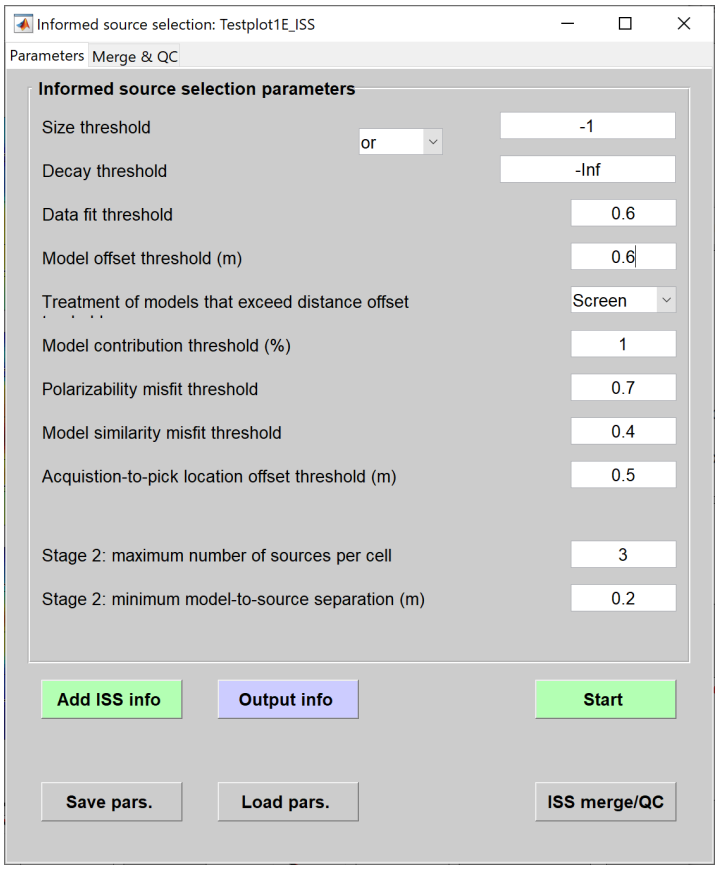

Figure 88. Informed Source Selection Parameters

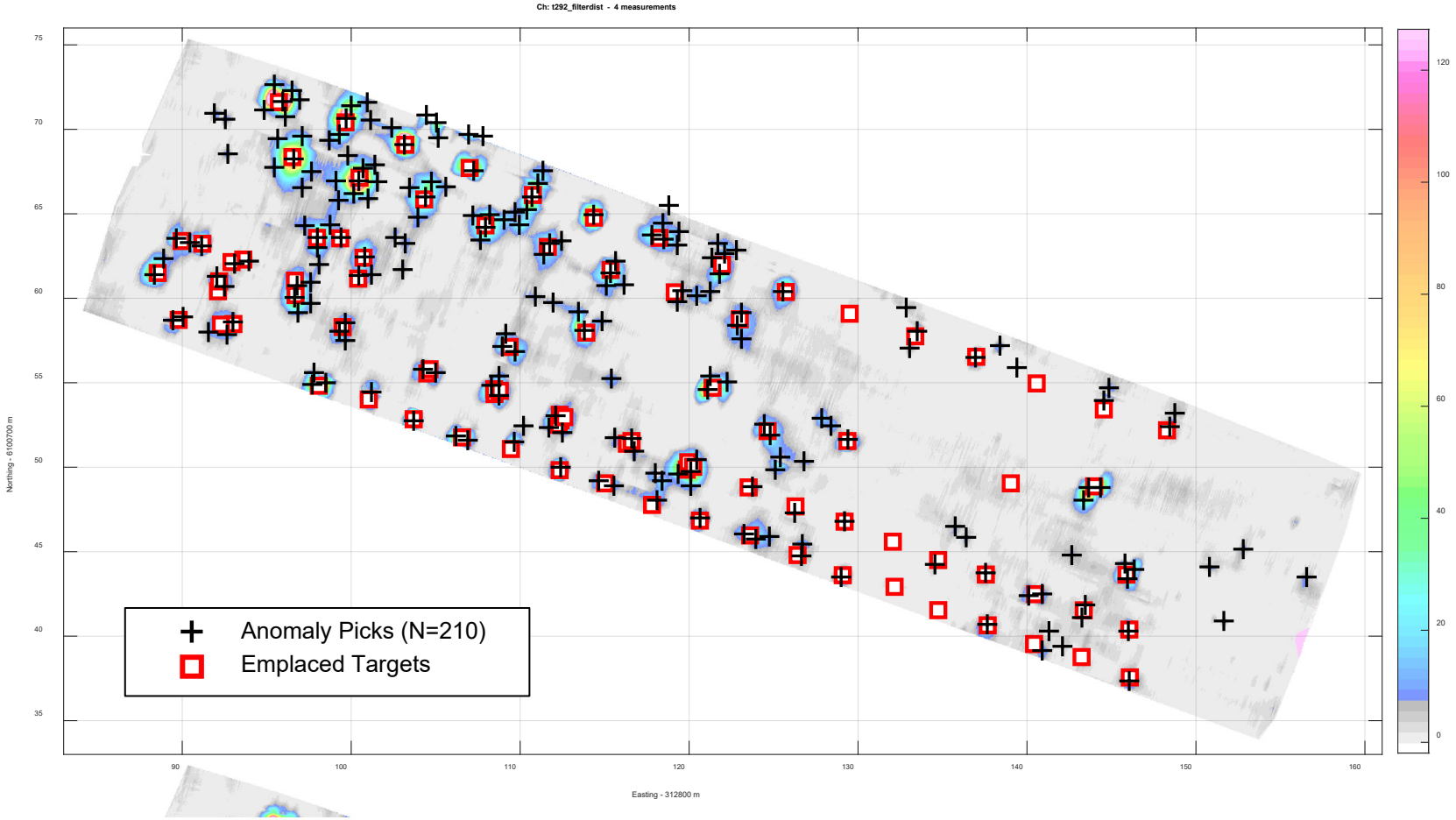

Figure 89. A Threshold of 7.6 Was Used to Select Data Anomalies.

All ISOs within the required clearance depth were picked.

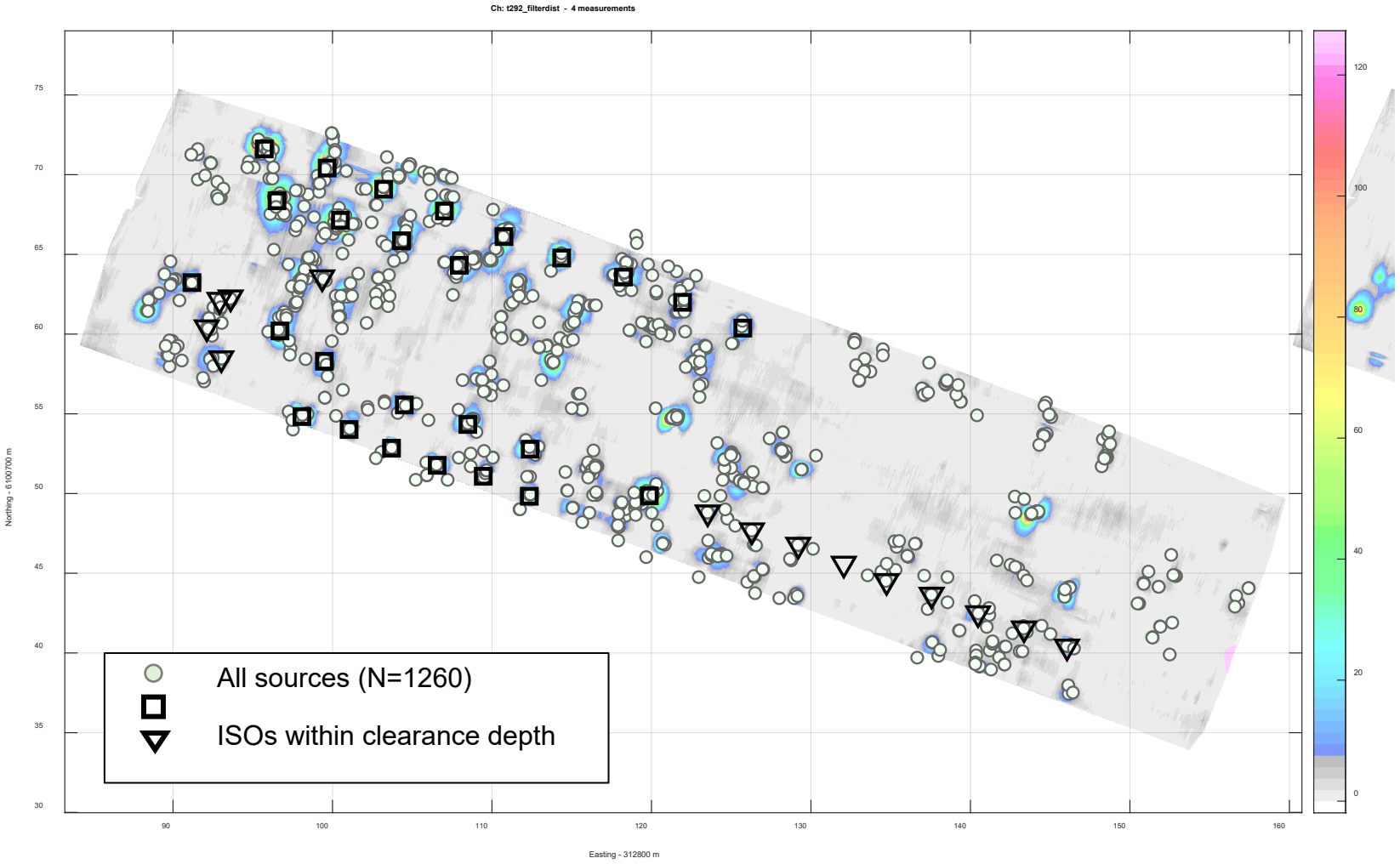

Figure 90. Dipole Source Locations from Inverting Each Data Anomaly with a 1, 2, and 3, Source Inversion.

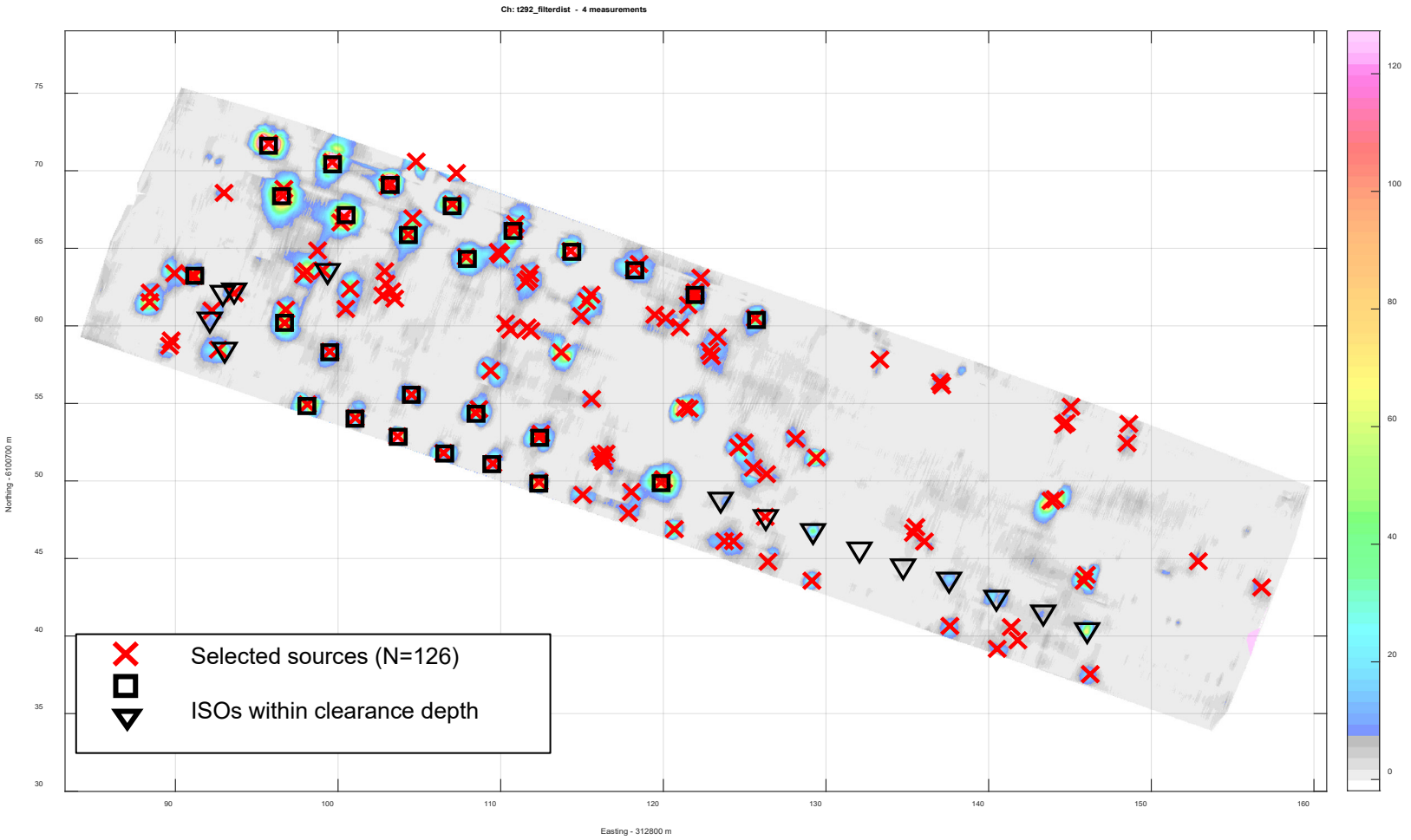

Figure 91. Selected Sources. All ISOs Within the Clearance Depth (i.e., Black Squares) Have Selected Sources.

We note that several of the ISOs deeper than the clearance depth were retained.

Table 3. TOI Locations and Nearest Selected Source

Emplaced Target information					Nearest Selected Source			
Type	Easting (m)	Northing (m)	Depth (m)	Orientation	dx (m)	dy (m)	dr (m)	Comment
Small ISO	312898.08	6100754.83	0.20	Axial	0.03	0.11	0.11	single target
Small ISO	312901.04	6100754.02	0.18	Cross track	0.02	0.05	0.05	single target
Small ISO	312903.70	6100752.84	0.20	Vertical	-0.03	0.03	0.05	single target
Small ISO	312906.56	6100751.77	0.28	Axial	-0.07	0.04	0.08	single target
Small ISO	312909.45	6100751.08	0.35	Cross track	0.07	0.04	0.08	single target
Small ISO	312912.34	6100749.83	0.33	Vertical	0.02	0.10	0.10	single target
Medium ISO	312895.72	6100771.61	0.25	Axial	0.02	0.14	0.14	single target
Medium ISO	312899.66	6100770.41	0.25	Cross track	-0.02	0.15	0.15	single target
Medium ISO	312903.21	6100769.09	0.32	Vertical	-0.02	0.12	0.13	single target
Medium ISO	312907.01	6100767.72	0.48	Axial	0.01	0.13	0.13	single target
Medium ISO	312910.75	6100766.12	0.53	Cross track	0.07	0.04	0.08	single target
Medium ISO	312914.37	6100764.77	0.52	Vertical	-0.06	0.06	0.09	single target
Medium ISO	312918.25	6100763.58	0.72	Axial	-0.05	0.11	0.12	single target
Medium ISO	312921.95	6100761.99	0.78	Cross track	-0.05	-0.06	0.08	single target
Medium ISO	312925.73	6100760.38	0.80	Vertical	-0.08	0.12	0.14	single target
Large ISO	312896.52	6100768.36	0.75	Cross track	0.09	0.03	0.09	single target
Large ISO	312900.50	6100767.14	0.75	Vertical	-0.13	-0.13	0.18	single target
Large ISO	312904.32	6100765.85	0.98	Cross track	0.00	0.04	0.04	single target
Large ISO	312907.95	6100764.32	1.07	Vertical	-0.07	0.13	0.15	single target
Small ISO	312904.50	6100755.55	0.30	Axial	0.02	0.02	0.03	multi: 23cm between iso and EOD9154
Small ISO	312908.48	6100754.33	0.30	Axial	-0.01	0.05	0.05	multi: 24cm from eod9150 28cm from eod9148 25cm from each other
Small ISO	312912.40	6100752.78	0.30	Axial	-0.04	0.04	0.05	multi: 24cm from eod9147 26cm from 9151 21cm from 9160
Medium ISO	312919.86	6100749.86	0.50	Axial	0.00	0.05	0.05	multi: 24cm from eod9246 34cm from eod9157
Small ISO	312899.49	6100758.30	0.31	Cross track	0.01	0.04	0.04	Saturated
Medium ISO	312896.71	6100760.20	0.50	Cross track	0.01	0.00	0.01	Saturated
Small ISO	312891.19	6100763.23	0.28	Vertical	-0.02	-0.01	0.02	Saturated

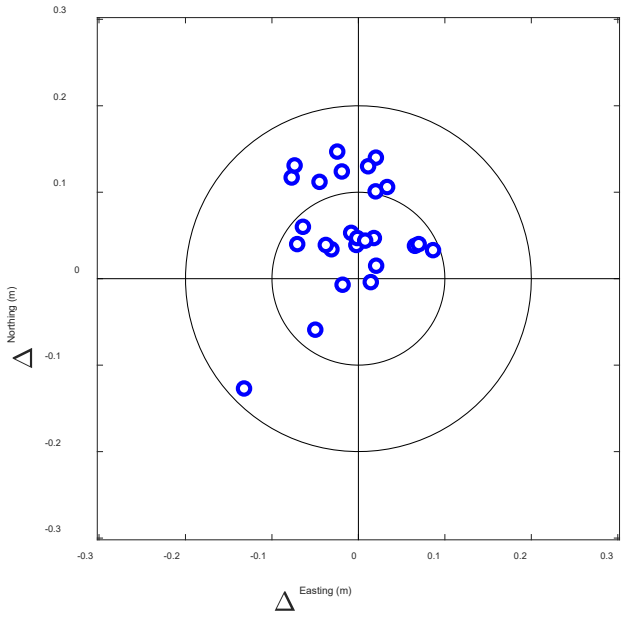

Figure 92. Nearest Selected Source Offset from Ground Truth for Seeded ISOs.

All sources are within 0.2 m of the target's ground truth location.

Table 4. 20mm Simulant Locations and Nearest Selected Source

Easting (m)	Northing (m)	Depth (m)	Orientation	Comment	Distance to Nearest Source (m)
312923.525	6100748.809	0.15	Axial	Single Target	2.71
312926.2985	6100747.682	0.15	Cross track	Single Target	0.03
312929.204	6100746.782	0.15	Vertical	Single Target	3.08
312932.0607	6100745.594	0.25	Axial	Single Target	3.48
312934.7424	6100744.506	0.25	Cross track	Single Target	2.06
312937.565	6100743.65	0.25	Vertical	Single Target	2.87
312940.4764	6100742.486	0.07	Axial	Single Target	2.12
312943.3587	6100741.533	0.07	Cross track	Single Target	2.19
312946.0566	6100740.394	0.08	Vertical	Single Target	2.86
312900.4132	6100761.166	0.21	Axial	Multi	0.1
312899.3542	6100763.553	0.21	Vertical	Multi	0.31
312893.613	6100762.295	0.21	Axial	Multi	0.19
312892.9179	6100762.145	0.25	Axial	Multi	0.70
312892.1164	6100760.418	0.25	Cross track	Multi	0.58
312893.0295	6100758.479	0.21	Vertical	Multi	0.39

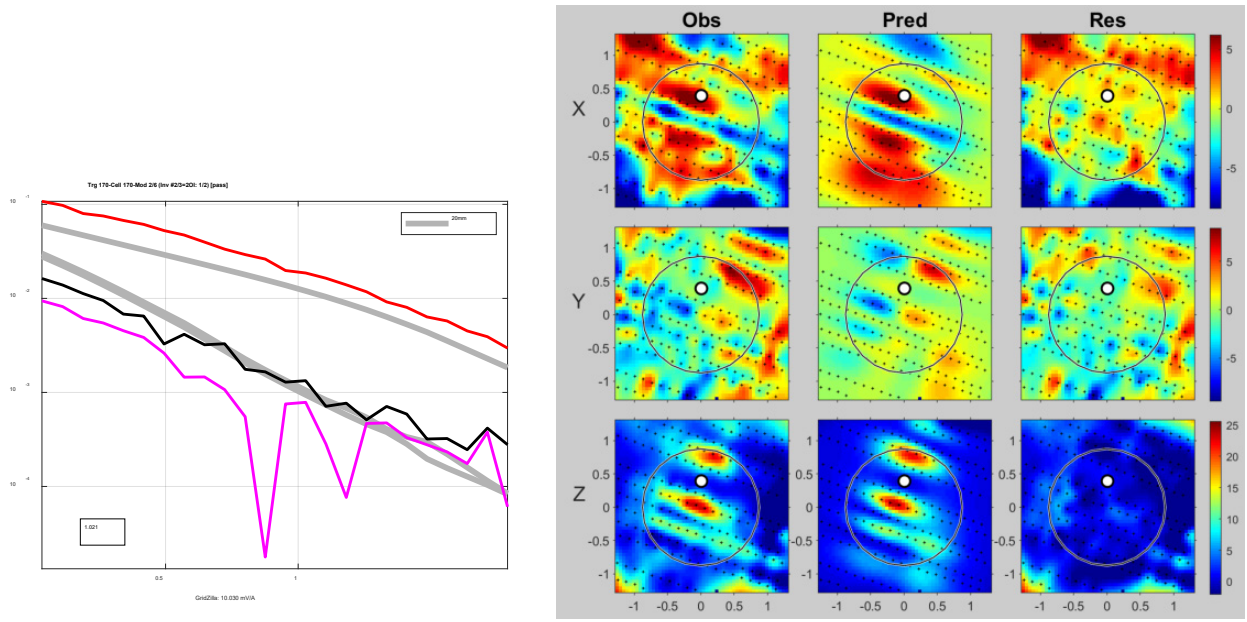

Figure 93. Left: Source Polarizability for Isolated 20 mm Not Screened by ISS. The Source Has a 3 cm Offset from the Groundtruth. However, the Depth for this Source Was Over Estimated, Resulting in a Size Metric of -0.96, Which was slightly higher than the -1 Size Threshold Used by the ISS. Right: The Data Fit for This Target, Showing Observed, Predicted, and Residual Data.

B.7 CONCLUSION

Our analysis of the Strathalbyn test data indicates that target locations and polarizabilities estimated from UltraTEM Screener data can be reliably used for informed source selection.